USP10 is a *de novo* tumour-specific regulator of β-Catenin and contributes to cancer stem cell maintenance and tumour progression

USP10 ist ein *de novo* tumorspezifischer Regulator von β-Catenin und trägt zur Erhaltung von Krebsstammzellen und zur Tumorprogression bei

Doctoral Thesis
for a doctoral degree
at the Graduate School of Life Sciences,
Julius-Maximilians-Universität Würzburg,
Section Biomedicine

submitted by
Michaela Reissland

from Friedrichroda

Würzburg 2022

Members of the thesis committee:

Chairperson:	Prof. Dr. Alexander Buchberger
Primary supervisor:	Dr. Markus E Diefenbacher
Second supervisor:	Prof. Dr. Amir Orian
Third supervisor	Prof. Dr. Martin Eilers
Forth supervisor	Prof. Dr. Ivan iki

Submitted on:

Date of Public Defence:

Date of Receipt of Certificates:

Contents

Summary

Colorectal Cancer (CRC) is the third most common cancer in the US. The majority of CRC cases are due to deregulated WNT-signalling pathway. These alterations are mainly caused by mutations in the tumour suppressor gene *APC* or in *CTNNB1*, encoding the key effector protein of this pathway, β-Catenin.
In canonical WNT-signalling, β-Catenin activates the transcription of several target genes, encoding for proteins involved in proliferation, such as MYC, JUN and NOTCH. Being such a critical regulator of these proto-oncogenes, the stability of β-Catenin is tightly regulated by the Ubiquitin-Proteasome System. Several E3 ligases that ubiquitylate and degrade β-Catenin have been described in the past, but the antagonists, the deubiquitylases, are still unknown.
By performing an unbiased siRNA screen, the deubiquitylase USP10 was identified as a *de novo* positive regulator of β-Catenin stability in CRC derived cells. USP10 has previously been shown in the literature to regulate both mutant and wild type TP53 stability, to deubiquitylate NOTCH1 in endothelial cells and to be involved in the regulation of AMPKα signalling. Overall, however, its role in colorectal tumorigenesis remains controversial.
By analysing publicly available protein and gene expression data from colorectal cancer patients, we have shown that *USP10* is strongly upregulated or amplified upon transformation and that its expression correlates positively with *CTNNB1* expression. In contrast, basal USP10 levels were found in non-transformed tissues, but surprisingly USP10 is upregulated in intestinal stem cells.
Endogenous interaction studies in CRC-derived cell lines, with different extend of *APC*-truncation, revealed an APC-dependent mode of action for both proteins. Furthermore, by utilising CRISPR/Cas9, shRNA-mediated knock-down and overexpression of USP10, we could demonstrate a regulation of β-Catenin stability by USP10 in CRC cell lines.
It is widely excepted that 2D cell culture systems do not reflect complexity, architecture and heterogeneity and are therefore not suitable to answer complex biological questions. To overcome this, we established the isolation, cultivation and genetically modification of murine intestinal organoids and utilised this system to study Usp10s role *ex vivo*. By performing RNA sequencing, dependent on different Usp10 levels, we were able to recapitulate the previous findings and demonstrated Usp10 as important regulator of β-dependent regulation of stem cell homeostasis.
Since genetic depletion of USP10 resulted in down-regulation of β-Catenin-dependent transcription, therapeutic intervention of USP10 in colorectal cancer was also investigated. Commercial and newly developed inhibitors were tested for their efficacy against USP10, but failed to significantly inhibit USP10 activity in colorectal cancer cells.
To validate the findings from this work also *in vivo*, development of a novel mouse model for colorectal cancer has begun. By combining CRISPR/Cas9 and classical genetic engineering with viral injection strategies, WT and genetically modified mice could be transformed and, at least in some animals, intestinal lesions were detectable at the microscopic level.
The inhibition of USP10, which we could describe as a *de novo* tumour-specific regulator of β-Catenin, could become a new therapeutic strategy for colorectal cancer patients.

Zusammenfassung

Darmkrebs ist die dritthäufigste Krebsart in den USA. Die Mehrheit der Darmkrebsfälle sind auf einen deregulierten WNT-Signalweg zurückzuführen. Diese Veränderungen werden hauptsächlich durch Mutationen im Tumorsuppressor-Gen *APC* oder in *CTNNB1* verursacht, welches für das zentrale Protein dieses Signalwegs, β-Catenin, kodiert.
Beim kanonischen WNT-Signalweg aktiviert β-Catenin die Transkription mehrerer Gene, die für, an der Proliferation beteiligte Proteine wie MYC, JUN und NOTCH, kodieren. Da β-Catenin ein kritischer Regulator dieser proto-Onkogene ist, wird die Stabilität von β-Catenin durch das Ubiquitin-Proteasom-System streng reguliert. In der Vergangenheit wurden mehrere E3-Ligasen beschrieben, die β-Catenin ubiquitylieren und abbauen, aber die Deubiquitylasen, sind gröSStenteils noch unbekannt.
Mit Hilfe eines unvoreingenommenen siRNA-Screens wurde die Deubiquitylase USP10 als *de novo* Regulator der β-Catenin-Stabilität in Darmkrebs-Zellen identifiziert. In der Literatur wurde bereits gezeigt, dass USP10 sowohl die Stabilität von mutiertem als auch von wild typ TP53 reguliert, NOTCH1 in Endothelzellen deubiquityliert und an der Regulation des AMPKα Signalwegs beteiligt ist. Insgesamt bleibt seine Rolle in der kolorektalen Tumorgenese aber bisher umstritten.
Anhand der Analyse öffentlich zugänglicher Protein- und Genexpressionsdaten haben wir gezeigt, dass *USP10* bei der Transformation stark hochreguliert oder amplifiziert wird und dass seine Expression positiv mit der von *CTNNB1* korreliert. Im Gegensatz dazu wurden in nicht transformiertem Gewebe basale USP10-Spiegel gefunden, aber überraschenderweise ist USP10 in intestinalen Stammzellen hochreguliert.
Endogene Interaktionsstudien in Darmkrebs-Zelllinien mit unterschiedlichem AusmaSS an APC-Trunkierung zeigten eine APC-abhängige Interaktion für beide Proteine. Darüber hinaus konnten wir mit Hilfe von CRISPR/Cas9, shRNA-vermitteltem Knock-down und Überexpression von *USP10* eine Regulation der β-Catenin-Stabilität durch USP10 in Darmkrebs-Zelllinien nachweisen. Es ist allgemein bekannt, dass 2D-Zellkultursysteme die Komplexität, Architektur und Heterogenität nicht widerspiegeln und daher nicht geeignet sind, um komplexe biologische Fragen zu beantworten. Um dies zu überwinden, haben wir die Isolierung, Kultivierung und genetische Veränderung von murinen Darmorganoiden etabliert und dieses System genutzt, um die Rolle von Usp10 *ex vivo* zu untersuchen. Durch die Durchführung von RNA-Sequenzierungen in Abhängigkeit von unterschiedlichen Usp10-Spiegeln konnten wir die bisherigen Ergebnisse rekapitulieren und Usp10 als wichtigen Regulator der β-Catenin-abhängigen Regulation der Stammzellhomöostase nachweisen.
Da die genetische Depletion von *USP10* zu einer Herunterregulierung der β-Catenin-abhängigen Transkription führte, wurde auch die therapeutische Intervention von USP10 in Darmkrebs untersucht. Kommerzielle und neu entwickelte Inhibitoren wurden auf ihre Wirksamkeit gegen USP10 getestet, konnten jedoch die Aktivität von USP10 in Darmkrebs- Zellen nicht hemmen. Um die Erkenntnisse aus dieser Arbeit auch *in vivo* zu validieren, wurde mit der Entwicklung eines neuartigen Mausmodells für Darmkrebs begonnen. Durch die Kombination von CRISPR/Cas9 und klassischer Gentechnik mit viralen Injektionsstrategien konnten WT- und gentechnisch veränderte Mäuse transformiert werden und zumindest bei einigen Tieren waren Darmläsionen auf mikroskopischer Ebene nachweisbar.
Die Inhibtierung von USP10, als *de novo* tumorspezifischer Regulator von β-Catenin, könnte eine neue therapeutische Strategie für Darmkrebs-Patienten werden.

1 Introduction

1.1 Colorectal cancer

Cancer represents one of the most leading causes of death worldwide in 2020 and is responsible for one in six deaths, according to the world health organisation (WHO). Especially in high income countries, lung and colon cancer are among the six leading causes of death, together with ischaemic heart disease, stroke and pulmonary disease [1]. In the American cancer statistics 2021, colorectal cancer (CRC) is the third most common cancer for both, men and women, with 8 % estimated new cases and 8 to 9 % estimated deaths in 2021 [2]. Interestingly, the probability of developing invasive CRC increases with age. The reasons for age differences probably reflect variations in exposure to environmental risk factors and the mutational burden, accumulating over time.
It is widely accepted that environmental risk factors, such as diet, obesity, low level of exercise, alcohol and tobacco consumption increase the risk of developing CRC, as summarized by the Cancer Research UK. In line with that, Correa *et al.* demonstrated in 1977 that the risk to develop colon cancer also increases in individuals migrating from low-risk to high-risk-countries, providing an additional evidence for environmental factors determining the risk of CRC development [3]. Besides these environmental risk factors, inherited forms of CRC, characterised by distinct mutations, are known. Although the majority of patients show an overall good survival after diagnosis, only 10 % of patients diagnosed in stage 4, survive longer than 5 years [4]. This poor prognosis for late-stage patients punctuates the necessity of revealing the molecular mechanism underlying sporadic and hereditary colorectal cancers.

1.1.1 The adenoma-to-carcinoma sequence

For the development of colorectal cancer, several hypotheses are proposed. Among these, the so called *adenoma-to-carcinoma sequence* is widely accepted in the field. It was first proposed by Lockhart-Mummery and Dukes in 1928 as *polyp-cancer sequence* and afterwards described more precisely by Jackman and Mayo in 1951 as the *adenoma-to-carcinoma sequence* [5],[6]. Although not proven directly, clinicopathological and genetic evidences support the concept sufficiently.
In principle, the adenoma-carcinoma sequence describes the stepwise transformation from normal to carcinoma tissue via adenomas. As mentioned before, the risk of developing colon cancer increases with age and interestingly, adenomas are diagnosed at least five years earlier than carcinomas. Early adenomatous polyps are characterised as small and with low malignant potential and the majority do not evolve to carcinomas during life-time [7]. As reviewed in Leslie *et al.*, approximately 40 % of the western population will eventually develop adenomas during their life-span, but only 3 % out of these will develop colon cancer [8]. This raises the question, which factors determine the progression from benign polyps to malignancies.

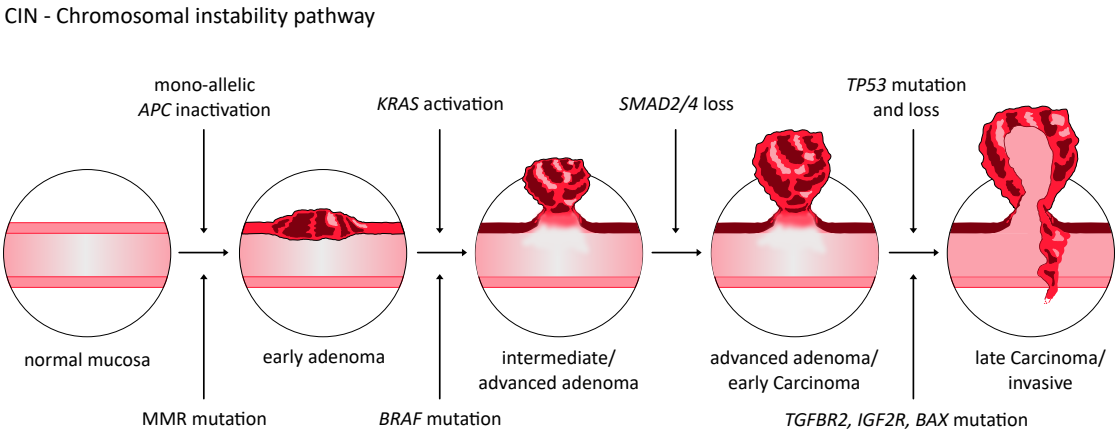

Figure 1.1: **The adenoma-to-carcinoma sequence**
Overview of the conventional adenoma-to-carcinoma sequence. Sequential occurring mutations are shown for the chromosomal instability (CIN) subtype (upper part) and for the mircosatellite instability (MSI) subtype (lower part). Figure is based on De Palma *et al.*, 2019 [9].

The smallest detectable transformations are polyps, which arise within aberrant crypts. Out of these polyps only 10 % evolve into adenomas and than further into colon cancer, worth mentioning that this process can take up to 10 - 15 years and is mainly determined by sequential mutations (reviewed in [10]). For the *adenoma-to-carcinoma sequence*, two different mechanism of tumourigenesis need to be considered: genetic instability caused by the chromosomal instability (from herein after referred to as CIN) mechanism and the microsatellite instability (from herein after referred to as MSI) phenotype (see figure 1.1 upper and lower part, respectively). CIN is detected in up to 85 % of sporadic colon cancers and therefore accounts for the majority of CRC patients (reviewed in [9]). From a genetic perspective, early adenomas arise from disordered, hyper-proliferating stem cells in the crypt, caused by mono-allelic mutations in the tumour suppressor gene Adenomatous Polyposis coli (*APC*) [11]. In contrast to that, MSI driven tumours mainly harbour changes in the methylation status of the DNA, followed by *BRAF* mutations (fig 1.1 lower part) [12]. Besides that, other distinct genetic features are frequently found, except for polyps smaller than 1 cm. Adenomas with a size greater than 1 cm are classified as dysplasia or intermediate/ late adenomas and, most importantly, in at least 50 % of the cases, those adenomas harbour mono-allelic hyper activating mutations in *KRAS* [11]. The next step in transformation to severe dysplasia or early carcinomas is caused by allelic loss of chromosome 18q. Its loss occurs in 70 % of patients with late carcinoma and for a long time it remained unclear, which tumour suppressor in this region is affected [13]. In the meantime, the tumour suppressors *SMAD2* and *SMAD4* were identified. SMAD2/4 are involved in the regulation of transforming growth factor (TGF)-β pathway and thereby regulate important cellular processes such as cell growth, differentiation and apoptosis [14]. Additionally, loss of chromosome 17p occurs in the majority of patients, leading to inactivating mutations in one allele of the tumour suppressor gene *TP53*, together with loss-of-heterozygosity (LOH) for *APC* and, in some cases, *KRAS* mutations (fig 1.1 upper part). The inactivating mutation of *TP53* together with LOH of the second allele, are considered as major candidate for the transition of early carcinomas to advanced invasive colon carcinomas. This is especially prompted

by the observation, that the mutation or loss of both *TP53* alleles accounts for only 3 % of advanced adenomas but for 75 % of invasive carcinomas [15]. While adenomas and carcinomas undergo LOH for the tumour suppressors *APC* and *TP53*, also other mutations accumulate in these advanced stages.

1.1.2 Molecular subtypes of colorectal cancer

As described before, characterisation of colorectal cancer types so far mainly relies on the two different types of genomic instability, CIN and MSI. Besides that, further classification into other subtypes failed to be consistent between different studies, most likely due to various individual analysing methods. In 2015, the first consensus molecular subtypes of colorectal cancer were described by Guinney *et al.*, based on data-integration from an international consortium. By sharing and analysing large-scale data among these expert groups, four distinct molecular subtypes could be established: CMS1, CMS2, CMS3 and CMS4 (see figure 1.2 A).
Tumours with MSI mainly cluster in the CMS1 subtype, characterised by hypermethylation and hypermutation, but show low abundance of somatic copy number alterations (SCNAs). Driver mutations, commonly detected in this subtype, are activating $BRAF^{V600E}$ mutations, simultaneously occurring with mutations in the DNA damage repair pathway, for example. Additionally, CMS1 subtype tumours are characterised by a strong infiltration of the immune system (fig 1.2 A and B).
Tumours representing the characteristic of CIN are further subdivided into the three remaining molecular subtypes, depending on their molecular features: CMS2, 3 and 4 (see Fig 1.2 B). CMS2 and CMS4 tumours are microsatellite stable and show low levels of CpG island methylator phenotype ($CIMP^{low}$). Even though both subtypes cannot be discriminated by their SCNA pattern, they can be distinguished by their distinct pathway activations. The CMS2 subtype is classified as the canonical colorectal cancer, driven by mutation in the tumour suppressor *APC* and WNT pathway activation. With accounting for 37 % of all CRC cases, CMS2 also represents the largest subgroup.
In contrast, the CMS4 subtype, is characterised by alterations in the TGF-β signalling pathway and by undergoing epithelial-to-mesenchymal transition (EMT). The mesenchymal characteristics of this subgroup also correlates with a higher risk for relapse and a poor survival rate for patients.
The last molecular subgroup CMS3, represented by 13 % of CRC cases, shows mixed CIN and MSI status and is also characterised by lower methylation as well as lower SCNAs. This subgroup is mainly driven by mutations in *KRAS* along with other genomic alterations, leading to metabolic deregulations (Fig 1.2 A) [16],[17].

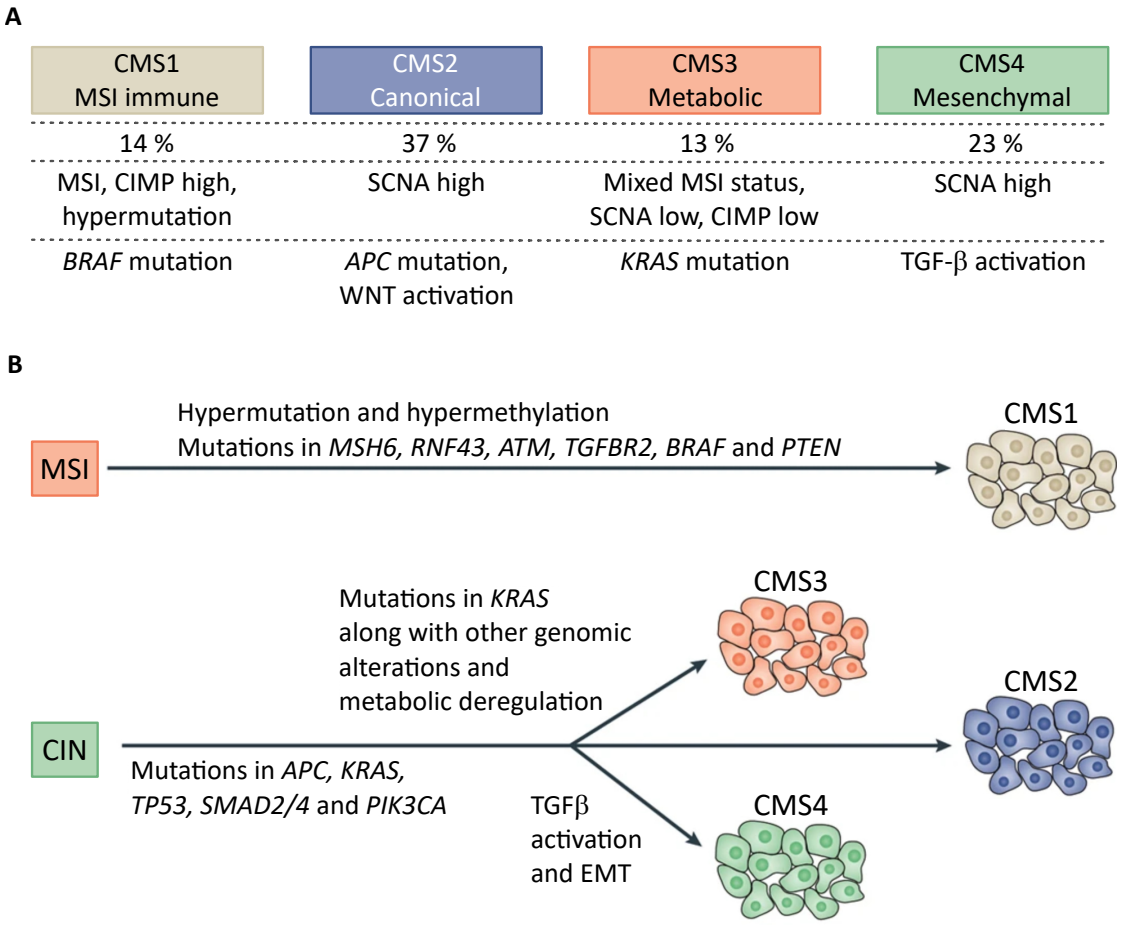

Figure 1.2: **Classification of colorectal cancer according to the molecular subtypes** **A** Proposed classification of colorectal cancer according to relevant changes in gene-expression profiles, based on Guinney *et al.*, 2015 [16] **B** Overview of potential routes of development of MSI and CIN tumours. MSI and CIN cancers develop mainly in the described molecular subtypes. Figure is based on Dienstmann *et al.*, 2017 [17].

1.2 The molecular basis of colorectal cancer

As described earlier, colorectal cancer is caused by various environmental and hereditary risk factors. However, the majority of CRC is characterised by alterations in one distinct signalling pathway - the canonical WNT pathway. The previously introduced molecular subtypes CMS2, 3 and 4 are mainly driven by mutations in the tumour suppressor gene *APC*, which is an important scaffolding protein in the WNT signalling pathway. To be able to identify novel mechanisms leading to CRC and thereby opening new therapeutic options, a detailed knowledge of the underlying pathway and the origin of CRC, the intestinal crypts, is inevitable.

1.2.1 The intestinal crypt

It is widely accepted that the specific organisation of the intestinal epithelium provides the basis for the self-renewal capacity of the gut. It consists of villi, which are long,

into the gut lumen projecting structures and crypts, containing a population of cells able to self-renew. The intestinal crypts consist of various progenitor cells, defined by the gradients of signalling factors and the expression of distinct markers (*LGR5*, *BMI1* and *LRIG1*) [18]. In the upper part of the crypt, non-dividing, differentiated cells are present, connected via the transit-amplifying cells with the bottom of the crypt (summarized in figure 1.3, left side).

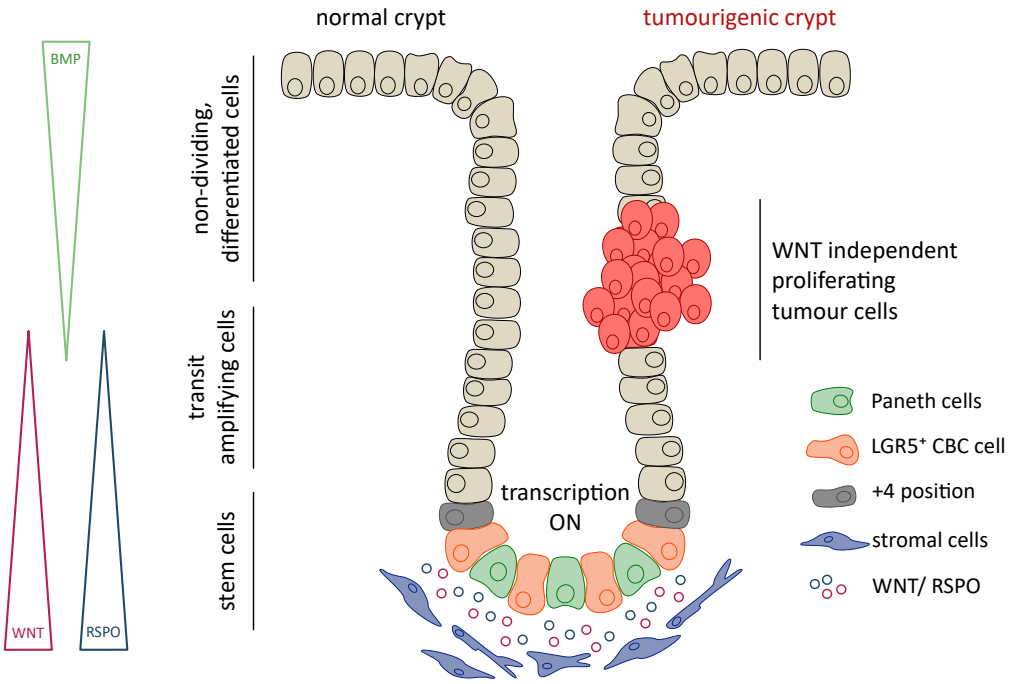

Figure 1.3: **Schematic model of the intestinal crypt**
WNT/RSPO ligands are secreted by stromal cells and drive proliferation of LGR5$^+$ CBC and paneth cells. Cells migrate and proliferate through the transit-amplifying zone, followed by differentiation into all epithelial lineages. BMP signalling antagonises the WNT/RSPO gradient. On the right side of the crypt (in red), WNT-independent proliferating tumour cells are shown. Figure is based on Parsons, Tammela and Dow 2021 [19].

At the bottom of the crypt, exposed to the secretion of WNT and R-spondin (RSPO) ligands, LGR5$^+$ crypt base columnar (CBC) cells can be found. These cells are considered as the stem cells of the crypt/ intestine. In between LGR5$^+$ cells, paneth cells are located. These are exclusive to the small intestine and constitute the niche for LRG5$^+$ cells [20]. However, cell-proliferation at the bottom of the crypt is driven by active WNT signalling. Throughout the transit-amplifying zone cells are still proliferating, but when migrating to the top of the crypt, the concentration of WNT and RSPO decrease and the antagonistic bone morphogenetic protein (BMP) signalling increases. With inactivation of the WNT signalling pathway, cells stop proliferating and differentiate into all epithelial lineages.

1.2.2 The WNT signalling pathway

The WNT signalling pathway can be divided into the canonical (β-Catenin-dependent) and the non-canonical (β-Catenin-independent) pathways. Since there is no clear evidence for the non-canonical pathway as a primary driver of the disease (reviewed in [19]), the canonical, β-Catenin-dependent WNT signalling, is of main interest and will be discussed in detail.

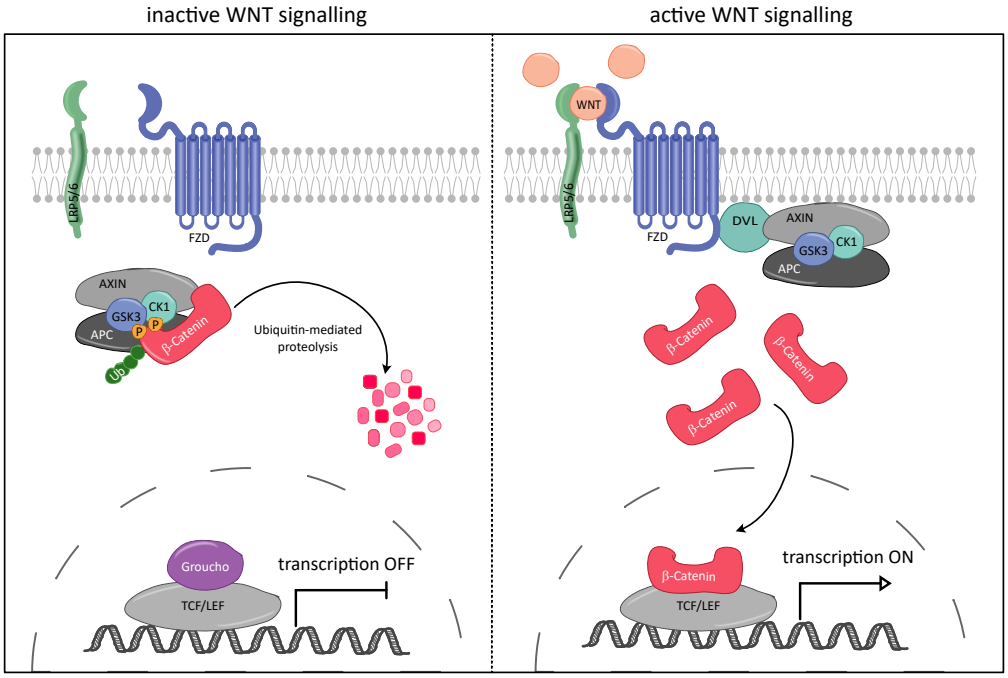

Figure 1.4: **Overview of canonical WNT signalling pathway**
Left side: In the absence of WNT ligand, cytosolic β-Catenin is bound by the destruction complex and phosphorylated by the kinases CK1α and GSK3β. Phosphorylated β-Catenin is marked for ubiquitylation and degradation. Transcription of its target genes is inhibited by the repressor Groucho. Right side: Secreted WNT ligands bind the membrane receptors LRP5/6 and Frizzled (FZD), leading to the recruitment of Dishevelled (DVL) and the disassembly of the destruction complex. β-Catenin molecules accumulate and translocate into the nucleus, displace Groucho and activate the TCF/LEF-dependent transcription of its target genes. Figure is based on Parsons, Tammela and Dow 2021 [19].

In the absence of WNT ligand, which is normally secreted by adjacent stromal cells, the β-Catenin-dependent transcriptional program is OFF. Being such an important transcriptional co-activator as β-Catenin, its abundance needs to be tightly controlled. When no WNT ligand is secreted, β-Catenin is bound by the so-called destruction complex, which results in its continuous degradation (see figure 1.4, left side). The scaffolding proteins AXIN1/2 and APC bind β-Catenin, together with the two kinases casein kinase 1 (CK1α) and glycogen synthase kinase 3 (GSK3β). Both kinases phosphorylate β-Catenin subsequently at its N-terminus and therefore mark it for ubiquitylation. First, CK1α adds the priming phosphorylation on Ser45, followed by GSK3β- mediated Ser33,

Ser37 and Thr41 phosphorylation ([21], [22]). The phosphorylated β-Catenin is then recognised by a E3-Ligase complex comprising of β-tranducin repeat containing E3 ubiquitin protein ligase (βTrCP) and subsequently degraded by the ubiquitin-proteasome system (UPS) [23],[24].
In contrast, active WNT signalling is induced by the secretion of WNT ligand by adjacent stromal cells, as summarised on the right side of figure 1.4. The WNT ligand binds to the membrane receptors LRP5/6 and Frizzled (FZD), leading to the recruitment of the scaffolding proteins AXIN1/2 and Dishevelled (DVL). With the recruitment of AXIN1/2 to the membrane, the destruction complex disassembles, resulting in a stabilisation of β-Catenin. The stabilized and accumulated β-Catenin translocates into the nucleus, displaces the transcriptional repressor Groucho and activates the transcription of its target genes (reviewed in [19]).

1.2.3 APC truncating mutations in colorectal cancer

In 80 % of cases, CRC is characterised by deregulated WNT signalling, which is almost twice as much compared to other cancer types with a high incidence of WNT alterations (see figure 1.5 A). Furthermore, it is of very high interest that in colorectal cancer the majority of WNT- driven tumours show mainly truncating mutations in the tumour suppressor gene *APC*. In contrast, in uterine and hepatocellular carcinoma (HCC), the most abundant mutations in WNT signalling occur in the proto-oncogene *CTNNB1* (see figure 1.5 B). Several efforts have been undertaken to elucidate the preference for *APC* mutation over *CTNNB1* mutation in colorectal cancer, but it is still not fully understood. One possible explanation was found by Quyn *et al.* in 2010: the authors showed that *APC* truncating mutations additionally cause problems in the orientation and asymmetry of cell division, leading to a delay in the transition of cells from the crypt base to the top [25]. With these additive effect on tumour growth, a putative prevalence for *APC* truncating mutations over other mutations could be explained.
However, the major oncogenic driver of CRC is the inability of the destruction complex to bind and degrade β-Catenin, caused by truncating mutations in *APC*. As a consequence, cells proliferate independently of the presence of WNT ligand (see figure 1.3, right side).

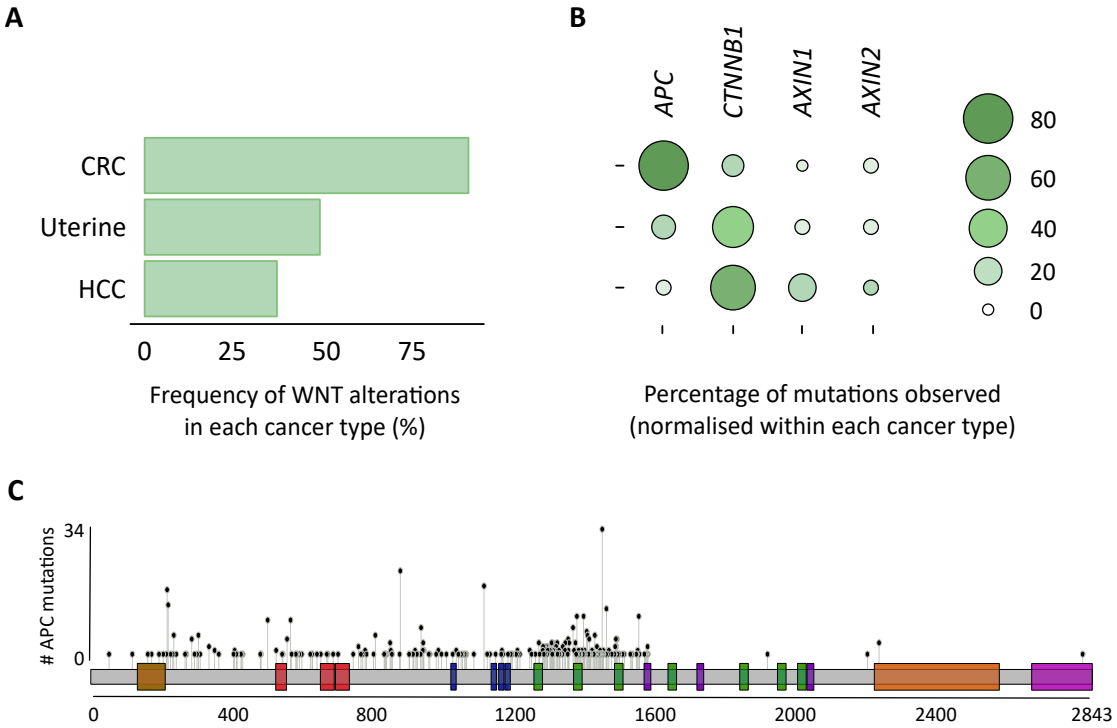

Figure 1.5: **Alterations in WNT pathway across different cancer types**
A Bar graph representing the occurrence of WNT pathway mutations in colorectal cancer, uterine cancer and hepatocellular cancer (HCC). **B** Bubble graph of mutations in *APC*, *CTNNB1*, *AXIN1* and *AXIN2* in different cancers. Percentages within the WNT altered subset are shown. Figure adapted from Parsons, Tammela and Dow 2021 [19]. **C** Lollipop plot showing number and position of *APC* truncating mutations in colorectal cancer. Lollipop plot was generated using cBioportal with the PanCancer TCGA dataset.

The tumour suppressor gene *APC* was identified in 1991 by Groden *et al.* as an important gene in the development of colorectal cancer. With its 213 kDa it is the largest scaffold protein in the destruction complex, providing several binding sites for other proteins [26]. In figure 1.5 C the domains of *APC* are shown, together with the number and position of mutations, occurring in CRC patients. Interestingly, most mutations accumulate in the region between codon 1200 and 1600, where the catenin inhibitory domain (CID) and the β-Catenin binding 20 amino acid repeats (20 AAR) are located. This region is therefore also called the mutational cluster region (MCR).
In genetic mouse models it was shown that the activity of WNT signalling corresponds to the degree of APC truncation. Therefore, heterozygous APC truncation ($APC^{1322T/+}$) in mice results in the most severe version of intestinal polyps, followed by the $APC^{Min/+}$ model (will be introduced in the following), which is already truncated at codon 850. Based on these observations, the hypothesis of the "just right" level of WNT signalling for the progression of colorectal cancer, was developed [27]. Albuquerque *et al.* found out that the first mutational hit in the *APC* gene also determines the mutation for the second allele. For example, when the germline mutation in *APC* leads to the loss of all 20 AAR, then the second mutation will most likely occur either at a position that only one or, less frequent, two of the 20 AAR sides remain. Conversely, if the germline mutation in *APC* is downstream of the 20 AAR and results in one or two remaining 20

AAR sites, then, the second hit on the *APC* allele will result in the complete removal of the 20 AARs or even in LOH of the second allele [27], [28].
All the above mentioned mutations result in the inactivation of the β-Catenin destruction complex. Whether this occurs due to the removal of the AXIN binding sites (the SAMP repeats), the β-Catenin binding sites or mutations in the CID will influence the extent of resulting WNT signalling, but besides that, always results in the abolished degradation of β-Catenin by the UPS.

1.3 Regulation of WNT signalling through the ubiquitin-proteasome system

An important developmental process, such as the WNT signalling pathway, needs to be tightly controlled, since its dysregulation is associated with severe diseases as cancer, Alzheimer's disease and metabolic diseases. The regulation of such an integral pathway is frequently mediated via post-translational modifications (PTMs) and, in case of WNT signalling, these PTMs are mainly ubiquitylation and de-ubiquitylation. An enzyme-family called E3 ubiquitin ligases attaches ubiquitin moieties on its substrates and thereby, in the majority of cases, initiates its subsequent degradation by the 26S proteasome. However, this process can also be counteracted by deubiquitylating enzymes (DUBs). These proteins remove ubiquitin from substrates and therefore stabilise them. In the following section the molecular basis of the ubiquitin-signalling pathway and its important role in the regulation of the WNT signalling pathway will be discussed.

1.3.1 The ubiquitin-proteasome system

When the small molecule (76 amino-acid long) ubiquitin (from hereinafter referred to as Ub) was identified in 1980, it was described as a post-translational modification, labelling some proteins for degradation exclusively (reviewed by Ciechanover 2015 [29]). However, after years of extensive research it became clear, that almost every protein eventually will face ubiquitylation during its life-span and, more importantly, that this process not only marks its substrates for degradation but also controls various processes such as proteostasis, selective autophagy, DNA repair, cell cycle control, cell signalling cascades and programmed cell death (reviewed in [30]).
Independent of the resulting function of ubiquitylation, as summarised in figure 1.6 A, the process starts with an ATP-dependent attachment of ubiquitin to the E1 ubiquitin-activating enzyme, followed by the transfer of the activated ubiquitin onto the E2 Ub-conjugating enzyme. Substrate ubiquitylation can occur via two different mechanism, dependent on the E3 Ub-ligase: the ubiquitin molecule can be transferred to a homologous to the E6-AP Carboxyl Terminus (HECT) E3 ligase or to a RING-in-between-RING (RBR) E3 ligase and then subsequently attached to the substrate or, in case of really interesting new gene (RING) E3 ligases, directly from the E2 enzyme onto the substrate (reviewed in [30]). Interestingly, the substrate-specificity of this process is most likely mediated via the E3 ubiquitin ligases, of which more than 600 different ones are known in the human genome. In contrast, only 2 E1 and 40 E2 enzymes are known to date.

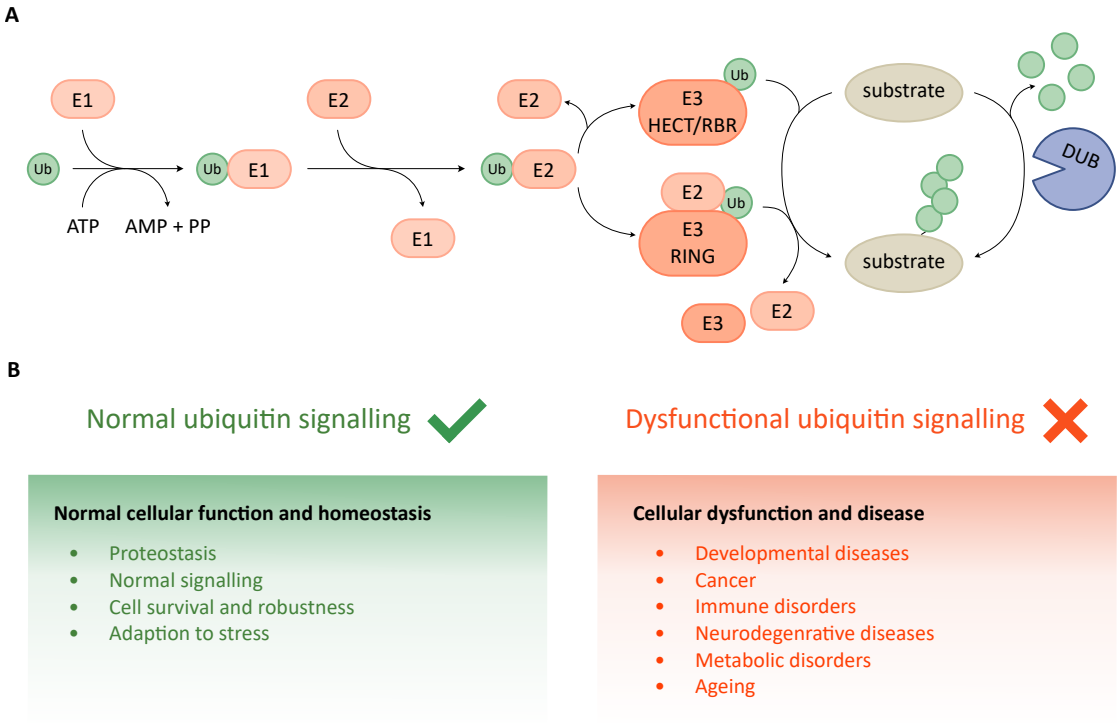

Figure 1.6: **Ubiquitin signalling in cell biology and disease**
A Schematic of the ubiquitin signalling pathway. In an ATP-dependent manner ubiquitin is attached to the Ub-activating enzyme (E1) before it gets transferred to the Ub-conjugating E2 enzyme. Next, the E2-conjugated Ub gets either transferred directly to a lysine-residue on the substrate, via a RING E3 Ub ligase, or transferred to a HECT/RBR E3 ligase before getting attached to the substrate. Deubiquitylases (DUBs) can revert that process by deubiquitylating Ub chains from the substrate. **B** Dysregulation of ubiquitin signalling can cause dysfunctional cellular processes and diseases, for example: developmental diseases, immune disorders and cancer, etc. Modified according to Damgaard 2021 [30].

Independent of the E3 Ub ligase, the process of ubiquitylation always starts with a single ubiquitin molecule binding a lysine-residue of the substrate protein, followed by poly-ubiquitylation via any of the seven lysine-residues of the ubiquitin molecule (Lys6, Lys11, Lys27, Lys29, Lys33, Lys48 and Lys63) or via the N-terminal methionine (Met1) of ubiquitin. It is well known that any composition of these linear or branched homo- and heterotypic poly-ubiquitin chains can result in structural and functional differences. For example Lys48-linkages label their substrates for proteasomal degradation, whereas all other linkage-types can serve as proteolytic and non-proteolytic signals. The composition of the linkage and its resulting cellular functions are summarised as 'the Ubiquitin code' (reviewed by Komander and Rape 2012 [31]).
Noteworthy, the process of substrate ubiquitylation is reversible and mediated by DUBs. Approximately 100 different human DUBs are identified so far and can cleave different linkage types. They are classified into eight different subgroups, with the ubiquitin-specific-proteases (USPs) being the largest subgroup. The balance between ubiquitylation and deubiquitylation is an important process for physiological cellular functions and homeostasis, like proteostasis, signalling, cell survival and adaption to stress. As a consequence, if the ubiquitin signalling is altered or deregulated, cellular dysfunctions and diseases, as cancer, metabolic disorders and ageing can occur (see figure 1.6 B).

1.3.2 Ubiquitin-dependent regulation of WNT signalling

The key protein of WNT signalling pathway, β-Catenin, is not only a transcriptional co-activator, it also mediates cell-cell contacts at the cell membrane together with E-cadherine [32]. To ensure the right amount of cytosolic β-Catenin, it is produced continuously and in case of inactive WNT signalling, the pool of β-Catenin, which is not required for transcriptional activation, is subsequently degraded by the UPS. As explained before, β-Catenin is phosphorylated and therefore marked for ubiquitylation by the substrate-binding subunit of Skp1-Cullin-F-box (SCF) RING-type E3 ligase, called β-TrCP.
However, several E3 ligases have been described, which ubiquitylate β-Catenin under certain circumstances (an overview is shown in figure 1.7 A). SIAH-1 is an E3 ligase highly expressed upon genotoxic stress induced p53 activation and ubiquitylates β-Catenin independent of its phosphorylation status [33]. Interestingly, not only destabilising E3 ligases are described for β-Catenin. In 2016, Abed *et al.* demonstrated that the E3 ligase RNF4 ubiquitylates its phosphorylated targets, including β-Catenin, MYC and JUN, thereby leading to target stabilisation [34]. RNF4 and SIAH-1 are only two examples of other E3 ligases in the regulation of the cytosolic pool of β-Catenin, however also the nuclear, non-phosphorylated active proportion of β-Catenin, can be ubiquitylated. In renal cancer a von Hippel-Lindau (VHL)- dependent ubiquitylation of nuclear β-Catenin by the plant homeodomain (PHD) E3 ligase JADE-1 was described. However, whether this mechanism is conserved in other tissues remains unclear [35].
Other members of the WNT signalling pathway are also regulated via the UPS, such as the membrane receptor protein FZD, the scaffolding protein DVL and the destruction complex member AXIN (figure 1.7 A). FZD is normally regulated by ubiquitylation of the transmembrane E3 ligase RNF43/ZNRF3, which ubiquitylates and degrades FZD. In active WNT signalling, when the ligand RSPO is present, the binding of RSPO to LGR4/5 and RNF43/ZNRF3 leads to its auto-ubiquitylation, subsequent degradation and thereby to an increase of WNT receptors and enhanced signalling [36].
Besides activation, WNT signalling can also be repressed e.g., by the regulation of the cytosolic effector protein DVL. The BTB-protein Kelch-like 12 (KLHL12)-Cullin3 E3 ligase complex directly binds and ubiquitylates DVL upon stimulation by WNT. Additionally to KLHL12, also the HECT E3 ligase HUWE1 can bind and ubiquitylate DVL, causing its subsequent degradation and therefore providing WNT-sensitive negative regulators of the pathway [37], [38].
Since the scaffolding proteins APC and AXIN are the major negative regulators of WNT signalling pathway, also their stability is tightly controlled. Three different E3 ligases are known to bind and ubiquitylate AXIN. SIAH-1, RNF146 and SMURF-2 were described to specifically decorate AXIN with Lys48-linkages, leading to its proteasomal degradation [39].

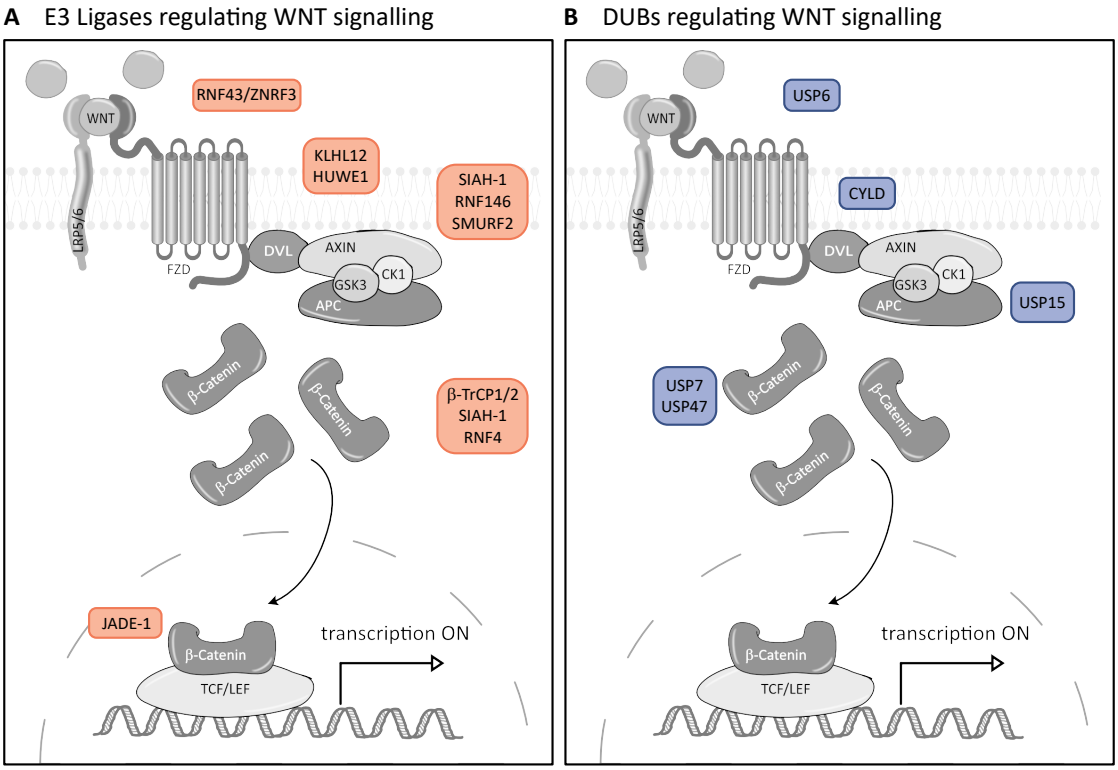

Figure 1.7: **Ubiquitin as an important regulator of the WNT signalling pathway** **A** E3 ligases regulate the activity and stability of signalling factors from the WNT pathway by ubiquitylation. **B** To increase stability of members of the WNT signalling pathway, de-ubiquitylases (DUBs) cleave ubiquitin chains from substrates. Mostly, members of the USP family are involved. Figure based on Park, Kim and Beak 2020 [40].

As introduced before, the process of ubiquitylation is reversible and DUBs can remove ubiquitin chains from substrates. In the past, several DUBs regulating the stability of members from the WNT signalling pathway have been described. In an siRNA based DUB screen USP6 was identified as a strong regulator of the WNT signalling pathway. Madana *et al.* showed in 2016 that USP6 de-ubiquitylates the membrane receptor FZD, leading to its stabilisation [41]. Furthermore, the cytosolic effector protein DVL is ubiquitylated and the the familial cylindromatosis tumour suppressor gene (CYLD), belonging to the USP family of DUBs, could be identified to cleave Lys63 chains from DVL, resulting in decreased WNT signalling activity. Correspondingly, loss of CYLD in tumours leads to increased WNT signalling [42]. Another negative regulator of WNT signalling, the scaffold protein APC, can be regulated via ubiquitylation and de-ubiquitylation. The DUB USP15 is a component of the COP9 signalosome (CSN), which normally regulates the activity of E3 ligase complexes. In WNT signalling, the CSN associates with the β-TrCP E3 ligase and the resulting super complex enhances the activity of β-TrCP E3 ligase and USP15 can stabilise APC. These interaction guarantees high levels of APC and Axin proteins [43].
As summarised above, several E3 ligases have been described regarding ubiquitylating β-Catenin. Some of these E3 ligases are phosphorylation dependent or independent, and the ubiquitylation can result in either stabilisation or destabilisation, in accordance

to the attached poly-ubiquitin chains. Hence, it is highly likely that several counteracting DUBs must exist. Until now, extensive research for identification and validation of novel β-Catenin regulating DUBs has been conducted. For example, in 2015 Shi *et al.* could identify USP47 as a regulator of β-Catenin stability. In HEK293T cells but also in *Drosophila melanogaster* the authors could show that reduction of USP47 levels decreased β-Catenin protein level and cell proliferation [44].
Interestingly, two years later Novellasdemunt *et al.* described a tumour-specific DUB for β-Catenin. In a very elegant study the authors identified USP7, by using CRISPR/Cas9, as an APC truncation dependent DUB which regulates the stability of β-Catenin and confirmed their findings in an *ex vivo* intestinal organoid system [45].
While several E3 ligases and DUBs have been described, which contribute to regulating members of the WNT signalling pathway up- and downstream of β-Catenin, however for this thesis, only a brief overview of the most important ones was given.
To identify novel DUBs in the context of colorectal cancer, an siRNA based DUB library screen was conducted by our research group. Aiming the identification of DUBs specifically regulating β-Catenin stability in a human CRC-derived cell line HT-29, an siRNA library was transfected and the intensity of β-Catenin stability upon DUB knock-down was measured and quantified using Operetta high content microscopy. In figure 1.8 the schematic overview of the screen and the volcano plot of the results is shown. Among known regulators, which served as positive controls, also unknown DUBs, affecting the stability of β-Catenin, were identified.

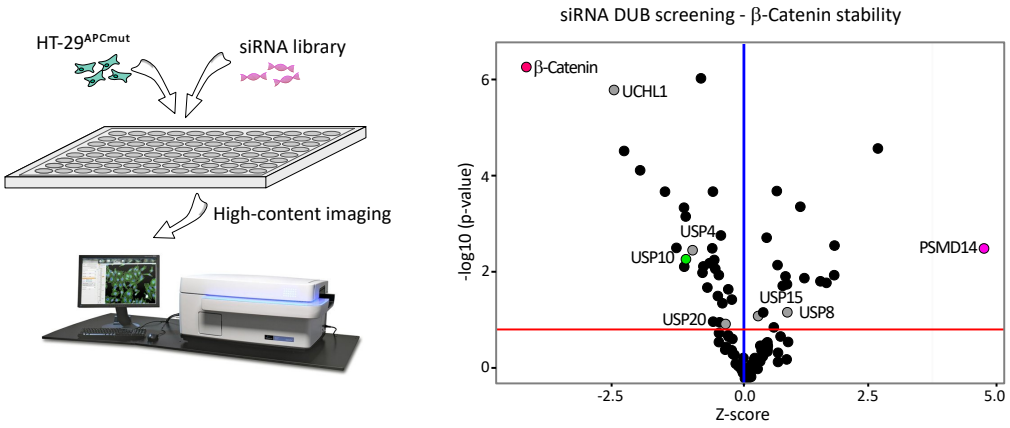

Figure 1.8: **siRNA based DUB library screen to identify USP10**
A Schematic model of DUB library screen. HT-29 cells were transfected with siRNA DUB library and β-Catenin fluorescence was imaged and measured using Operetta high content microscopy. Screen was performed by Dr. Markus E Diefenbacher. **B** Volcano plot of quantified β-Catenin intensity. Positive controls in pink, novel regulators in grey and USP10 is shown in green. Screen was analysed by Cristian Prieto-Garcia.

By performing validation experiments the ubiquitin-specific-protease USP10 showed the most promising effects on β-Catenin (data not shown). Therefore, it was decided to investigate USP10 and β-Catenin in CRC as the major aim of this thesis.

1.4 The deubiquitylase USP10

The aforementioned DUB USP7 belongs to the largest familiy of DUBs, the ubiquitin-specific proteases (USPs). The USP domain, which all USPs have in common, is thought to be the catalytic domain and consists of three regions, fingers, thumb and palm. Although only crystal structures from USP5, 7 and 8 are solved, the following mode-of-action is considered to be conserved for most of the USPs: with the binding of ubiquitin, a conformational change of this domain leads to the formation of the catalytical triad. Thereby, the active-site loop moves from its initial position to bind the C-terminal end of the substrate, leading to the cleavage of the ubiquitin molecule from the target protein. Although there is no crystal structure of human USP10 yet, it is known that the 798 amino acid long protein also consists of the described USP domain and therefore a similar mode-of-action is considered. USP10 is one of the most investigated proteins among the USPs and several target proteins are already known. Due to the importance of its substrates, it is clear that USP10 plays an enormous role in maintaining cellular function and therefore it is not surprisingly that deregulation of USP10 can lead to malignancies e.g., cancer.
Interestingly, it remains unclear whether USP10 functions as a tumour suppressor or oncogene in the context of cancer. When studying the present literature, it becomes obvious that a tissue-specific function of USP10 determines its role in tumourigenesis. The role of USP10 as tumour suppressor and oncogene will be discussed in the following parts.

1.4.1 USP10s role as tumour suppressor

One of the first evidences, that USP10 could play a role as a tumour suppressor, was provided in 2010 by Yuan *et al.*. In this study USP10 was described to control the deubiquitylation of the major tumour suppressor P53, and thereby, directly counteracting the E3 ligase MDM2. The authors showed that ATM-dependent phosphorylation and activation of USP10, upon genotoxic stress, induces a fraction of USP10 to shuttle into the nucleus where it deubiquitylates and stabilises P53. Interestingly, when the authors analysed the expression level of *USP10* in renal cell carcinoma (RCC) they found that in *TP53* WT patients, *USP10* was downregulated, prompting its role as a tumour suppressor, however in patients with mutant *TP53*, *USP10* levels were upregulated [46]. In a comment in *Cell* in 2010, Jochemsen and Shiloh discussed a potential explanation for that finding. USP10 seems to deubiquitylate WT P53 as well as mutant P53 and thereby either acts as a tumour suppressor or oncogene, depending on the P53 status of tumours [47].
Without discussing the *TP53* status any further, also other studies reported USP10 as a tumour suppressor. Sun *et al.* analysed the function of USP10 in lung cancer patients and cell lines and could identify the tumour suppressor phosphatase and tensin homolog (PTEN) as a novel target for USP10 [48].
In three additional studies, published in 2018, 2019 and 2020, several groups analysed USP10 and its target protein p14ARF in ovarian cancer and intestinal adenocarcinomas. Also in these studies a downregulation of USP10 and p14Arf could be observed in tumour tissues compared to WT tissue and could have been correlated to poor prognosis of patients [49], [50], [51].

1.4.2 USP10s role as oncogene

However, considering the dual role of USP10 in the context of TP53 regulation, several studies described USP10 as oncogene.
Additionally to its controversial role in the regulation of P53, another interesting example for its function as tumour suppressor and oncogene is the regulation of PTEN by USP10. As described before, in lung cancer, USP10 deubiquitylates and stabilises the tumour suppressor PTEN. However, in breast cancer it was also shown that USP10 stabilises the E3 ligase ITCH, resulting in a downregulation of MEK1 and thereby reduced PTEN localisation to the plasma membrane. By downregulating *USP10* expression a decreased activation of AKT could be observed, resulting in reduced colony formation. Correspondingly, an increased expression of *USP10*, which correlates with poor survival of the patients, is found in breast cancer patients [52].
In glioblastoma patients, furthermore, an upregulation of *USP10* was found by using a novel real-time quantitative low density array (RTQ-LDA). Together with thymidylate synthetase (TS) and *BIRC5*, *USP10* was found to be upregulated in patients with a poor prognosis compared to healthy individuals and patients with an overall good prognosis. Grunda *et al.* therefore described USP10, survivin (encoded by *BIRC5*) and TS as novel prognostic markers and maybe also therapeutic targets for glioblastoma [53].
The most prominent target of USP10 is the the GTPase-activating protein-binding protein 2 (G3BP2) which is involved in stress granule formation. In 2018, Takayama *et al.* analysed USP10 and G3BP2 in prostate cancer. It was described that USP10 associates with G3BP2 to inhibit P53 signalling thereby leading to a poor outcome for prostate cancer patients. In agreement, a high expression of *USP10* and *G3BP2* can be observed in patients with prostate cancer [54].
With the aforementioned examples of USP10s role in various tumour-types it is obvious that its function as tumour suppressor or oncogene is highly context depending, including the tissue-type and the mutational landscape of the tumour entity at question.

1.5 Advances in modelling colorectal cancer

For colorectal cancer, as well as for the majority of other cancers, the time of diagnosis is the most predictive factor in determining the outcome of the disease. Patients with diagnosis of stage 4 disease show a poor overall survival, prompting the need of novel therapies and the identification of markers, which allow an earlier diagnosis. To identify novel early-stage markers and to develop novel targeted therapies, patient-relevant mouse models are indispensable, which will be summarised in following (see figure 1.9).

1.5.1 Genetically engineered mouse models

The identification of the tumour suppressor gene *APC*, as a driver mutation for the majority of sporadic cancers in the gastrointestinal tract, as well as genetic cause of the

familial adenomatous polyposis (FAP), sparked the development of the first colorectal cancer mouse models [55]. In 1990, Moser *et al.* developed the multiple intestinal neoplasia (MIN) model, harbouring a heterozygous loss-of-function mutation in codon 850 of the *Apc* gene (referred to as $Apc^{Min/+}$). Although mutations in *APC* occur in the majority of CRC patients, the $Apc^{Min/+}$ model does not reflect patient relevant CRC. The majority of adenomas are induced in the small intestine and only few lesions arise in the colon [56],[57]. While this mouse model paved the way to broaden our understanding of this disease, it faithfully recapitulates FAP rather than CRC.
In parallel also carcinogen-induced models of CRC have been developed, such as through application of aoxymethan (AOM), 1,2-dimethylhydrazine and methylazoxymethyl acetate (reviewed in [58]). Besides these chemicals, repeated ingestion of dextran sulfate sodium (DSS) was successful in inducing acute and chronic ulcerative colitis, leading to erosions, crypt abscesses and dysplasia of the colonic mucosa. However, the use of carcinogens for tumour induction comes along with multiple limitations, as only a few animals develop tumours and these show a large variability in number, localisation and differentiation [59],[60]. An attempt for improving the two pre-existing models was described in 2001 by Cooper *et al.* Here they compare wild-type (WT) and $Apc^{Min/+}$ mice, upon exposure to DSS. Interestingly, the number of tumours increased by about 40 % compared to untreated $Apc^{Min/+}$ mice. Additionally, 90 % of the dysplasias showed LOH of *Apc*, which is in line with, and an important step in the *adenoma-to-carcinoma sequence* [61].

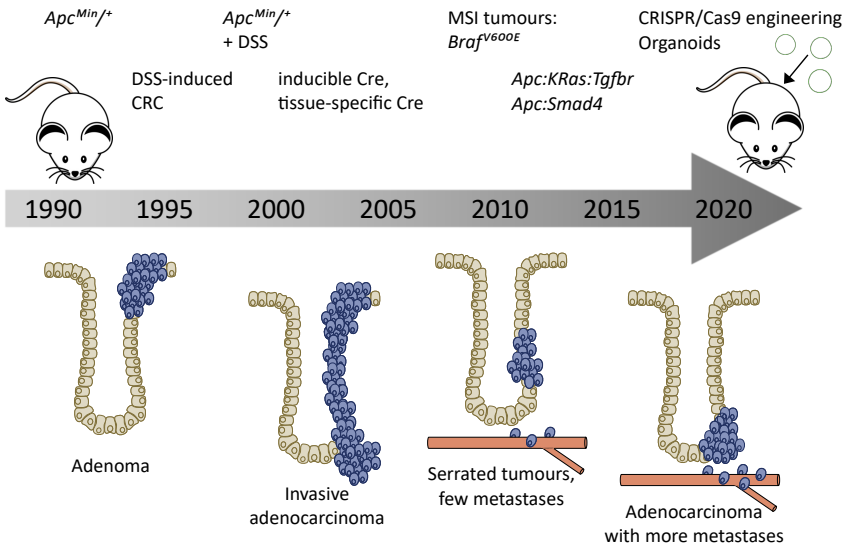

Figure 1.9: **Timeline for the development of CRC mouse models**
The development of genetic engineered mouse models for colorectal cancer. Important models and reflecting stage of CRC are shown. Figure based on Jackstadt and Sansom, 2016 [62].

As described by Moser *et al.* in 1990, homozygous $Apc^{Min/Min}$ mutation are embryonically lethal [56]. Various attempts to overcome this issue have been undertaken over the following years. For example, conditional targeting of *Apc* via adenoviral induction of the Cre-recombinase enabled homozygous deletion of codon 580 and therefore led to development of adenomas already within four weeks [63]. Another strategy to

overcome embryonic lethality was the development of a conditional tissue-specific *Apc* kock-out. Sansom *et al.* described in 2004 a napthoflavone-inducible Cre-recombinase under the control of the intestine-specific *Cyp1A* promoter. By utilizing this system homozygous $Cre^{+}Apc^{fl/fl}$ mice were developed and demonstrated for the first time that acute loss of *Apc* activates WNT signalling, and targeted cells maintained a so called crypt-progenitor-like phenotype [64]. By using a similar strategy, el Marjou *et al.* developed the Villin-Cre mouse in 2005, which is still today, widely used for targeting genes specifically in the intestine [65].
Although *APC* mutations account for the majority of CRCs, approximately 15 % of all cases molecularly belong to the MSI phenotype and harbour activating mutations in the oncogene *BRAF*. The mouse genetic tools described above were used to subsequently generate a MSI phenocopying mouse model, using the Villin-Cre in combination with conditional mutant Braf ($Vil\text{-}Cre;Braf^{LSL\text{-}V637E/+}$). These mice provided for the first time an ideal model to recapitulate the alternative hyperlasia/ adenoma/ carcinoma sequence *in vivo*. The use of this mouse model showed that targeting *Mek* or *Pi3k/Braf* provides a novel opportunity for targeted therapies in CRC [66].
As described earlier, for a longer timespan it was not clear which gene on chromosome 18p is lost in many human CRCs. Takaku *et al.* were able to show in 1998 that heterozygous deletion of the murine SMAD4 homologue *Dpc4* combined with mono-allelic mutation of *Apc* led to advanced carcinomas with more malignant tumours [67]. This proves again the importance of patient-relevant mouse models to identify novel mechanism of CRC and is one example for the combination of different oncogenic mutations to investigate the molecular mechanism underlying different stages of CRC. 20 years later, in 2018, Sakai and Nakayama *et al.* combined various mutations identified in CRC, such as *Apc,* $Kras^{G12D}$ *Tgfbr2*, to prove that this combination leads to the highest incidence of metastases in mice [68]. Since late stage diagnosed patients also show a poor overall survival and the highest-risk of relapsing, it is important to develop genetic models for late-stage CRC, enabling potential implications in finding novel therapeutic strategies.

1.5.2 CRISPR-Cas9/ Organoid - based models

Although the development of genetically engineered mouse models (GEMMs) provided a suitable system to model advanced disease and led to the identification of important mechanism in the development of CRC, it still comes with several limitations. The generation of GEMMs is an immense time-consuming progress and relies on extensive breeding of mice. With the establishment of the 3R rule (Replacement, Reduction and Refinement) in 1960 and the development of the organoid technique by Toshiro Sato in 2009, novel, fast and less breeding intensive options have been established [69], [70].
The first important step was the development and characterisation of the organoid-culture by the Clevers Laboratory. Sato and colleagues described long-term culture conditions for isolated intestinal crypts and single stem cells, which are able to grow in the absence of non-epithelial niches. These 3D cellular objects grow in the typical crypt-villus structure and show all differentiated cell types, which are also found *in vivo* [70]. Even more strikingly, only two years later, it was also described how to isolate and expand human colonic organoids in a long-term culture [71]. From then on, human and murine intestinal organoid-techniques were combined with the CRISPR/Cas9 genome

editing tools ([72],[73]) to modify and generate genetically engineered organoids, depicting various disease specific genetic aspects. As an example, one of the first reported studies, published by Schwank *et al.* in 2013, utilised CRISPR/Cas9 technology, to repair the cystic fibrosis transmembrane conductance regulator (*CFTR*) gene in intestinal organoids of cystic fibrosis patients [74].
In 2015, Matano *et al.* introduced various patient-relevant mutations into normal human intestinal organoids and selected for isogenic lines by modulating the culture media and growth conditions. With the introduction of mutations in *APC, SMAD4, TP53* and *KRAS* and/or *PIK3CA*, oncogenic organoids were generated and injected under the kidney subcapsule in mice. Although the genetically engineered organoids engrafted and led to micrometastases, no liver metastases could be found. In contrast, when genetically engineered adenoma-derived organoids were implanted, macrometastases were observed, suggesting that classical driver mutations are not enough for invasive behaviour [75].
One year later, in 2016, Fujii *et al.* established a living biobank of 55 colorectal tumour organoid lines, including primary and metastatic tumours. The organoid lines were analysed for gene expression and transplanted into mice as xenografts. Matched pair comparison of primary tumour and metastatic organoids revealed that organoids derived from metastases showed highest metastatic capacity in xenografts. This highlights the importance of phenotype-genotype analysis on a single-patient level [76]. However, to study not only the behaviour of the engrafted tumour organoids, but also the impact of the microenvironment, it is necessary to implant organoids into the gastrointestinal (GI) tract directly.
In a very elegant study from 2017, Fumagalli *et al.* orthotopically transplanted genetically engineered human organoids directly into the colon of mice and analysed the metastatic capacity of different driver mutations. By targeting the WNT, EGFR, P53 and TGF-β pathway, the authors were able to recapitulate migration and metastasis *in vivo* for the first time and could prove that the ability of metastasising is caused by the loss of dependency on specific niche factors [77].
Only a few months later, two additional studies were published back-to-back, describing the orthotopic engraftment of organoids into the colon of mice. OtRourke *et al.* pretreated mice with 3 % DSS, to induce inflammation, and successfully implanted organoids from genetically engineered mice, organoids egineered *ex vivo* as well as patient-derived organoids. While being a very rapid procedure (<5 minutes per animal), organoid engraftment succeeded in two-third of mice and was suitable to model the adenoma-to-carcinoma sequence, including liver-metastases, in a time-span of only 21 weeks post implantation [78]. A similar result was achieved by implanting autochthonous *Apc*Δ/Δ; *Kras*$^{G12D/+}$; *Trp53*Δ/Δ (AKP) organoids into NSG mice [79].
With these novel experimental systems the rapid generation and recapitulation of tumour progression and metastases was achieved and can be utilized to characterise and study new cancer-associated genes *in vivo*.

1.6 Aim of the thesis

Colorectal cancer is predominantly driven by deregulated and aberrant WNT signalling, leading to altered transcription of β-Catenin target genes. The stability of β-Catenin is mainly regulated via the UPS and many E3 ligases ubiquitylating β-Catenin are known already. However, the counteracting proteins, namely DUBs, remained elusive at the beginning of this work.
The aim of this thesis was to identify and validate USP10 as a novel regulator of β-Catenin stability in colorectal cancer.
Firstly, a putative interaction between USP10 and β-Catenin in different CRC-derived cells should be investigated. Then, by altering USP10 abundance via CRISPR/Cas9 or shRNA, consequences in the transcriptional program upon loss of USP10 should be analysed in 2D cell culture.
Since 2D cell culture is not an ideal system to study complex physiological questions, the isolation, cultivation and modification of murine intestinal organoids should be established. By depleting, silencing or overexpressing Usp10 in these genetically engineered organoids, the phenotypic consequences of this novel interaction should be investigated using RNA sequencing and will be compared to results from 2D cell culture.
Secondly, if genetic targeting of USP10 leads to promising effects in model systems of CRC, a therapeutical intervention by inhibiting USP10 will be investigated. Commercially available as well as novel small molecule inhibitors will be tested for targeting USP10 in CRC cell lines.
Thirdly, it will be worked on a novel CRISPR/Cas9 based mouse model for CRC. In light with the 3-R rule for animal work, a viral infection- based model, which will reduce breeding-time and the number of animals needed, will be developed.

2 Materials and Methods

2.1 Materials

2.1.1 Experimental models

Human cell lines

Cell lines were tested for mycoplasma contamination on a regular basis.

Name	Description (Source)
HEK293T	Human embryonic kidney cell line (ATCC)
HEK293T AAV pro	Human embryonic kidney cell line, derived from HEK293, optimised for AAV production (Takara)
HCT116	male APC wild-type human CRC cell line (ATCC)
LS174T	female APC wild-type human CRC cell line (ATCC)
SW480	male APC mutated human CRC cell line (ATCC)
SW620	cell line derived from a metastasis of the same patient as SW480 (ATCC)
DLD-1	male APC mutated human CRC cell line (ATCC)
HT-29	female APC mutated CRC cell line (ATCC)
Colo320	female APC mutated CRC cell line (ATCC)
L17-Rspo	murine L cells stable expressing Rspo1 (Gift from O. Sansom)
HEK293-Nog	HEK293 cells stable expressing murine Noggin (Gift from O. Sansom

Murine organoid lines

Murine small intestinal organoids were isolated as described in 2.2.2.2.

Name	Description (Source)
Cas9 organoids	small intestinal organoids from a $Rosa26^{SOR\text{-}CAGG\text{-}Cas9\text{-}IRES\text{-}GFP}$ expressing mouse

Bacterial strains

Name	Description
DH5α	*Escherichia coli*, genotype: F- , Φ80lacZΔM15, Δ(lacZYA-argF) U169, recA1, endA1, hsdR17 (rK-, mK+), phoA, supE44, λ-, thi-1, gyrA96, relA1
XL1 blue	*Escherichia coli*, genotype: recA1, endA1, gyrA96, thi-1, hsdR17, supE44, relA1 lac [F$\acute{}$proAB lacIqZΔM15 Tn10 (Tetr)]

Mice strains

Name	Company	Identifier
B6(C)-Gt(ROSA)26Sor$^{em1.1(Cag\text{-}Cas9*,\text{-}EGFP)Rsky}$/J	the Jackson laboratory	stock no.: 028555
C57BL/6J	the Jackson laboratory	stock no.: 000664
B6.129S4-*Kras*^{tm4Tyi}/J	the Jackson laboratory	stock no.: 008179
B6.129-*Kras*$^{tm4Tyi/}$:*Trp53*^{tm1Brn}/J	the Jackson laboratory	stock no.: 032435

2.1.2 Cultivation media and supplements

All chemicals were obtained from Sigma Aldrich and Roth, changes in suppliers are mentioned.

Cultivation media for cell culture

For cultivation of human colorectal cancer cell lines and HEK293T cells DMEM (Thermo Fisher Scientific) and RPMI-1640 (Thermo Fisher Scientific) were used. Additional components are as following:

FCS	10 % (v/v) heat-inactivated fetal calf serum (Biochrom)
Pen/Strep	1 % (v/v) Penicillin/Streptomycin (100.000 U/mL, PAA)
Trypsin/EDTA	0.025 % Trypsin (Thermo Fisher Scientific)
	5 mM EDTA
	22.3 mM Tris pH 7.4
	125 mM NaCl

Cultivation media for 3D organoid culture

For cultivation of murine organoids ENR medium was used. The supplements used for the media were prepared as following:

murine recombinant EGF (Peprotech)	500 µg/mL 0.2 % BSA/PBS
Noggin	conditioned medium (see 2.2.2.1)
Rspondin	conditioned medium (see 2.2.2.1)
Cultrex RGF BME Type2 Select (Biotechne)	1:2.5 diluted with medium
Geltrex™LDEV-Free RGF (Thermo Fisher Scientific)	1:2.5 diluted with medium

Supplements and inhibitors for cell culture and 3D organoid culture

Compound (Company)	Description	Stock concentration	Final concentration
B27 Supplement (Thermo Fisher Scientific)	Supplement-mix for organoids	50x	1x
Blasticidin (Invivogen)	Antibiotic	10 mg/mL	20 ţg/mL
Doxycycline	activation of TRE	1 mg/mL in EtOH	0.5 ţg/mL
Gibco™ Anti-Anti	Antibiotic, Antimycotic	100x	1x
HBX19818 (MedChem Express)	USP7 Inhibitor	10 mM in DMSO	cell line dependent
MG-132 (Sellekchem)	Proteasome Inhibitor	10 mg/mL	25 ţg/mL
N2 Supplement (Thermo Fisher Scientific)	Supplement-mix for organoids	100x	1x
P22077 (MedChem Express)	USP7/10 Inhibitor	10 mM in DMSO	cell line dependent
Primocin (InvivoGen)	Antimicrobial agent	50 mg/mL	100 ţg/mL
Puromycin (Invivogen)	Antibiotic	10 mg/mL	1 to 2 ţg/mL
Spautin-1 (MedChem Express)	USP13/10 Inhibitor	10 mM in DMSO	cell line dependent
TMV-05 (Frankfurt University)	USP10 Inhibitor	10 mM in DMSO	cell line dependent
TMV-06 (Frankfurt University)	USP10 Inhibitor	10 mM in DMSO	cell line dependent
TMV-07 (Frankfurt University)	USP10 Inhibitor	10 mM in DMSO	cell line dependent
TMV-12 (Frankfurt University)	USP10 Inhibitor	10 mM in DMSO	cell line dependent

Cultivation media and supplements for bacteria

Supplements were, if not stated otherwise, obtained from Roth. Stock solution were prepared by dissolving the powder in ddH_2O and sterile filtration.

Compound	Composition/ Concentration
Lysogeny broth (LB) medium	10 % (w/v) Bacto tryptone 0.5 % (w/v) Yeast extract 1 % (v/v) NaCl
LB agar	LB medium with 1.2 % Bacto agar autoclaved, antibiotics were added at 50 °C temperature 10 cm plates were prepared
Ampicillin	100 ţg/mL
Carbenicillin	100 ţg/mL
Kanamycin	30 ţg/mL

2.1.3 Buffers and solutions

All chemicals were obtained from Sigma-Aldrich and Roth, if not stated otherwise. Buffers and Solutions were prepared in ddH_2O and stored at 4 °C, changes are indicated. Buffers specific for an experiment are listed in the according method-section.

Buffers and Solutions	Composition
Ammonium persulfate (APS; 10 %)	100 mg/mL, aliquots stored at −20 °C
Blueing solution	350 mL MilliQ water
	150 mL Tap water
	1.5 mL $NH_4(OH)$
Bradford Reagent	0.01 % (w/v) Coomassie Brilliant Blue G250
	1 x Bis-Tris
DNA loading buffer (6x)	10 mM EDTA pH 8.0
	0.2 % (w/v) Orange G
	40 % (w/v) Sucrose, stored at −20 °C
Lysis Buffer	200 mM NaOH
	1 % SDS
Neutral buffered formalin (NBF; 4 %)	10 % (v/v) Formaldehyde (37 %)
	1x PBS
Neutralisation Buffer	3.1 M Potassium-acetate pH 5.5
Phosphate Buffered Saline (PBS)	137 mM NaCl
	2.7 mM KCl
	10.1 mM Na_2PHO_4
	1.76 mM KH_2PO_4
Polybrene	200 mg dissolved in 50 mL H_2O
	aliquots stored at −20 celsius
Primary antibody solution	0.1 % Casein
	1x PBS
Protease Inhibitor cocktail	Protease Inhibitor cocktail (Biotool)
	used 1:1000, aliquots stored at −20 °C
RIPA lysis buffer	50 mM HEPES pH 7.9
	140 mM NaCl
	1 % (v/v) Triton X-100
	0.1 % (w/v) SDS
	0.1 % (w/v) sodium deoxycholate
	10 mM sodium fluoride
	10 mM sodium pyrophosphate
	10 mM β-glycerophosphate
Resuspension Buffer	1 M Tris
	0.5 M EDTA
sample Buffer (5x)	1 g SDS
	5 mg bromophenol blue
	3.9 mL 100 % (v/v) glycerol
	1 mL 0.5 M Tris, pH 6.8
	0.78 g DTT
SDS- Running buffer (10x)	250 mM Tris base

	2.5 M glycine
	1 % SDS
SDS- separating gel 10 %	10 % (v/v) acrylamide/bisacrylamide
	375 mM Tris HCl pH 8.8
	0.1 % (w/v) SDS
	0.1 % (w/v) APS
	0.1 % (w/v) TEMED
SDS- stacking gel	4 % (v/v) acrylamide/bisacrylamide
	125 mM Tris HCl pH 6.8
	0.1 % (w/v) SDS
	0.1 % (w/v) APS
	0.1 % (w/v) TEMED
Transfer-buffer (10x)	250 mM Tris base
	1.5 M glycine
Tris-Acetate-EDTA buffer (TAE) 50X	2 M Tris pH 8
	5.7 % (v/v) acetic acid
	50 mM EDTA
Tris Buffered Saline (TBS) (20x)	200 mM Tris
	1.5 M NaCl
	pH 7.4
TBS with Tween-20 (TBS-T)	1x TBS
	0.2 % (v/v) Tween-20
TE	10 mM Tris pH 7
	1 mM EDTA pH 8
Secondary antibody solution	0.1 % Casein
	1x PBS
	0.1 % SDS

2.1.4 Commercial kits

FastPure Gel DNA Extraction Mini Kit	Vazyme
ImmPRESS Horse anti-rabbit IgG Kit	Vector Laboratories
ImmPRESS Horse anti-mouse IgG Kit	Vector Laboratories
NEBNext Poly(A) mRNA Magnetic Isolation Module	NEB
NEBNext® Ultra™II Directional RNA Library Prep Kit for Illumina®	NEB
ReliaPrep™ RNA Miniprep Systems	Promega
SignalStain® DAB substrate Kit	Cell Signaling

2.1.5 Chemicals, enzymes and standards

Agencourt AMPure XP Beads	Beckman Coulter
Blocker™FL Fluorescent Blocking Buffer (10X)	Thermo Fisher Scientific
Calf Intestinal Phosphatase (CIP)	NEB
DNase	Applichem
Dynabeads™Protein G for IP	Thermo Fisher Scientific
Dynabeads™Protein A for IP	Thermo Fisher Scientific
Eosin	Sigma-Aldrich
5x GC-buffer	Mobidiag
Gene Ruler 1 kb Plus DNA ladder	Thermo Fisher Scientific
Gibco™ Horse Serum	Thermo Fisher Scientific
GlutaMAX™	Thermo Fisher Scientific
Glutathion-Sepharose 4B	GE Healthcare
Hematoxylin	Sigma-Aldrich
HEPES	Biochrom
Differentiation Solution	Sigma Aldrich
M-MLV reverse transcriptase	Promege
Mowiol® 40-88	Sigma-Aldrich
PageRuler Prestained Protein Ladder	Thermo Fisher Scientific
PNK Ligase	Thermo Fisher Scientific
Protease Inhibitor Cocktail	Roche
Protein A Sepharose™4B beads	Thermo Fisher Scientific
Polyethylenimine, Linear (PEI)	Polysciences
Restriction Enzymes	New England Biolabs
RNase A	Roth
S7 Fusion Polymerase™	Mobidiag
SYBR® Green qPCR Master Mix	Thermo Fisher Scientific
T4 DNA Ligase	Vazyme
2x Taq MasterMix Dye Plus	Vazyme
TriFast™	Vazyme
Warhead ubiquitin suicide probe	UbiQ

2.1.6 Nuclei acids

2.1.6.1 Primers

All oligos were synthesized and obtained by Sigma-Aldrich at 0.025 µmol scale and purified by desalting (DST), if not stated otherwise. Each oligo was re-suspended in ddH_2O to a concentration of 100 µM and used at a final concentration of 10 µM, if not stated otherwise. Stock primer were stored at $-20\,^{\circ}C$.

Primer for cloning

Name	Sequence
EFs rev	GCCTGTGTTCTGGCGGCAAACCCG
shRNA mirE XhoI fwd	TACAATACTCGAGAAGGTATATTGCT GTTGACAGTGAGCG
shRNA mirE EcoRI rev	TTAGATGAATTCTAGCCCCTTGAAGTC CGAGGCAGTAGGCA
U6 short fwd	GGGCCTATTTCCCATGATTC

Primer for CRISPR/Cas9

Name	Sequence
APC ex9 fwd	caccGCCGCTAGAACTCAAAACAC
APC ex9 rev	aaacGTGTTTTGAGTTCTAGCGGC
Apc ex10 fwd	caccGCTTTTACAGTCCCAGGCGG
Apc ex10 rev	aaacCCGCCTGGGACTGTAAAAGC
KRas fwd	caccGACTGAGTATAAACTTGTGG
KRas rev	aaacCCACAAGTTTATACTCAGTC
$KRAS^{G12D}$ HDR fwd	TTTTGTGTAAGCTTTGGTAACTCCAT GTATTTTTATTAAGTGTT
$KRAS^{G12D}$ HDR rev	GAGCTTATCGATACCGTCGACACACC CAGTTTAAAGCCTTGGAA
Trp53 fwd	caccGATGGTGGTATACTCAGAGC
Trp53 rev	aaacGCTCTGAGTATACCACCATC
USP10 ex2 fwd	caccgCTTACCTCAACTGAAGATCG
USP10 ex2 rev	aaacCGATCTTCAGTTGAGGTAAGc
USP10 ex10 fwd	caccGCTCTTCTTCATTGACCGAG
USP10 ex10 fwd	aaaCTCGGTCAATGAAGAAGAGC

Primer for Fellmann shRNA

Name	Sequence
shUSP10-1	TGCTGTTGACAGTGAGCGATACCCTTTAGTTTTT GATAAATAGTGAAGCCACAGATGTATTT ATCAAAAACTAAAGGGTAGTGCCTACTGCCTCGGA
shUSP10-2	TGCTGTTGACAGTGAGCGCGGTGTCGATG AAGTCATTGAATAGTGAAGCCACAGATGTATT CAATGACTTCATCGACACCATGCCTACTGCCTCGGA
shUsp10-1	TGCTGTTGACAGTGAGCGCGGGTACTACAG TTATTTGAAATAGTGAAGCCACAGATGTATTT CAAATAACTGTAGTACCCATGCCTACTGCCTCGGA
shUsp10-2	TGCTGTTGACAGTGAGCGATGGGTAC TACAGTTATTTGAATAGTGAAGCCACAGATGT ATTCAAATAACTGTAGTACCCAGTGCCTACTGCCTCGGA
shNTC	TGCTGTTGACAGTGAGCGCAGGAATTAT AATGCTTATCTATAGTGAAGCCACAGATGTATAGAT AAGCATTATAATTCCTATGCCTACTGCCTCGGA

Primer for Broad shRNA

Name	Sequence
shUSP10-1 fwd	CACCGACCAGCAACAACACTTGTAAATT
	CAAGAGATTTACAAGTGTTGTTGCTGGTCTTTTT
shUSP10-1 rev	AAACAAAAAGACCAGCAACAACACTTGT
	AAATCTCTTGAATTTACAAGTGTTGTTGCTGGTC
shUSP10-2 fwd	CACCGCCTATGTGGAAACTAAGTATTTT
	CAAGAGAAATACTTAGTTTCCACATAGGCTTTTT
shUSP10-2 rev	AAACAAAAAGCCTATGTGGAAACTAAGT
	ATTTCTCTTGAAAATACTTAGTTTCCACATAGGC
shUsp10-1 fwd	CACCGTCATTAGAGATCGCTCTTACTTC
	AAGAGAGTAAGAGCGATCTCTAATGACTTTTT
shUsp10-1 rev	AAACAAAAAGTCATTAGAGATCGCTCTT
	ACTCTCTTGAAGTAAGAGCGATCTCTAATGAC
shUsp10-2 fwd	CACCGCACAGCCTACCTCCTATATTTTC
	AAGAGAAATATAGGAGGTAGGCTGTGCTTTTT
shUsp10-2 rev	AAACAAAAAGCACAGCCTACCTCCTATA
	TTTCTCTTGAAAATATAGGAGGTAGGCTGTGC

Primer for qRT-PCR

Name	Sequence forward	Sequence reverse
Actb	CTAAGGCCAACCGTGAAAAG	ACCAGAGGCATACAGGGACA
Usp10	CGATTTCAGCCCTGATGAAT	CTGGCAGTTCATCTTCAGCC
Ctnnb1	TGCTCAACAAAACAAACGTGA	TTTACTAAGGCTTGGGGTCCA
Myc	GTGCTGCATGAGGAGACACC	AGGGGTTTGCCTCTTCTCC
Ccnd1	CAGAGGCGGATGAGAACAA	AGGGTGGGTTGGAAATGAA
Lgr5	CGAGCCTTACAGAGCCT	TTGCCGTCGTCTTTATTC
	GATACC	CATTGG
ACTB	CCAACCGCGAGAAGATGA	CCAGAGGCGTACAGGGATAG
USP10	GGATCCTGTAGCCATAA	GGTTGCAACGACACT
	AGATTG	GGTTT
CTNNB1	TGTTAAATTCTTGGCTATT	CCACCACTAGCCAGTAT
	ACGACA	GATGA
KRT20	AACTGCAAAATGCTCGGTGT	CAGGCCTTGGAGATCAGCTT
LGR5	CTCCCAGGTCTGGTGTGTTG	GAGGTCTAGGTAGGAG
		GTGAAG
GAPDH	AGCCACATCGCTCAGACAC	GCCCAATACGACCAAATCC

2.1.6.2 Plasmids

Empty vectors

AAV	selfmade from AAV backbone (Addgene#60224)
pLenti CRISPRv2	lentiviral backbone for CRISPR/Cas9 (Addgene#52961)
pLKO5	lentiviral Vector for Sp sgRNA delivery, GFP, (Addgene#57822)
pSico TRE	selfmade DOX-inducible from pSico p53 (Addgene#12089)

Packaging vectors

psPAX.2	lentiviral packaging plasmid (Addgene#12260)
pMD2.G	lentiviral packaging plasmid (Addgene#12259)
pAAV-DJ Vector	Cell Biolabs, INC. (VPK-420-DJ)
pHelper	Cell Biolabs, INC. (VPK-400-DJ)

Plasmids available in the laboratory of Markus Diefenbacher

AAV sgApc^{exon9}	AAV targeting Apc exon9
AAV sgApc^{exon9} KRas^{G12D}	AAV targeting Apc exon9, KRas with HDR^{G12D}
AAV sgApc^{exon9} Trp53 KRas^{G12D}	AAV targeting Apc exon9, Trp53, KRas with HDR^{G12D}
pSico CTNNB1^{S45A} Cre-RFP	pSico overexpressing Ctnnb1^{S45A} and Cre-RFP

Plasmids from collaboration partners

pGEX-6P-1-4x-UBA-GST (TUBE)	plasmid for recombinant TUBE production (Gift from David Komander)
pLVX-TetOne-puro-cycle3 GFP	pLVX-TetOne-puro GFP control (Gift from Michael Potente)
pLVX-TetOne-puro-cycle3 GFP USP10	pLVX-TetOne-puro GFP USP10 WT (Gift from Michael Potente)
pLVX-TetOne-puro-cycle3 GFP USP10 CA	pLVX-TetOne-puro GFP USP10 CA (Gift from Michael Potente)

Plasmids generated during this thesis

pLKO shUSP10-1	pLKO shRNA targeting *USP10*#1
pLKO shUSP10-2	pLKO shRNA targeting *USP10*#2
AAV shUsp10-1	AAV backbone shRNA targeting *Usp10*#1
AAV shUsp10-2	AAV backbone shRNA targeting *Usp10*#2
pSico TRE shUSP10-1	pSico shRNA targeting *USP10*#1
pSico TRE shUSP10-2	pSico shRNA targeting *USP10*#2
pCRISPRv2 sgUSP10 exon2	pCRISPRv2 sgRNA targeting USP10 exon 2
pLKO sgUSP10 exon10	pLKO sgRNA targeting USP10 exon10
AAV USP10 WT	AAV USP10 WT overexpression
pCRISPRv2 sgApc^{exon10}	pSico targeting *Apc* exon10
pCRISPRv2 sgApc^{exon10} Trp53	AAV targeting *Apc* exon9, *Trp53*

2.1.6.3 Antibodies

Primary antibodies

Antibody	species	cat. no	company	dilution
USP10	rabbit	HPA006731	Sigma Aldrich	WB: 1:1000 IP: 1 µg IF/IHC: 1:300
β-Catenin	mouse	610154	BD Transduction	WB: 1:1000 IP: 1 µg IF/IHC: 1:300
active β-Catenin	mouse	05-665	Millipore	IHC: 1:100
KI67	rabbit	RM-9106-S1	Thermo Fisher	IHC: 1:100
β-Actin	mouse	sc-47778	Santa Cruz	WB: 1:1000
LGR5 (discontinued)	rabbit	21833-1-ap	PTGlab	WB: 1:1000
GAPDH	rabbit	10494-1-ap	PTGlab	WB: 1:1000
Lamin B1	mouse	66095-1-lg	PTGlab	WB: 1:1000
α-Tubulin	mouse	66031-1-lg	PTGlab	WB: 1:1000
ERK1/2	rabbit	A5029	Bimake	WB: 1:1000
p-ERK1/2	mouse	sc-7383	Santa Cruz	WB: 1:1000
E-Cadherin	mouse	60335-1-lg	PTGlab	WB: 1:1000
N-Cadherin	rabbit	22018-1-ap	PTGlab	WB: 1:1000
USP7	rabbit	A300-033A	Bethyl	WB: 1:1000
OLFM4	mouse	PA5-73003	Thermo Fisher	IF: 1:100
ASCL2	rabbit	PA5-40474	Thermo Fisher	IF: 1:100
LGR5	rabbit	MA5-25644	Thermo Fisher	IF: 1:100
CD44	mouse	60224-1-lg	PTGlab	IF: 1:100

Secondary antibodies

Antibody	species	cat. no	company	dilution
AlexaFluor800 α-rabbit	donkey	A32808	Thermo Fisher	WB: 1:10000
AlexaFluor680 α-mouse	donkey	A32788	Thermo Fisher	WB: 1:10000
AlexaFluor647 α-rabbit	donkey	A32795	Thermo Fisher	WB: 1:400
AlexaFluor555 α-mouse	donkey	A32773	Thermo Fisher	WB: 1:400
AlexaFluor488 α-rabbit	donkey	A32790	Thermo Fisher	IF: 1:400

2.1.7 Equipment

Cell culture incubator	BBD 6220 (Heraeus)
Cell counter	Countess 3 FL automated Cell Counter system (Thermo Fisher Scientifific)
Centrifuges	Avanti J-26 XP (Beckman Coulter) Eppendorf 5417 R (Eppendorf) Eppendorf 5425 (Eppendorf) Eppendorf 5430 (Eppendorf) Galaxy MiniStar (VWR) Optima L-90K Ultracentrifuge (Beckman Coulter)
Deep-sequencer	NextSeq 500 (Illumina) NextSeq 2000 (Illumina)
Fragment analyzer system	Fragment analyzer (Agilent)
Histology	Microm Stp-120 (Thermo Fisher Scientifific) Microm EC 350-1 (Thermo Fisher Scientific)
Immunoblot detection	Odyseey®CLx Imaging System (LI-COR)
Microscope	Operetta®High-Content Imaging System (Perkin Elmer)
Photometer	Ultrospec™3100 pro UV/Visible (Amersham Biosciences) Spectrofluorometer NanoDrop 1000 (Thermo Fisher Scientific)
PVDF transfer membrane	PVDF Transfer Membran 0.2 ţm (Thermo Fisher Scientific)
Quantitative RT-PCR machine	StepOne™plus (Applied Biosystem)
Slide scanner	Ventana DP 200 slide scanner (Roche)

2.1.8 Software and online programs

Name	Company or Provider
Acrobat	Adobe
Affinity Designer	Serif
Bowtie2 v2.3.4.1	[80]
Broad institute shRNA	https://portals.broadinstitute.org/
cBioportal	https://www.cbioportal.org

ChopChop	http://chopchop.cbu.uib.no/
edgeR	[81]
FASTQC	http://www.bioinformatics.babraham.ac.uk/projects/fastqc/
featureCounts	[82]
GEPIA	http://gepia.cancer-pku.cn
GSEA v2.2	http://software.broadinstitute.org/gsea/downloads.jsp
Harmony® High-Content Analysis software v4.6	Perkin Elmer
Image Studio®version 5.2.5	LI-COR
Office 365	Microsoft Inc.
Panther Classification system	http://pantherdb.org
Prism8	GraphPad Software Inc.
Qupath	https://qupath.github.io
R v4.0.0	https://www.r-project.org
R2: Genomics Analysis and Visualization Platform	http://r2.amc.nl
Samtools	[83]
Splash RNA	http://splashrna.mskcc.org/
StepOne software v2.3	Applied Biosystem
tidyverse	[84]
UCSC Genome Bioinformatics	http://genome.ucsc.edu
Venn diagram	http://bioinformatics.psb.ugent.be/webtools/Venn/
Zhang lab gRNAs design resource	https://zlab.bio/guide-design-resources

2.2 Methods

2.2.1 Cell-biological Methods

2.2.1.1 Cultivation of eucaryotic cells

The human colorectal cancer cell lines HCT116, SW480, SW620 and HT-29 as well as HEK293T cells were cultivated in DMEM 10 % FCS. The colorectal cancer cell lines LS174T, DLD-1 and Colo320 were cultivated in RPMI-1640, supplemented with 10 % FCS. DMEM and RPMI-1640 will be from here on referred to as "medium". All stable transformed cell lines were cultivated in medium additionally supplemented with 1 % Penicillin/Streptomycin. Cells were incubated at 37 °C and 5 % CO_2. For passaging of cells, the medium was removed and cells were washed with PBS. Trypsin/EDTA was added to detach the cells and incubated for 3 to 5 min at 37 °C. To stop the reaction, pre-warmed medium was added and cells were individualized and split into a new cell culture dish. In case a specific number of cells was needed, cells were counted by using either a Thoma counting chamber or the Countess 3 FL automated Cell Counter system. For freezing, cells were trypsinized and centrifuged for 4 min, 1500 rpm at RT. Freezing medium (50 % medium, 40 % FCS and 10 % DMSO) was added and cells were frozen in a freezing container at −80 °C. For thawing, cells were quickly thawed and added to a tube with fresh medium. Cells were centrifuged for 4 min at 1500 rpm, RT to remove the remaining DMSO, re-suspended in fresh medium and transferred to a new cell culture dish. If necessary, medium was changed the next day.

2.2.1.2 Transfection of cells

For transient transfection, cells were seeded in a 6-well plate the day before the experiment. The transfection mix was prepared as following: 200 µL medium without FCS and antibiotics was prepared in a 1.5 mL reaction tube and mixed with 6 µL PEI. 3 µg of plasmid DNA of choice were added and the reaction was mixed by pipetting up and down. After 15 min of incubation, the transfection mix was added drop-wise to the cells.

2.2.1.3 Virus production

Lentivirus production

10x 10^6 HEK293T cells were seeded on a 15 cm dish. On the next day, the transfection mix for lentiviral production was prepared as following: 2 mL medium (without FCS and antibiotics) were mixed with 75 µL PEI. 10 µg of each of the packaging plasmids psPAX2 and pMD2G and 15 µg of the lentiviral expression plasmid were added to the mixture and incubated for 15 min at RT. After incubation, the mix was added drop-wise to the cells.

The virus-containing supernatant was harvested every 24 h and filtered through a 0.45 µL filter. To concentrate the virus it was precipitated using 40 % PEG8000, overnight at 4 °C and centrifuged the next morning (20 min, 2200 g, 4 °C). The pellet was re-suspended in 1 mL PBS and stored until further usage at −80 °C.
For organoid infection and *in vivo* experiments, the lentivirus was concentrated using ultra-centrifugation (25 000 g, 4 °C, 90 min). The resulting pellet was re-suspended in 1 mL PBS and stored at −80 °C until further usage.

Adeno-associated virus (AAV) production

For the production of AAVs, 10x 10^6 HEK293T cells were seeded on a 15 cm dish. On the next day, the transfection mix was prepared as following: 2 mL medium (without FCS and antibiotics) were mixed with 75 µL PEI. 10 µg of each of the packaging plasmids ΔF6 and DJ and 15 µg of the AAV-expression plasmid were added to the mixture and incubated for 15 min at RT. After the incubation, the mix was added drop-wise to the cells. After three days, the virus-containing supernatant and cells were harvested. To purify the virus, the cells were lysed with 0.5 mM NaCl for 1 h at 4 °C, rotating. Afterwards, 10 % Chloroform were added and the mixture was incubated for another 30 min at 4 °C, rotating. The phases were than separated by centrifugation (2000 g, 30 min at 4 °C) and the upper phase was carefully transferred to a new falcon. With the addition of 10 % PEG8000, the virus was pelleted over night. On the next day, the mixture was centrifuged for 20 min, 2000 g at 4 °C and the supernatant discarded. The remaining pellet was re-suspended in 200 µL AAV-resuspension buffer, 2 µL DNAse were added and the reaction was incubated for 2 h at 37 °C. After the DNA digestion, Chloroform was added in a 1:1 ration, centrifuged (12 000 g, 15 min at 4 °C), and the upper phase transferred to a fresh reaction tube. The Chloroform precipitation was repeated once more and the resulting AAV was stored at −80 °C until further usage.

2.2.1.4 Viral infection

To generate stable transformed cell lines, cells were plated on a 6-well plate.
For lenti-viral infection, either 1 mL of supernatant or 50 µL concentrated virus (see 2.2.1.3) were added to the cells, together with polybrene (to a final concentration of 6 µg/mL). On the next day, cells were washed with PBS and fresh medium was added.
For AAV-infection, approximately 50 µL of AAV were added per cavity of a 6-well plate, without polybrene.
For selection of infected cells, cells were either selected with corresponding antibiotics (concentration dependent on cell line) or, in case a fluorescent marker was used, proceeded to FACS sorting by a FACSAria™III machine.

2.2.2 3D organoid culture

2.2.2.1 Production of growth factors

The organoid-medium supplements R-spondin and Noggin were produced as conditioned medium (CM). For tumour and murine small intestinal organoids, R-spondin and Noggin were sufficient. Each batch of produced CM was tested for functionality by side-by-side culturing of organoids.
For production of CM, Advanced DMEM/F12 with supplements (from hereinafter referred to as ADF base medium) was prepared as following:

Advanced DMEM F12	500 mL
100x Anti-Anti	5 mL
HEPES	100 mM
100X GlutaMAX™	5 mL
Gibco™Horse Serum	500 µL

R-Spondin conditioned medium

For production of R-spondin conditioned medium L17-Rspo1 cells were used. Cells were grown in DMEM 10 % FCS supplemented with 1 mg/mL G418 for selection. When confluent, cells were expanded to 5x T175 flasks and grown without G418. When confluent, the medium was changed to ADF base medium and cells were incubated for 5 d. Then, CM was collected in 50 mL falcon tubes and centrifuged for 5 min, 300 g. The supernatant was passed trough a 0.2 µm filter, 10 mL were kept for testing and the remaining CM was stored in aliquots at −20 °C.

Noggin conditioned medium

For production of Noggin CM HEK293 cells, stable transfected with murine Nog, were used. Cells were cultured in DMEM 12 % FCS supplemented with G418 (500 µg/mL for selection. When cells were confluent, G418 was removed and cells were expanded to 10x T175 flasks. When cells were confluent, growing medium was changed to ADF base medium and the cells were incubated for one week. For harvesting of CM medium, the medium was collected in 50 mL falcons, centrifuged for 5 min at 1500 rpm and passed through a 0.2 µm filter. A small aliquot of medium was used for testing and the remaining CM was stored in small aliquots at −20 °C until further usage.

2.2.2.2 Isolation of murine intestinal organoids

Murine intestinal organoids were isolated and cultured as described by Sato *et al.* in 2009 [70] and in this thesis adapted as following:
Mice were sacrificed and an approximately 4 to 5 cm long piece of the small intestine cut out. The piece of intestine was directly transferred to ice cold PBS in a petri-dish and flushed with PBS, using a syringe. Remaining fat tissue, surrounding the intestine, was carefully removed and the intestine was cut longitudinal. Next, the tissue was cut into small (3 to 5 mm) pieces and transferred to a 50 mL falcon tube containing PBS. Pieces were washed thoroughly using a 25 mL pipette. To isolate the crypts out of the intestine, the pieces were transferred to 20 mL PBS containing 25 mM EDTA and incubated for 30 min at 4 °C rotating. After the incubation, isolation of crypts was checked under the microscope and the suspension was filtered through a 70 nm cell strainer into a new falcon tube. The isolated crypts were washed twice with PBS by centrifugation (900 g, 4 °C, 10 min). After the last centrifugation step, PBS was carefully removed, the crypt-containing pellet was re-suspended in approximately 1 mL of Geltrex™ and plated drop-wise onto a pre-warmed 24-well ultra-low attachment plate. When the Geltrext™ solidified, murine ENR-Isolation medium was added. On the next day, the medium was exchanged to normal murine ENR medium.

murine ENR medium

R-Spondin CM	10 %
Noggin CM	1 %
murine EGF	0.05 ţg/mL
100X N2	500 ţL
50X B27	1 mL
ADF base medium	ad to 50 mL

Note: For isolated and thawed organoids 10 ţM *Rock inhibitor Y-27632 was added.*

2.2.2.3 Cultivation of organoids

For passaging of organoids, medium was removed without disturbing the geltrex-dome and PBS was added. The organoids were re-supended and mechanically disrupted into small fragments by pipetting. The suspension was transferred to a falcon tube and centrifuged at 900 g for 5 min. After centrifugation, the supernatant was discarded and organoids were re-suspended in fresh geltrex and plated. When the geltrex solidified, medium was added.
For freezing, the organoid-pellet was re-suspended in freezing medium (50 % medium, 40 % FCS and 10 % DMSO) and stored at −80 °C. For thawing, organoids were quickly thawed and transferred to a falcon with medium. To remove the DMSO from freezing medium, organoids were centrifuged for 5 min at 900 g, the supernatant was discarded and the remaining pellet was re-supended in geltrex and plated. When the geltrex solidified, ENR medium for thawing was added. Medium was changed to normal ENR medium as soon as little organoids were visbile under the microscope.

2.2.2.4 Viral infection of organoids

For AAV- infection of organoids the spinoculation method was utilised. Per infection, six approximately 20 µL organoid-domes were used. Organoids were washed twice with PBS and afterwards re-suspended in 250 µL medium. The organoid suspension was mixed with 250 µL concentrated AAV (see 2.2.1.3) and transferred to a 24-well ultra-low attachment plate. For spinoculation the plate was centrifuged for 90 min at 900 g and 37 °C. Afterwards, the plate was incubated for another 4 h in the incubator. After the incubation time, the organoid-virus suspension was transferred to a fresh 1.5 mL reaction tube and centrifuged (5 min, 900 g). The virus-containing supernatant was discarded and the pellet was washed with PBS. The organoid-pellet was then re-suspended in 60 µL geltrex and plated onto a 24-well plate. Medium was added when the geltrex solidified. After two days, selection of infected organoids was started by adding corresponding antibiotics to the medium.

2.2.3 Biochemical Methods

2.2.3.1 Transformation of competent bacteria

For transformation, competent bacteria were thawed on ice. Plasmid DNA or Ligation mixture was added and incubated for 30 min on ice. Afterwards, bacteria-DNA mixture was applied to heat-shock for 1 min at 42 °C followed by a 2 min incubation on ice and after that 300 µL pre-warmed LB medium was added to the mixture. The suspension was incubated up to 1 h on 37 °C shaking and plated on Agar-plates or transferred to 50 mL LB medium, supplemented with corresponding antibiotic, for selection of single cell clones or amplification of plasmid DNA, respectively.

2.2.3.2 Isolation of plasmid DNA from bacteria (midi-preparation)

Plasmid DNA isolation was performed using alkaline lysis. 50 mL overnight culture was pelleted by centrifugation and lysed in 5 mL resuspension Buffer. 5 mL lysis buffer was added and the mixture was incubated for 5 min on ice. For precipitation of proteins 5 mL of neutralisation buffer were added and thoroughly mixed. To separate proteins and soluble phase, the mixture was centrifuged for 20 min 2000 g at 4 °C. Afterwards, the mixture was filtered through a pleated filter into a fresh 50 mL falcon, 10 mL isopropanol were added and mixed by shaking. The DNA was pelleted using centrifugation (20 min, 4000 g, 4 °C), the pellet was re-suspended in 400 µL desalted water and transferred to a fresh 1.5 mL reaction tube. 1 mL Phenol/Chloroform was added and phases were separated by centrifugation (15 min 10 000 g at RT). The upper phase was transferred to a fresh reaction tube and DNA was precipitated by adding 1 mL isopropanol. Pelleted DNA was washed twice with 70 % ethanol, air-dried and solubilised in desalted water. Concentration of DNA was measured using the NanoDrop 1000 system.

2.2.3.3 Ligation of DNA fragments into plasmids

For cloning of DNA inserts into linearised vectors, ligation using T4 DNA ligase was performed as following:

Vector	100 ng
Insert (3x excess to Vector)	x ng
10X T4 DNA ligase buffer	1 µL
T4 DNA ligase	0.5 µL
ddH_2O	ad 10 µL

The reaction was incubated for 1 h at 37 °C and subsequently transformed into competent bacteria (2.2.3.1).

2.2.3.4 Gel electrophoresis and extraction

For analysing the size of nucleic acids, gel electrophoresis was used. Dependent on the size of the DNA-of-interest 1 to 2 % agarose-gels were prepared. Therefore, the appropriate amount of agarose was solved in 1x TAE buffer and boiled in the microwave until it was completely dissolved. Ethidium-bromide was added to a final concentration of 0.3 µg/mL and after gentle mixing, the gel was poured into a gel-chamber. Samples were prepared by adding 1x DNA loading dye and 1 kb Plus DNA ladder was used as a reference. The separation according to size was achieved by running the gel with 120 V for 1 h. Ethidium-bromide intercalates DNA and therefore, DNA-bands could be detected with UV light (254/365 nm).

2.2.3.5 Extraction and purification of DNA from agarose gels

DNA fragments, separated by gel-electrophoresis, were cut out of the gel and extracted using FastPure Gel DNA Extraction Mini Kit (Vazyme) according to manufacturer‘s instructions with minor changes: Two washing steps were performed and DNA was eluted in desalted water.

2.2.3.6 Colony PCR

To validate cloning experiments, colony PCR was performed on single colonies. The following reaction mix was prepared:

1:10 diluted Primer 2	1 µL
1:10 diluted Primer 2	1 µL
2X Taq MasterMix Dye Plus (Vazyme)	10 µL
ddH_2O	8 µL

For each cloning experiment up to 5 single colonies were picked, by using a yellow pipette-tip, dipped into the reaction-mix and transferred to 200 µL LB medium (supplemented with antibiotics for selection) in a 96-well stock plate. The plate was incubated at 37 °C until further usage.
The PCR was performed with an initial denaturation at 95 °C for 2 min followed by 35 cycles of: denaturation (95 °C, 30 s), annealing (60 °C, 30 s) and elongation (72 °C, 45 s). A final elongation step at 72 °C for 10 min was added. The amplified PCR product was analysed using gel electrophoresis (2.2.3.4) and after identification of positive clones, 100 µL bacteria suspension from the stock-plate were transferred to 50 mL LB with antibiotics for midi-preparation (see 2.2.3.2).

2.2.3.7 Cloning

Oligo cloning

To clone single and double guide RNAs into pCrisprV2 and pLKO plasmids, the Oligo cloning protocol https://www.addgene.org/crispr/zhang/ was adapted.
Guide RNAs were chosen from UCSC genome browser (https://genome.ucsc.edu/) and prepared for cloning as following:

Oligo 1	1 µL
Oligo 2	1 µL
T4 DNA ligase buffer	1 µL
PNK ligase	0.5 µL
ddH_2O	6.5 µL

Reactions were incubated for 30 min at 37 °C followed by 5 min at 95 °C. After cooling down slowly, reaction was filled up with 200 µL desalted water.
The vectors pCrisprV2 and pLKO were digested using the restriction enzyme BsmBI and its corresponding buffer by incubating the mixture for 1 h at 55 °C. After digestion, vectors were de-phosphorylated by adding 1 µL Calf intestinal phosphatase (CIP) directly to the reaction and incubation for 30 min at 37 °C. Vectors were subsequently purified via gel electrophoresis (2.2.3.4 and 2.2.3.5). Annealed oligos were ligated into purified Vectors (2.2.3.3) and transformed into competent bacteria (2.2.3.1). Transformed bacteria were plated on LB agar plates and positive clones were checked the next day using colony PCR (2.2.3.6).

shRNA cloning

Short-hairpin RNAs (shRNAs) were cloned into the home-made pSico-TRE-miR-E plasmid. Sequences targeting the protein-of-interest were obtained from either [85] or http://splashrna.mskcc.org/.
First, oligos were amplified by a polymerase chain reaction as following:

miR-E primer 1 (1:10)	2.5 µL
miR-E primer 2 (1:10)	2.5 µL
shRNA oligo (1:30)	5 µL
dNTPs	10 mM
5X GC-buffer (Mobidiag)	10 µL
S7 Fusion Polymerase™(Mobidiag)	0.5 µL
ddH_2O	ad 50 µL

For PCR the mix was heated for 3 min at 98 °C. Afterwards, the reaction was denatured (25 s, 98 °C), annealed (30 s, 54 °C) and elongated (60 s, 72 °C) for 25 cycles, followed by a final elongation step of 5 min at 72 °C. The PCR product was purified and eluted in 20 µL desalted water.
To insert the amplified shRNA into the pSico-TRE-miR-E based backbone, both, the vector and the shRNA were digested with restriction enzymes EcoRI and XhoI as following:

Insert or Vector	10 µL
EcoRI	0.5 µL
XhoI	0.5 µL
10X Cutsmart	5 µL
ddH_2O	ad 50 µL

After incubation, samples were applied to gel electrophoresis, cut out and purified (2.2.3.5), followed by ligation (2.2.3.3) and transformation into competent bacteria (2.2.3.1). Transformed bacteria were plated on LB agar plates and positive clones were checked the next day using colony PCR (2.2.3.6). The plasmid DNA of validated clones was sequenced (Macrogen) to confirm correct orientation of the inserted oligo.

2.2.3.8 Nucleic acid isolation

RNA isolation with TriFast

For RNA isolation the medium was carefully removed and cells were scraped in 1 mL TriFast™ and transferred to a rection tube. 200 µL chloroform were added and tubes were thoroughly mixed by vortexing. To separate phases, tubes were centrifugated for 15 min at full speed, RT and the upper aqueous phase was carefully transferred to a new reaction tube. To precipitate the RNA, 500 µL isopropanol were added, the solution was mixed by inverting and centrifuged for 20 min, full speed at 4 °C. The resulting RNA pellet was washed twice with 1 mL 70 % ethanol and centrifuged one additional time empty. The air-dried pellet was dissolved in 20 µL RNAse-free water and concentration was measured using the NanoDrop 1000. RNA samples were either stored at −80 °C or directly used for cDNA synthesis (2.2.3.9).

RNA isolation with ReliaPrep™RNA Miniprep Systems

For RNA-sequencing (2.2.6), the RNA was isolated using the ReliaPrep™RNA Miniprep Systems according to manufacturer‘s instructions.

2.2.3.9 complementary DNA (cDNA) synthesis

cDNA synthesis is used to transcribe total RNA into complementary DNA. Therefore, 1 to 2 ţg of total RNA were mixed with 1 ţL random hexanucleotide primer and RNAse-free water to a final volume of 14 ţL. The mixture was incubated for 5 min at 65 °C. After a short incubation of ice, the following mix was added to the reaction:

10 mM dNTPs	1 ţL
5X first-strand buffer	4 ţL
M-MLV reverse transcriptase	1 ţL

The RNA was transcribed in a step-wise protocol for 5 min at each 25 °C, 30 °C and 35 °C, followed by 60 min at 42 °C and a final incubation for 15 min at 72 °C.
The resulting cDNA was diluted with water to a final volume of 200 ţL and directly used for qRT-PCR (2.2.3.10) or stored at −20 °C.

2.2.3.10 quantitative real-time PCR (qRT-PCR)

qRT-PCR is a method to analyse gene expression by measuring the abundance of mRNA. The fluorescent dye SYBR® Green was used, as it intercalates into newly synthesized DNA.
For each gene-of-interest (GOI) a master mix, consisting of 2.4 ţL SYBR® Green Master Mix, 0.5 ţL 1:10 diluted forward and reverse primer and 3.6 ţL water was prepared and dispensed into a 96-well plate. 3 ţL of cDNA was added to each well and the mixture was collected at the bottom of the plate by short centrifugation. The reaction was performed using a StepOne® plus machine with an initial denaturation (15 min, 95 °C), followed by 38 cycles of denaturation (30 s, 95 °C), annealing (20 s, 60 °C) and extension (15 s, 72 °C).
For analysis the Δ ΔCt method, described by Schmittgen and Livak in 2008, was used. Fold-changes in the expression of a gene, normalized to a housekeeping-gene (expected to not change among different conditions), between different conditions were calculated using the following formula (with HS : housekeeping gene, FC: fold change):

$$FC = 2^{-((Ct^{\mathrm{GOI}} - Ct^{\mathrm{HS}})_{\mathrm{sample}} - (Ct^{\mathrm{GOI}} - Ct^{\mathrm{HS}})_{\mathrm{control}}))}$$

2.2.4 Protein biochemical methods

2.2.4.1 Harvesting and lysis of cells

To prepare cell lysates, the medium was removed and cells were scratched in 1x PBS and transferred to a reaction tube. For pelleting, cells were centrifuged (3 min at 1500 rpm, RT), the supernatant was discarded and the pellet was re-suspended in approximately three-times pellet-volume lysis-buffer (e.g. RIPA) supplemented with 1:1000 Protease Inhibitor cocktail (Biotool). For efficient lysis, three cycles of freeze-thaw (liquid nitrogen - 37 °C water bath) were performed, followed by centrifugation (13 000 g, 20 min, 4 °C). Protein concentration was measured using Bradford assay (see 2.2.4.2).

2.2.4.2 Quantification of protein using Bradford assay

The, in the Bradford-reagent used dye, Coomassie-brilliant blue G250 can bind to unpolar, hydrophobic and cationic side chains of amino acids. This binding causes a shift in the absorbent maxima from 465 to 595 nm.
For measuring the protein concentration of lysates, 1.5 µL of lysate were mixed with 1 mL of Bradford-reagent in a cuvette. The absorption was then measured at 595 nm using a Ultrospec™3100 pro photometer. Protein concentration was calculated using the measured absorption and a standard curve with known, increasing concentrations, of BSA.

2.2.4.3 TUBE pull-down

Tandem-Ubiquitin-Binding-Entities (TUBEs) are used to purify endogenous poly- ubiquitinated proteins from cell lysates, according to the manufacturer‘s (Life Sensors) recommendation. Self-made chain-unspecific GST-tagged TUBE was kindly provided by the Lab of David Komander.
One cavity of a 100 % confluent 6-well plate was washed with PBS, harvested and lysed in 100 µL RIPA+ buffer. To ensure protection of poly-ubiquitinated proteins from proteolysis and de-ubiquitination, TUBE must be added immediately at a concentration of 100 µg/mL to the lysates.
To avoid DNA contaminations, three cycles of freeze-thaw were performed and lysates were cleared subsequently by centrifugation (15 to 20 min, full speed, 4 °C).
For pull-down experiments, cleared lysate was transferred to a new reaction-tube and 10 % were kept as input sample. 2 µL 5x Laemmli buffer were added to the input samples, 5 min denaturated at 95 °C and stored at −20 °C until further usage.
Glutathion-Sepharose 4B (GE Healthcare) beads were washed twice in ice-cold PBS-T and 20 µL beads (50 % slurry) were added per 100 µL reaction. Lysate and beads were incubated rotating at 4 °C for 2 h up to over night. After incubation, beads were washed 4 times with ice-cold PBS-T and subsequently boiled in 20 µL 1x sample buffer at 95 °C

for 10 min, to elute the bound proteins from the beads.
Input and pull-down samples were separated by SDS-PAGE and transferred to a PVDF-membrane by western blotting.

RIPA+ Buffer

Tris pH 7.4	50 mM
NP-40	1 %
Deoxycholate	0.5 %
SDS	0.1 %
NaCl	150 mM
EDTA	2 mM
$MgCl_2$	5 mM

Note: Supplement with 1 mM DTT and 1x complete Protease inhibitor mix (Biotool) before usage.

2.2.4.4 Activity Profiling of DUBs

Warheads are ubiquitin-like suicide probes, used to profile the activity of DUBs in cells. Therefore, cells grown in one cavity of a 6-well plate were harvested and re-suspended in two pellet volumes of ice-cold HR-buffer. Lysis was performed as described in 2.2.4.1. To profile DUB activity, 25 tg of cell lysate were transferred to a new reaction tube and the volume was adjusted to 16 tL with HR-buffer. 3 tL of a 1:1:1 mixture of Ub-VME, UbVS and Ub-PA suicide-probes (dissolved in 50 mM NaOAc, 5 % DMSO) were added to the lysate and to adjust the pH, double the volume 50 mM NaOH (compared to probes) was added. Samples were mixed briefly and incubated for 1 h at 37 °C shaking. After addition of 6 tL of 5x sample buffer, samples were boiled for 5 min and applied to SDS-PAGE, followed by western blotting (see 2.2.4.7 and 2.2.4.8). For active DUBs, binding of the suicide probe resulted in a 8 kDa size-shift of the proteins regular molecular weight.

HR-lysis Buffer

Tris pH 7.4	50 mM
NP-40	0.1 %
Sucrose	250 mM
$MgCl_2$	5 mM

Note: Supplement with 1x complete Protease inhibitor mix (Biotool) before usage.

2.2.4.5 Cellular- nuclear fractionation

One 15 cm dish of confluent cells was harvested by scratching in ice-cold PBS and centrifuged for 3 min at 4 °C. For lysis, cells were re-suspended in approximately 1 mL Buffer A (depending on pellet size) and incubated for 20 min on ice. Swollen cells were transferred to a pre-chilled 1 mL dounce homogenizer and cells were broken by 20 - 25 strokes of a tight pestle. Dounced cells were centrifuged in a 15 mL falcon for 5 min at 1000 rpm 4 °C. The supernatant, which is the cytosolic fraction, was transferred to a

fresh reaction tube. The remaining nuclear pellet was re-suspended in 1 mL S1 buffer and carefully layered over a cushion of 1 mL S2 buffer (in a fresh 15 mL falcon). To extract nuclear fraction, samples were centrifuged for 10 min at 3500 rpm , 4 °C. The supernatant was discarded and the remaining pellet re-supended in an appropriate volume of lysis buffer (e.g. RIPA)- this is the nuclear fraction.

Buffer A

HEPES pH 7.9	10 mM
$MgCl_2$	1.5 mM
KCl	10 mM
ddH_2O	up to 50 mL

Note: Supplemented with 0.5 mM DTT and 1x complete Protease inhibitor mix (Biotool) before usage.

Buffer S1

Sucrose	0.25 M
$MgCl_2$	10 mM
ddH_2O	up to 50 mL

Note: Supplemented with 1x complete Protease inhibitor mix (Biotool) before usage.

Buffer S2

Sucrose	0.35 M
$MgCl_2$	0.5 mM
ddH_2O	up to 50 mL

Note: Supplemented with 1x complete Protease inhibitor mix (Biotool) before usage.

2.2.4.6 endogenous co-Immunoprecipitation

To analyse the interaction of proteins, endogenous co-Immunoprecipitation (co-IP) experiments were performed. Therefore, cells were seeded on a 15 cm dish and when confluent, cells were harvested and lysed in RIPA+ buffer (see 2.2.4.1 and 2.2.4.3). Per reaction 1 ţg of antibody and 1 mg of protein-lysate were used and 3 % of lysate were kept as input-sample. Co-IPs were performed using either Protein A Sepharose™ 4B beads or Dynabeads™ (Thermo Fisher Scientific), as described below.
After binding of the antibody-coupled protein to the beads, the beads were washed four times in ice-cold lysis buffer. After the final washing step, the samples were eluted by boiling in 20 ţL 1x sample buffer for 10 min on 95 °C. Samples were than subjected to SDS-PAGE and Western Blot (see 2.2.4.7 and 2.2.4.8).

co-IP using Protein A Sepharose™ 4B beads

When using sepharose beads, 25 µL beads per reaction were washed twice in lysis buffer and re-suspended to a 50 % slurry solution. For pre-clearing of the lysate, beads were mixed with the lysate and incubated for 1 h at 4 °C rotating. Afterwards, beads were collected at the bottom by centrifugation (1500 rpm) and the lysate was transferred to a new reaction tube. Next, the antibody, targeting a specific protein, and corresponding IgG control antibody were bound to the lysate by overnight rotation at 4 °C. To precipitate the antibody-coupled lysate, 50 µL of a 50 % slurry bead-suspension were added and incubated for another 4 h at 4 °C rotating.

co-IP using Dynabeads™

For the usage of Dynabeads™, a 1:1 mixture of 2.5 µL Protein A and G coupled-beads was prepared and blocked in 5 mg/mL BSA in PBS. The beads were adjusted to a volume of 1 mL with 5 mg/mL BSA in PBS and antibody-of-interest as well as IgG control were added and incubated overnight at 4 °C rotating. On the next day, beads were washed twice and re-suspended in 50 µL BSA solution. For binding of proteins to the antibody-coupled beads, the lysate was added to the beads and incubated for another 6 h at 4 °C rotating.

2.2.4.7 SDS-PAGE

To analyse the composition of protein lysates, SDS poly-acrylamide gel electrophoresis (SDS-PAGE) was performed. Using this method, proteins are separated according to their molecular weight. For denaturation of proteins, samples were mixed with 5x sample buffer and boiled for 5 min at 95 °C. The sample buffer also contains DTT, which causes a disruption of disulfide-bonds and therefore, proteins loose their secondary and tertiary structure. The samples were loaded onto the acrylamide containing SDS gel and by applying a voltage of 90 to 120 V for 90 to 120 min the proteins run through the gel in the direction of the anode.
The poly-acrylamide forms, upon polymerisation, a mesh-like structure and denatured proteins run trough this mesh and get separated according to their size. The gel consists of a separation gel, which is overlaid by a stacking gel.
As a reference, 3 µL of PageRuler Prestained Protein Ladder, was loaded onto each gel together with equal amounts (25 µL) of each sample.

2.2.4.8 Immunoblotting

For visualisation of specific proteins, which were separated by SDS-PAGE, the proteins need to be immobilized on a membrane and stained with specific antibodies. Therefore, the western blot method was used.
Proteins were transferred to a PVDF-membrane using a wet blotting system. The membrane was activated for 5 min in MeOH. Six filter paper, two sponges and the SDS gel were equilibrated in 1x transfer buffer. The, so called, blotting sandwich was assembled as following in a blotting cassette: On the first sponge, three filter paper and the activated membrane were layered. The gel was carefully placed on top of the membrane, without any air bubbles between the two layers. Then, the next three filter papers were layered above and the second sponge was placed on top. The sandwich-containing cassette was fixed in the blotting chamber and filled with 1x transfer buffer. The negatively charged proteins in the gel were then transferred to the membrane, by running the blot with 300 mA for 3 h at 4 °C or 40 V overnight at 4 °C.
Afterwards, the membrane was blocked in 1:10 diluted blocking solution (Thermo Fisher Scientific) for 1 h at RT and then incubated in the primary antibody solution, containing the primary antibody-of-interest, for either 2 h at RT or over night at 4 °C. After that incubation, the membrane was washed three times with PBS-T to remove unbound antibody and then incubated for 1 h at RT in secondary antibody solution containing a secondary antibody coupled to an infra-red fluorophore. For detection of protein-bands the infra-red signal was detected using the Odyseey® CLx imaging system.

2.2.5 Animal models, human datasets and histological methods

2.2.5.1 Animal welfare and licences

All *in vivo* experiments were approved by the Regierung Unterfranken and the ethics comittee under the following licence 55.2-2-2532-2-555.
Mice are housed in standard cages located in pathogen free facilities on 12 hour- light / dark cycles with ad libitum access to food and water. The welfare of the mice was supervised by veterinarians every day and FELASA (Federation of European Laboratory Animal Science Associations) 2014 guidelines were followed for animal maintenance. By using sentinal animal screening, the animal health was monitored in general. In presence of obvious indicators of pain, stress or suffering, mice were immediately euthanised by cervical dislocation upon isoflurane anaesthesia.
All mice strains used in this thesis are listed in 2.1.1.

2.2.5.2 Mice euthanasia

For euthanisation, mice were placed in a chamber with access to isoflurane and the vaporizer was set at 3 %. Upon anaestisation, mice were euthanized by cervical dislocation. Death of the animal was verified by loss of consciousness, loss of reflex muscle response and the loss of noxious stimuli.

2.2.5.3 Colorectal infection of mice using lentivirus

The colorectal instillation of mice with concentrated lentivirus is described in detail in the results-section "Development of a novel mouse model for colorectal cancer".
In brief, mice were anaesthetised using a Ketamin/Xylazin mixture (for 10 mL solution: mix 1 mL Ketamin, 0.5 mL Xylazin and 8.5 mL NaCl). Upon anaestisation, the colon was flushed with 1 mL PBS and afterwards, approximately 500 µL concentrated virus were applied by the use of a round-tip needle. Mice were under constant observation until they fully recovered from anaesthetisation.

2.2.5.4 Histological processing of samples

Preparation of the gastrointestinal tract for histology

For histological analysis of the murine gastrointestinal (GI) tract the "swiss roles"-technique, described by Moolenbeek in 1981 [86], was utilized. Therefore, mice were euthanised and the complete GI tract, including colon and small intestine, were removed and directly flushed with PBS. The small intestine was cut into 3 pieces and the colon separated as well. The gut pieces were then carefully pulled over metal sticks and placed on a filter paper in a self-made device. The pieces were cut along the metal stick and carefully unwrapped on the filter paper. For fixation, a second filter paper was pressed on top and the tissue was incubated overnight in 4 % NBF. On the next day, the NBF was discarded and the tissue incubated for another 24 h in 70 % ethanol. To generate "swiss roles", each piece was then rolled longitudinal and fixated using small needles. The four pieces of the GI tract were paraffinised in a MICROM STP-120 (Thermo Fisher Scientific). After embedding the roles in paraffin blocks, using the MICROM EC 350-1 (Thermo Fisher Scientific), sections of 4 µm were prepared using a microtome.

Immunohistochemistry staining

Before staining, slides were de-paraffinised and rehydrated using the following protocol: 3 x 5 min xylene, 2 x 2 min 100 % ethanol, 2 x 2 min 95 % ethanol, 2 x 2 min 70 % ethanol, 1 x 2 min 50 % ethanol followed by 1 x 3 min water.
After rehydration, slides were subjected to either hematoxylin and eosin (H&E) or immunohistochemistry (IHC).
For H&E staining, the following protocol was performed: 4 min hematoxylin, rinse 2 min with water, 20 s differentiation solution, rinse 30 s with water, 20 s blueing solution, rinse with water for 2 min, 30 s eosin, rinse with water until colour changes to pink.
For IHC staining, sections were subjected to antigen retrieval by boiling in 1x sodium citrate buffer pH 6.0 for 5 min, 750 W, 5 min, 500 W and 5 min, 360 W in the microwave and finally cooled down by rinsing with water. After antigen retrieval, slides were washed

once in 1x TBS, followed by 10 min in 0.1 % TBS-T. After washing in 1x TBS, areas-of-interest were circled on the slide using a PAP pen (Sigma Aldrich). For blocking, sections were covered with 2.5 % horse-serum (Vector Laboratories) and incubated for 1 h at RT. For antibody-coupling, manufacturers instruction were followed. In general, antibodies were diluted in blocking solution and incubated overnight at 4 °C. On the next day, peroxidase block was performed. Therefore, slides were incubated for 10 min in 3 % H_2O_2, followed by another washing step in 1x TBS. Than, secondary antibody-solution ImmPRESS Horse anti-rabbit/mouse IgG Kit (Vector Laboratories) was added for 1 h at RT. Afterwards, slides were washed three times in 1x TBS and staining was performed using the SignalStain® DAB substrate Kit (Cell Signaling) according to manufacturers instructions. Upon DAB staining, nuclear counter-staining was performed by hematoxylin.
For H&E staining as well as IHC, slides were subjected to dehydration as following: 2x 20 s 70 % ethanol, 2x 2 min 95 % ethanol, 2x 2 min 100 % ethanol, 3x 5 min xylene. After dehydration slides were mounted with Mowiol® 40-88.
Slides were scanned using the Roche Ventana DP 200 slide scanner and analysed using QuPath software.

2.2.5.5 Human Colorectal Cancer patient samples

Human colorectal cancer patient samples were obtained from the Department of visceral surgery, University Hospital Wuerzburg and approved by the ethics committee of the University of Würzburg (no. 142/16-ge). Informed consent was obtained from all subjects and conducted experiments conform to the principles set out in the WMA Declaration of Helsinki and the Department of Health and Human Services Belmont Report. Human tissue samples were obtained as Tissue-Microarray (TMA) and subjected to IHC staining for USP10, β-Catenin and KI67 as described (2.2.5.4). Additionally, tumour and corresponding wild-type samples were obtained as frozen material and applied to protein analysis (see 2.2.4.7 and 2.2.4.8).

2.2.5.6 Analysis of human publicly available datasets

Publicly available CRC- patient mRNA data were obtained from the TCGA-COAD and GTEx data sets. Expression analysis for *USP10* and *CTNNB1* was performed using GEPIA website. For survival correlation, the Kaplan-Meier plot was generated using the R2: Genomics and Visualisation software with the Tumour Colon - Smith data set. All used software and webtools are listed in detail in 2.1.8.

2.2.6 RNA-sequencing

2.2.6.1 RNA isolation and library preparation

For RNA sequencing experiments, isolated RNA (see 2.2.3.8) was measured using NanoDrop spectrophotometer and the quality was analysed on a fragment analyser (Advanced Analytical). Only samples with RIN > 9 were used . 500 ng of RNA was used as

input and mRNA was purified using the NEBNext Poly(A) mRNA Magnetic Isolation Module (#E7490L) according to manufacturer‘s instruction. For library preparation, NEBNext® Ultra™II Directional RNA Library Prep Kit for Illumina® (#E7760L) was used, according to manufacturer‘s instruction with 10 cycles of PCR amplification.
The quality of the library was accessed using a fragment analyser and 50 fmol per sample were sequenced using Illumina NextSeq 500 or 2000.

2.2.6.2 Bioinformatic Analysis of RNA sequencing data

References and databases

The human reference genome build 38 (GRCh38) released in 2013 and the mouse genome build 39 (GRCm39) released in 2020 were used throughout the study for mapping of human and murine sequencing data, respectively. RefSeq genomic coordinates for all genes, exons, introns and rRNA cluster were downloaded from UCSC (University of California, Santa Cruz) table browser. Pre-built chromosome sizes and index for Bowtie were downloaded from NCBI.
For gene set enrichment analysis (GSEA) C2, C5 and Hallmark gene sets as well as mouse-orthologous hallmark, M2 and M5 were downloaded from Molecular Signature Database hosted by Broad Institute.

Read alignment

FASTQ files were downloaded from Illumina BaseSpace environment and checked for quality with FastQC software
(https://www.bioinformatics.babraham.ac.uk/projects/fastqc/).
Then, alignment to the corresponding genome was performed using Bowtie2 with one mismatch allowed and resulting .sam files were transformed into binary .bam files and sorted, using Samtools [80], [83].

Differential Gene Expression Analysis

Differential gene expression (DGE) analysis was performed in R (v 4.0.0.). Therefore, reads from sorted .bam files were counted using featureCounts, with exonic regions not considered [82]. Normalised counts were generated using the edgeR package and log2FC calculated from normalised reads over all replicates. Significance over DGE was calculated with Benjamini-Hoechberg algorithm, using edgeR package [81].
RPKM values, used for the generation of heatmaps, were calculated using rpkm() function of edgeR. All plots generated during RNA sequencing analysis were generated with ggplot2 package from the tidyverse [84].

3 Results

3.1 USP10 interacts with and regulates β-Catenin in APC mutant Colorectal Cancer

Colorectal cancer is mainly caused by alterations in the WNT signalling pathway, leading to constant transcription of its target genes. The hyper-activation of WNT singalling is caused either by stabilising mutations in *CTNNB1* or truncating mutations in the tumour suppressor *APC*, leading to the prevention of ubiquitylation and degradation of β-Catenin. Surprisingly, in previous experiments of this group, a remaining ubiquitylation on β-Catenin was found in CRC derived cell lines (data not shown) which led to the conclusion, that deubiquitylases (DUBs) may further stabilise β-Catenin.
To identify novel DUBs regulating the stability of β-Catenin, an siRNA based DUB-library screen was performed in APC mutant HT-29 cells. Here, the deubiquitylase USP10 was identified as a putative novel regulator of β-Catenin in CRC (1.8).

3.1.1 USP10 and β-Catenin are upregulated in Colorectal Cancer

To investigate whether USP10 does play a role in colorectal cancer, the expression of USP10 and β-Catenin was analysed by using publicly available datasets of colorectal cancer patients. The transcripts of *CTNNB1* and *USP10* were upregulated or amplified in tumour, when compared to adjacent wild-type tissue. Both demonstrated a significant correlation, with a Spearman coefficient of $R = 0.79$ (see figure 3.1 A and B). It is known that *CTNNB1* expression is elevated through out all stages of CRC (data not shown), however this is not clear for *USP10* yet. Analysis of public available data, accessible via the GEPIA platform (www.gepia2.cn), revealed that *USP10* expression was equally upregulated in all four stages of CRC, with no significant changes among the stages (figure 3.1 C). With this, one could speculate a role for USP10 not only in tumour initiation but also in tumour maintenance. This observation is reflected by an overall poor survival of patients with high *USP10* mRNA compared to patients with a lower expression, as seen by Kaplan-Meier analysis (figure 3.1 D).
Taken together, the analysis of *USP10* and *CTNNB1* expression data supports a putative role of USP10 in CRC patients and points towards a stage-independent function of USP10.
To further support our observations, which were based on public available expression data, we analysed the overall protein abundance of β-Catenin and USP10 in tissue micro arrays (TMA) as well as in primary tissue samples from local patients.

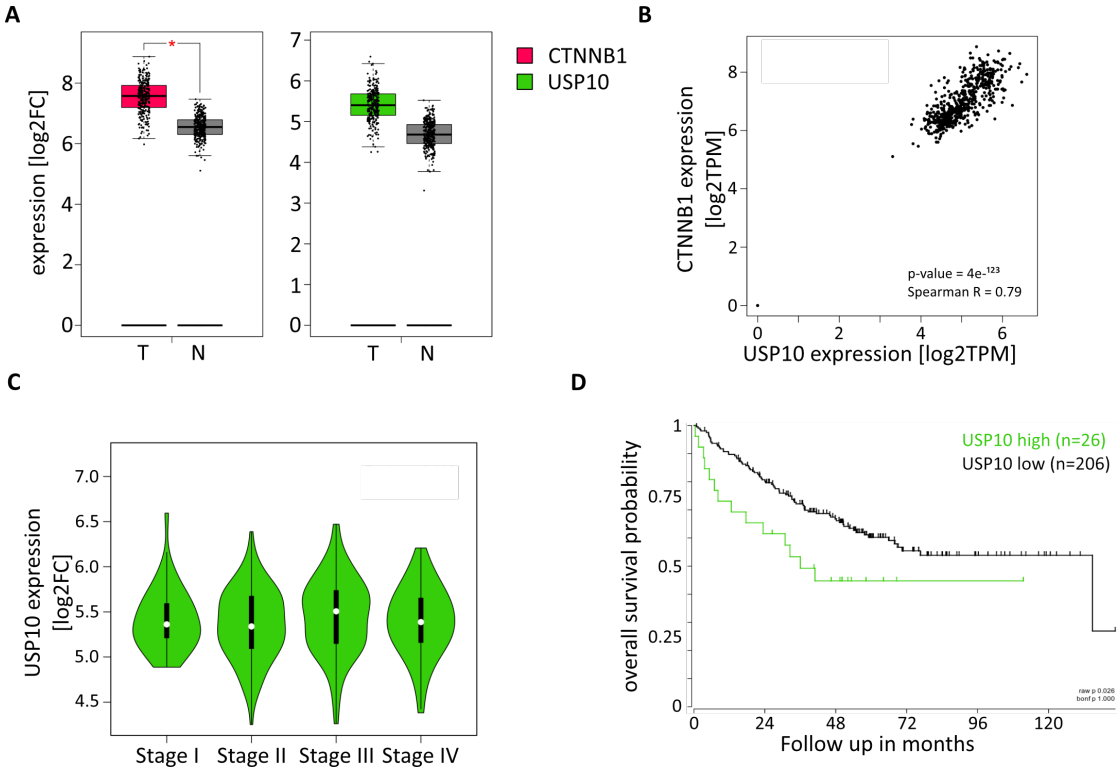

Figure 3.1: **USP10 and β-Catenin are upregulated in Colorectal Cancer**
A *CTNNB1* and *USP10* mRNA level are uprgeulated in tumour (T) compared to normal (N) tissue. Boxplots were generated using GEPIA website, using TCGA COAD tumour samples (n=275) and GTEx wild-type samples (n=349). **B** *CTNNB1* and *USP10* mRNA level correlate in CRC patients. Correlation analysis was performed using GEPIA website. **C** *USP10* mRNA is upregulated in all CRC stages. Violin plots were generated using GEPIA website. **D** High *USP10* expression correlates with poor overall survival for CRC patients. KM-plot was generated using R2: Genomics Analysis and Visualization Platform, using the Tumour Colon - Smith dataset.

For TMAs, small biopsies of tumours and adjacent wild-type (WT) tissue were embedded in paraffin and sections were subjected to Immunohistochemistry (IHC) staining. Representative images are shown in figure 3.2 A. USP10, β-Catenin and KI67 show a strong upregulation on protein-level in tumour tissues compared to the adjacent WT tissue. Furthermore, a difference in tissue organisation is observed between non-transformed and transformed tissue. Utilising the bioinformatic image analysis tool QuPath allowed for an unbiased analysis of overall staining intensity of each individual TMA core and enabled the direct comparison of protein abundance of the targets of choice. In figure 3.2 B the quantification of positive cells (%) per core from 37 tumour-cores and 35 WT-cores is shown. Indeed, we could observe that USP10, β-Catenin and KI67 were upregulated in transformed samples when compared to WT adjacent tissue (figure 3.2 A and B).
Additionally, to analyse protein level of USP10 and β-Catenin in non-fixed, fresh isolated human samples, tumour and adjacent WT tissue pieces were analysed on western blot. As shown in figure 3.2 C USP10 and β-Catenin were found to be upregulated in tumour samples compared to adjacent non-transformed patients samples. The upregulation of USP10 was about 2 - 3 fold when compared to the abundance in healthy control tissue.

A comparable observation was made for β-Catenin.

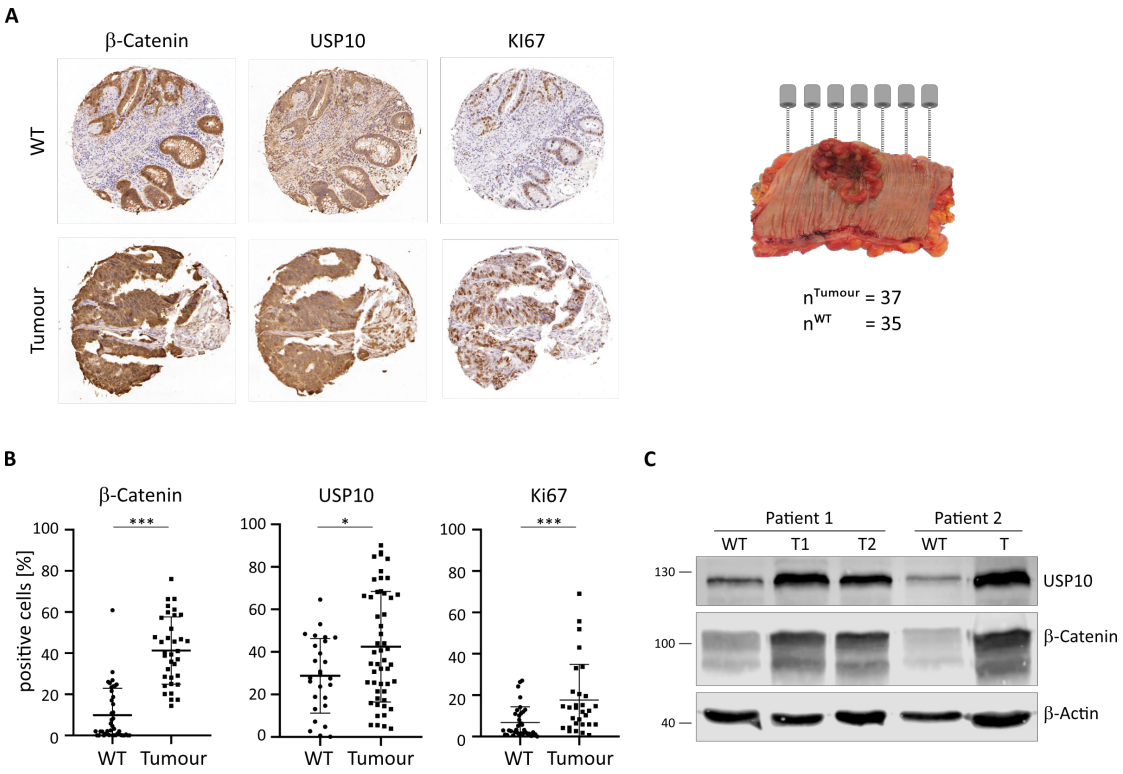

Figure 3.2: **Elevated protein-levels of USP10 and β-Catenin are found in in CRC patients**
A Tissue Micro Arrays (TMA) from local patients in Wuerzburg were subjected to Immunohistochemistry (IHC) and stained for USP10, β-Catenin and the proliferation marker KI67. 37 and 35 cores were classified as tumour and wild-type (WT) adjacent tissue, respectively. **B** Quantification of (A) using QuPath software. Significance was calculated using Mann-Whithney test. *p-value<0.05 **p-value<0.005 ***p-value<0.001 **C** Western blot of local patient samples. Tumour and WT adjacent tissue samples were blotted for USP10 and β-Catenin. β-Actin served as loading control.

With the analysis of USP10 expression in non-transformed tissue on transcript and protein level, we recognised that USP10 is not only expressed in colorectal cancer but also moderately expressed in healthy cells and even more in stem cell compartments (see normal core, figure 3.2 A). To further investigate the expression pattern of USP10 also in non-transformed tissue, immunofluorescence (IF) staining on a murine Apc^{ex10} small intestine was performed. In figure 3.3 an H&E staining as well as a high magnification of a transformed and non-transformed region are show. Interestingly, USP10 expression (green) is increased in the crypts compared to villi but gets overall upregulated upon transformation.
This data suggest an important function for USP10 not only in colorectal cancer, but also in stem cells.

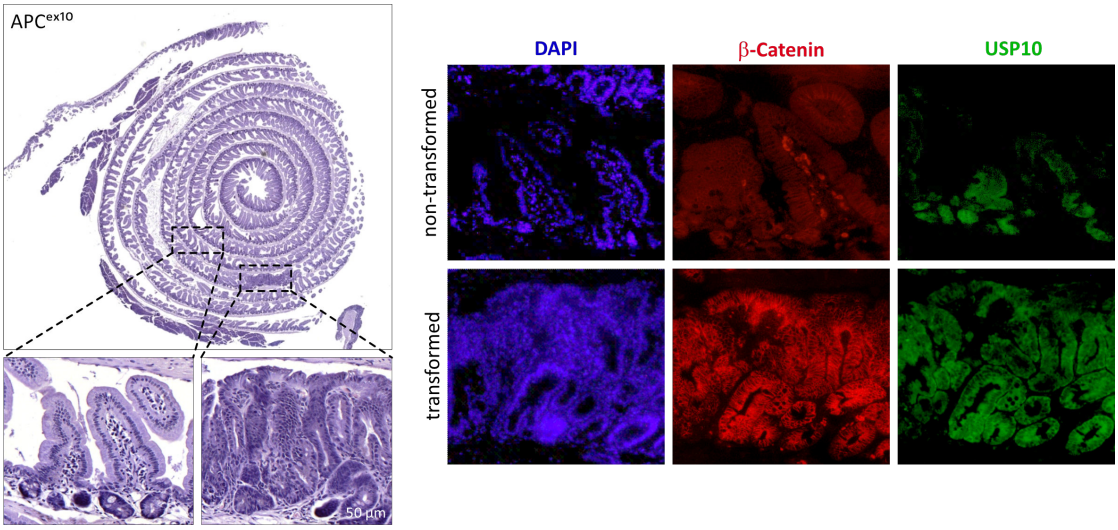

Figure 3.3: **USP10 expression localises to stem cells in untransformed tissue**
A left side: H&E staining of a murine Apc^{ex10} intestine with high magnification of a transformed and non-transformed region. Right side: IF staining of USP10 (green), β-Catenin (red) and DAPI as nuclear marker (blue). The expression of both proteins is restricted to crypt cells in the non-transformed intestine. In hyper-proliferative lesions USP10 and β-Catenin intensity increases throughout the whole transformed area.

Taken together, USP10 is indeed an important enzyme for colon tumours but also for highly proliferative cells, as seen by elevated levels of mRNA as well as protein in tumour samples and crypt cells, compared to untransformed tissue.

3.1.2 Binding of USP10 to β-Catenin is dependent on APC truncation mutation

Since in the initial siRNA-based DUB library screen changes in USP10 influenced β-Catenin protein abundance, a direct interaction of the proteins was hypothesised.
To test this proposed interaction, two different CRC derived cell lines were used, HCT116 as well as HT-29, and endogenous co-Immunoprecipiation (co-IP) experiments were performed. HT-29 cells were also used for the initial siRNA screen and are driven by an *APC* truncating mutation, while *CTNNB1* is genetically not altered. In contrast, HCT116 bear full-length *APC*, but carry a mutation in *CTNNB1* (S45A), resulting in degradation escape and aberrant, hence oncogenic, WNT signalling.
Both proteins, USP10 and β-Catenin were immunoprecipitated and subjected to SDS-PAGE followed by western blot. Interestingly, an interaction between USP10 and β-Catenin could only be observed in HT-29 cells, while in HCT116 cells no interaction was detected. It is important to note, that only by immunoprecipitating the bait, β-Catenin, the interaction with USP10 was observable. The reciprocal experiment, using USP10 as bait, failed to co-precipitate β-Catenin (figure 3.4 A).
Based on this result, it was hypothesised that the truncation mutation in *APC* could

lead to additional steric space in the destruction complex and thereby allows USP10 to enter and de-ubiquitylate β-Catenin (see hypothetical model in figure 3.4 B).

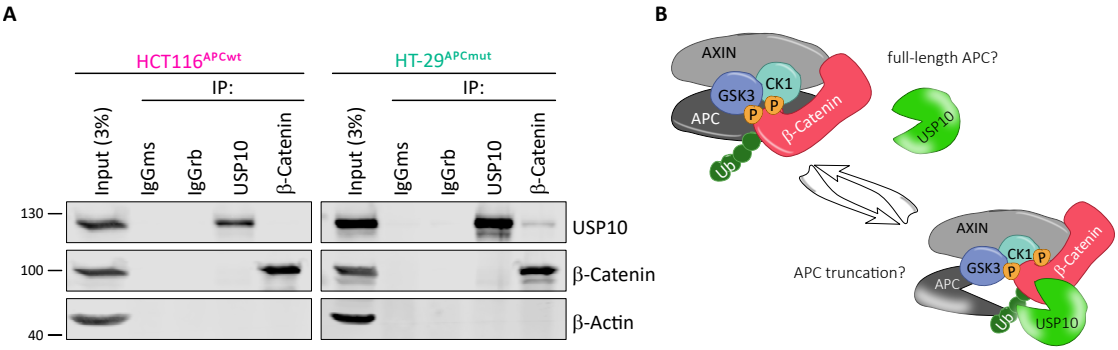

Figure 3.4: **USP10 and β-Catenin interact exclusively in APC truncated CRC-derived cell line**
A Endogenous co-IP of USP10 and β-Catenin in APC^{wt} HCT116 and APC^{mut} HT-29 CRC cell lines. **B** Model of putative mode of binding. APC truncation mutation enables interaction of USP10 and β-Catenin.

To further test the rationale that truncating mutations within *APC* are required to enable the interaction of USP10 and β-Catenin, six additional different CRC-derived cell lines, with different mutational background, were investigated. LS174T, like the previous introduced HCT116 cells, are driven by mutations in *CTNNB1* (S45F) and harbour no mutations in *APC*. Conversely, DLD-1, Caco-2 and SW480/SW620 originate from primary tumours driven by truncating mutations in *APC*, but still containing the 15- and 20- β-Catenin binding amino acid repeat (AAR) domains. Lastly, the CRC lines HT-29 and Colo320 were implied. HT-29 are heterozygous mutated in *APC*, bearing one allele with AAR left and one with a truncating mutation at amino acid 853. This mutation at amino acid 853 leads to the complete loss of 15- and 20- AAR, which is also the case for Colo320 cells, which have a homozygous truncation at aa811 in *APC* (as summarised in Fig 3.5 A)
The six cell lines where than subjected to an endogenous co-immunoprecipitation to elucidate the requirement of *APC* truncation, allowing the putative interaction of USP10 and β-Catenin. Surprisingly, and in contrast to our initial hypothesis, an interaction was, additionally to HT-29, observed in Colo320 cells, which have a very short remaining APC variant (figure 3.5 B).
Conclusively, these experiments indicate an interaction of USP10 and β-Catenin in an APC dependent manner. By performing endogenous co-immunoprecipitations in eight different colorectal cancer derived cell lines, which harbour various mutations, it could be demonstrated that at least heterozygous loss of the AAR domains was a prerequisite to facilitate binding of USP10 to β-Catenin. Hence, while several CRC-derived cell lines had mutations within *APC*, an interaction between USP10 and β-Catenin could exclusively be observed in HT29 and Colo320 cells.

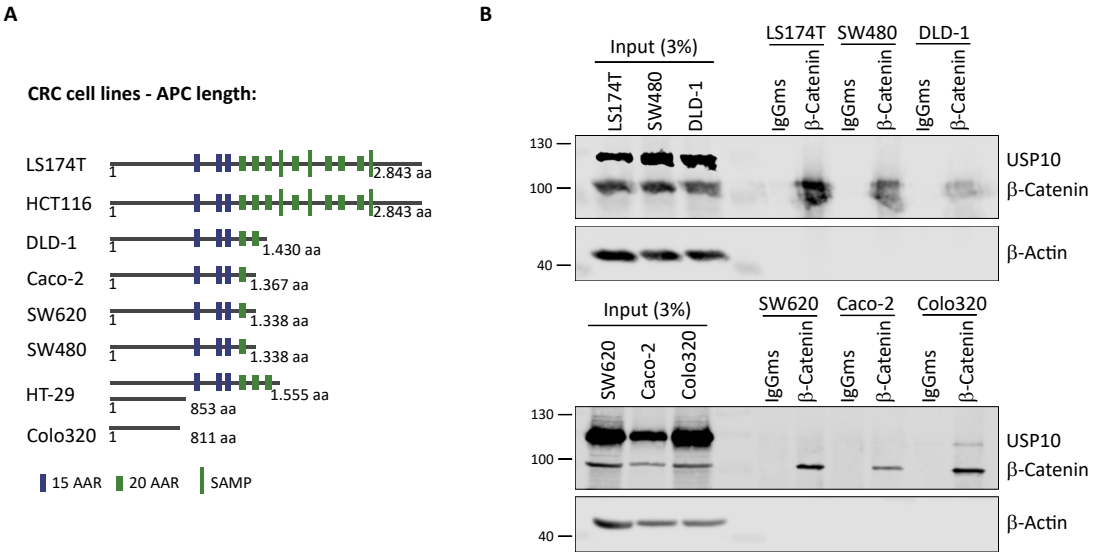

Figure 3.5: **A distinct truncating mutation in APC enables USP10-β-Catenin interaction**
A Schematic representation of APC protein domains for the different CRC-derived cell lines. 15- and 20-AAR = β-Catenin amino acid repeats; SAMP = Axin binding sites. **B** WB of endogenous co-IP in different cell lines. IP was performed by pulling on β-Catenin and IgG served as antibody-control.

3.1.3 USP10 regulates β-Catenin on protein level via its deubiquitylating activity

Until now, an *APC* truncation dependent interaction of USP10 and β-Catenin could be demonstrated. Additionally, in the initial siRNA screen, it was shown that USP10 knock-down also affected β-Catenin amount on protein level and therefore, a putative regulation of USP10 on β-Catenin stability should be investigated next.
Firstly, we strived for genetic deletion of USP10 in HT-29 cells. The CRISPR/Cas9 technology is a widely used tool to knock out a gene and thereby disrupt the protein completely. Here, a double guide approach, targeting two different exons of *USP10*, was utilized, as we assume that USP10 functions as proto-oncogene. While one guide RNA (gRNA) targeting exon 2 was cloned into the crisprV2 backbone, which also expresses the Cas9 enzyme and a puromycin-resistance cassette, enabling selection, a second gRNA, targeting exon 10, was cloned into the pLKO-GFP backbone (figure 3.6 A). The constructs were packaged as two individual lentiviruses and cells were co-infected with both particles simultaneously. For selection, puromycin as well as GFP were used. Since it was not possible to maintain USP10 knock-out (KO) single cell clones, cells were FACS sorted into GFP-low and GFP-high populations. The reduction of USP10 protein was equally good for the two individual populations as seen in figure 3.6 B. Upon depletion of USP10, a strong decrease in β-Catenin protein level was observed. Since β-Catenin regulates the transcription of several oncogenes and important intestinal stem cell markers, LGR5 was analysed as a surrogate marker for stemness. Indeed, an equally strong

decrease in LGR5 could be seen (figure 3.6 B). Next, the HT-29 USP10 KO cells were analysed on mRNA levels, to gain further insights into the patho-physiological consequences of loss of USP10 in CRC (see figure 3.6 C). CRISPR/Cas9-targeting of *USP10* yielded an mRNA depletion up to 50 %, when compared to control cells. Only mild changes were observed on *CTNNB1* mRNA levels, indicating that USP10 affects protein rather than mRNA levels. As a consequence, and in line with the observation made on overall protein abundance, the transcription of *LGR5*, a direct downstream target of β-Catenin, was moderately downregulated too.

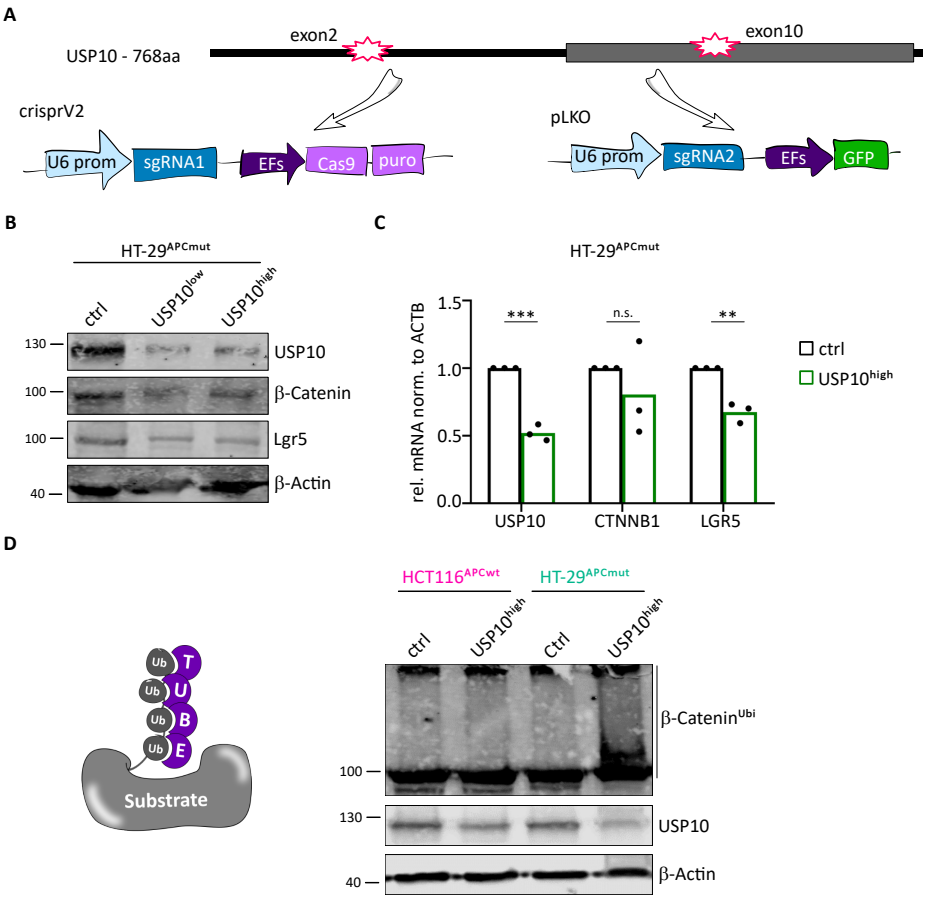

Figure 3.6: **Depletion of USP10 via Crispr/Cas9 alters β-Catenin on protein level** **A** Schematic model of the double guide approach, targeting *USP10* exon 2 and 10 by CRISPR/Cas9. **B** Representative western blot analysis of two different USP10 KO clones (low = FACS sorted clones with low GFP signal; high = FACS sorted clones with high GFP signal) compared to control cells. KO of USP10 also alters β-Catenin and Lgr5. β-Actin was used as loading control (n=3). **C** qRT-PCR analysis of USP10 high KO clones compared to control mRNA. Relative mRNA was normalised to *ACTB*. Three independent experiments are shown. Significance was calculated using unpaired t-test. *p-value<0.05 **p-value<0.005 ***p-value<0.001 **D** TUBE (Tandem Ubiquitin Binding Entities) experiment for the ubiquitylation pattern on β-Catenin upon depletion of USP10 in HCT116 and HT-29 cells. Representative western blot of two independent experiments is shown.

Taken together, these results indicate a regulation of β-Catenin by USP10 mainly on protein level, which could be, due to its deubiquitylating activity. To further proof this finding, Tandem Ubiqutin Binding Entities (TUBEs), which bind endogenous ubiquitin-chains on a substrate, were utilized. For the following experiment, and to reflect the observation regarding the mutational status of *APC* (wild-type or APC truncation), HCT116 and HT-29 USP10 KO cells were used. Control or USP10 KO HCT116 and HT-29 cells were incubated with the TUBE reagent and applied to SDS-PAGE followed by western blot. For APC wild-type HCT116 cells, no alteration in ubiquitinylated β-Catenin could be observed upon USP10 KO, compared to control cells. However, in the APC truncated HT-29 cell lines, a strong increase in ubiquitylated β-Catenin upon depletion of USP10 was detectable, when compared to control cells (figure 3.6 D).
As already mentioned before, it was not possible to maintain USP10 KO single cell clones, which is consistent with publicly available data (figure 3.7 A). When depleted via CRISPR/Cas9, 1064 out of 1086 cell lines showed a high dependency on USP10. Therefore, it was decided to utilise pooled populations in the previous experiments. Despite this effort, and in line with the large cancer cell screening data, also in pooled cell populations, a restoration of *USP10* mRNA could be observed via qRT-PCR, especially in longitudinal cell cultures (figure 3.7 B, data generated by Saskia Tauch and adapted from the corresponding Masterthesis).

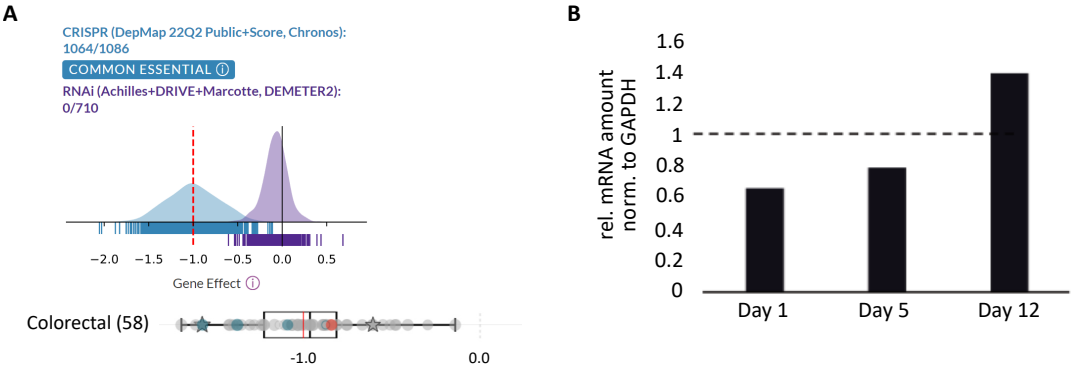

Figure 3.7: **USP10 is essential in CRC-derived cell lines**
A USP10 is considered as common essential in 513/769 cell lines, when depleted via CRISPR/Cas9. Data generated using www.depmap.org **B** qRT-PCR analysis of *USP10* mRNA in HT-29 USP10 KO cells, analysed at day 1, 5 and 12 after selection. Relative mRNA amount normalised to *GAPDH* (n=1).

Despite the strong data regarding essentiality of USP10 in the majority of human cancer cell lines, according to depmap.org data, it was suggested that modulation of USP10 levels via knock-down (KD) instead of knocking-out were feasible. To test this hypothesis and to generate a genetic tool to control USP10 abundance in cancer cell lines, constitutive as well as conditional shRNA mediated knock-down cells of USP10 were generated next.
For constitutive KD of USP10, two different shRNAs, as well as a non-targeting control (shNTC), were cloned into the pLKO-GFP backbone, followed by virual particle production and stable transduction of HT-29 cell. Successful reduction of USP10 was achieved using shUSP10-1 and -2, with the second one, showing strongest effects on β-Catenin

(figure 3.8 A). Additionally, the reduction of USP10 led to a decrease in proliferation, when compared to shNTC cells, as shown in the growth curve in figure 3.8 B. This finding is also consistent with the literature, where USP10 was described as an important regulator of proliferation in cancer [87], [88]. However, while longitudinal maintenance of USP10 depleted cells was possible, the extend of USP10 knock-down decreased and cells presented adaptive processes, negating the anti-proliferative phenotype over time (data not shown).

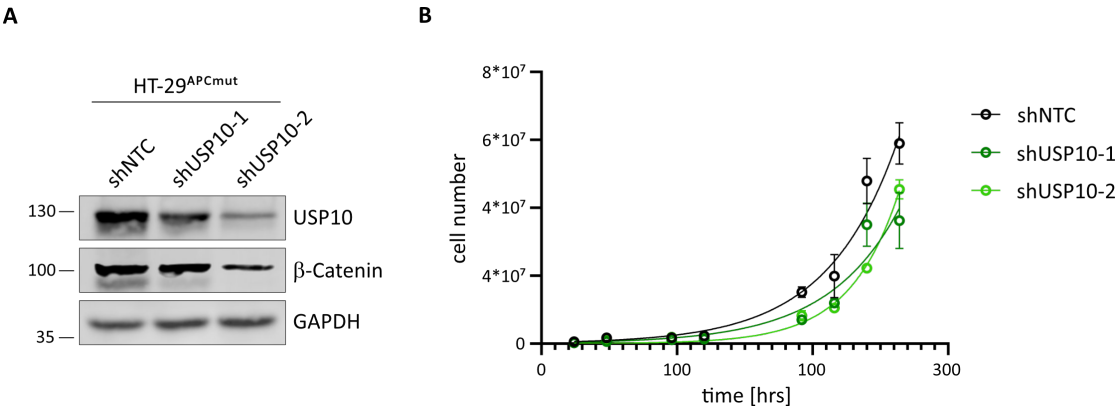

Figure 3.8: **Constitutive knock-down of USP10 alters β-Catenin protein level and decreases proliferation of cells**
A Representative western blot of shRNA mediated knock-down of USP10 compared to shNTC control cells. GAPDH served as loading control (n=3). **B** Growth-curve of shUSP10-1 and -2 knock-down cells compared to shNTC cells. Absolute cell number was counted over 10 days, error bars reflect S.D. (n=3).

In conclusion, this cellular system was not suitable to study the USP10-β-Catenin interaction on a physiological level. Therefore, a conditional knock-down of USP10 was established next. Two different shRNAs and a non-targeting control were cloned into a self-designed all-in-one lentiviral vector (pSico variant), encoding the reverse tetracycline-controlled transactivator (rtTA) under the control of a constitutive promoter (EFs) and a selection marker (puromycin). The expression of the individual shRNA was under the control of a tetracyclin-responsive element (TRE). Exposure of HT-29 cells, transduced with the viruses, to 0.5 ţg/mL doxycyclin (DOX) induces the binding of the rtTA to the TRE, hence, activating the expression of shRNAs. As shown in figure 3.9 A, the two shRNAs against USP10 lead to a strong reduction of USP10 protein upon DOX-treatment, however, no changes in protein level are observable for the ethanol control. To exclude any DOX-induced effects, shNTC and shUSP10 cells were treated with DOX and no ethanol control was used in the following experiments.

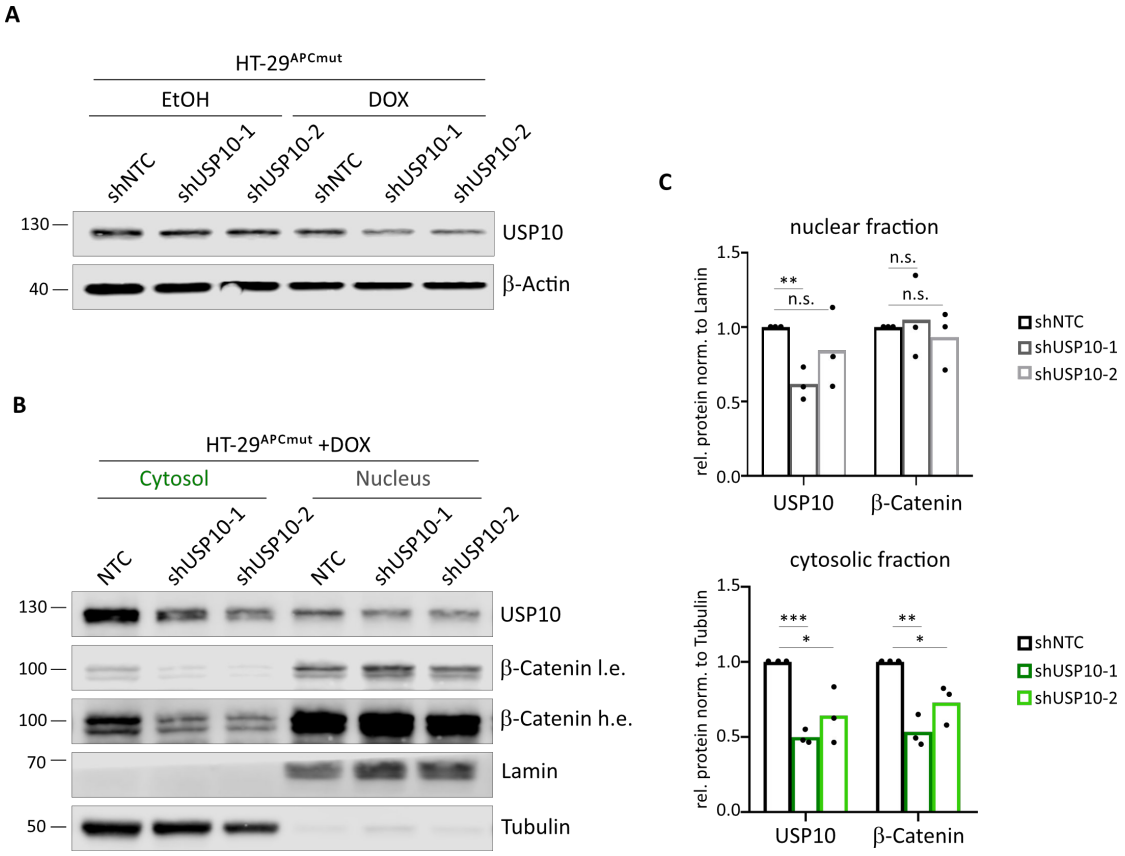

Figure 3.9: **Conditional knock-down of USP10 affects β-Catenin regulation mainly in the cytosol**
A Validation of DOX-inducible conditional knock-down in HT-29 cells with two different shRNAs against USP10. Cells were treated with doxycyclin for four days and than subjected to western blot (n=1). **B** Representative western blot of a cytosolic - nuclear fractionation in conditional shUSP10 HT-29 cells. Lamin and Tubulin serve as nuclear and cytosolic markers, respectively. **C** Quantification of changes in protein level for USP10 and β-Catenin from (B) for cytosolic and nuclear fractions. Significance was calculated using multiple unpaired t-tests of three independent experiments. *p-value<0.05 **p-value<0.005 ***p-value<0.001

To localise the USP10-β-Catenin interaction, a cytosolic-nuclear fractionation was performed. The inducible shNTC and shUSP10 cells were treated with DOX for four days and separated into a cytosolic, soluble fraction and the nuclear, membrane containing fraction. As shown in figure 3.9 B, the majority of USP10 protein can be found in the cytosol, but also a nuclear pool exists. However, for β-Catenin, the nuclear pool is the largest fraction, which is also consistent with the literature. For both proteins, the amount of cytosolic and nuclear protein were quantified and normalised to the corresponding marker proteins, lamin and tubulin (see figure 3.9 C). In both fractions, a significant reduction of USP10 upon shRNA mediated knock-down could be observed. But interestingly, only the cytosolic pool of β-Catenin is reduced significantly for both shRNAs targeting USP10.
Taken together, with an acute depletion of *USP10* it could be demonstrated that a reduction of USP10 effects mainly the cytosolic fraction of β-Catenin protein, indicating

a destruction complex dependent interaction of both proteins.

3.1.4 USP10-mediated regulation of β-Catenin leads to transcriptional changes in proliferation and stemness

With the aforementioned experiments, it was demonstrated that USP10 interacts with β-Catenin and regulates its stability via its deubiquitylating activity. Furthermore, interaction studies, performed in various CRC-derived cell lines, as well the cytosolic-nuclear fractionation immunoblotting upon USP10 KD suggest a destruction-complex depending role of the USP10-β-Catenin axis in the cytosol. However, the main function of β-Catenin during active WNT signalling is to activate the transcription of its target genes, such as *MYC*, *AXIN1/2*, *LGR5* and other stem cell and proliferation genes. The resulting transcriptional changes upon acute USP10 depletion should be investigated next by gene expression analysis.
For RNA sequencing, the strongest shRNA against USP10, shUSP10-1 and control shNTC expressing HT-29 cells were used. First, the amount of differentially expressed genes upon USP10 KD was analysed by generating an MA plot. Here, the log2FC is plotted against the log2CPM (counts per million reads) for the expression of shNTC vs shUSP10-1 and the extend of differential expression depends on the position of a gene relative to 0. Genes with a p-value below 0.05 are highlighted in red. Interestingly, only the minority of genes are significant differentially expressed between the two conditions. To further investigate which genes are differentially up- or downregulated upon *USP10* depletion, a volcano plot, showing log2FC in expression of shNTC vs shUSP10-1 against the -log10 p-value of the expression, was generated (see figure 3.10 B). Surprisingly, *USP10* and its known target gene *G3BP1* showed a mild log2FC around -0.4 (see figure 3.10 C). Nevertheless, known target genes of WNT signalling and proliferation were labelled on the left side in the volcano plot, showing a mild reduction upon USP10 KD. The log2FC of these genes was plotted in figure 3.10 C, together with USP10 and *G3BP1* as positive controls and *GAPDH* as a housekeeping gene. *KRT20*, which is a marker for differentiation, is upregulated. Interestingly, the main intestinal stem cell marker *LGR5* was the strongest differential expressed gene, with a log2FC of -0.5, among these chosen lists of genes. In line with these results, by performing gene set enrichment analysis (GSEA) against the Hallmarks of cancer data sets, both MYC target gene sets (MYC_targets_V1 and V2) as well as WNT target genes (WNT_β-Cat_signalling) were downregulated upon loss of USP10 when compared to shNTC (see figure 3.10 D). Interestingly, the G2M_checkpoint data set showed the strongest normalised enrichment score (NES) upon USP10 KD, which is in line with USP10s known function in regulating proliferation.

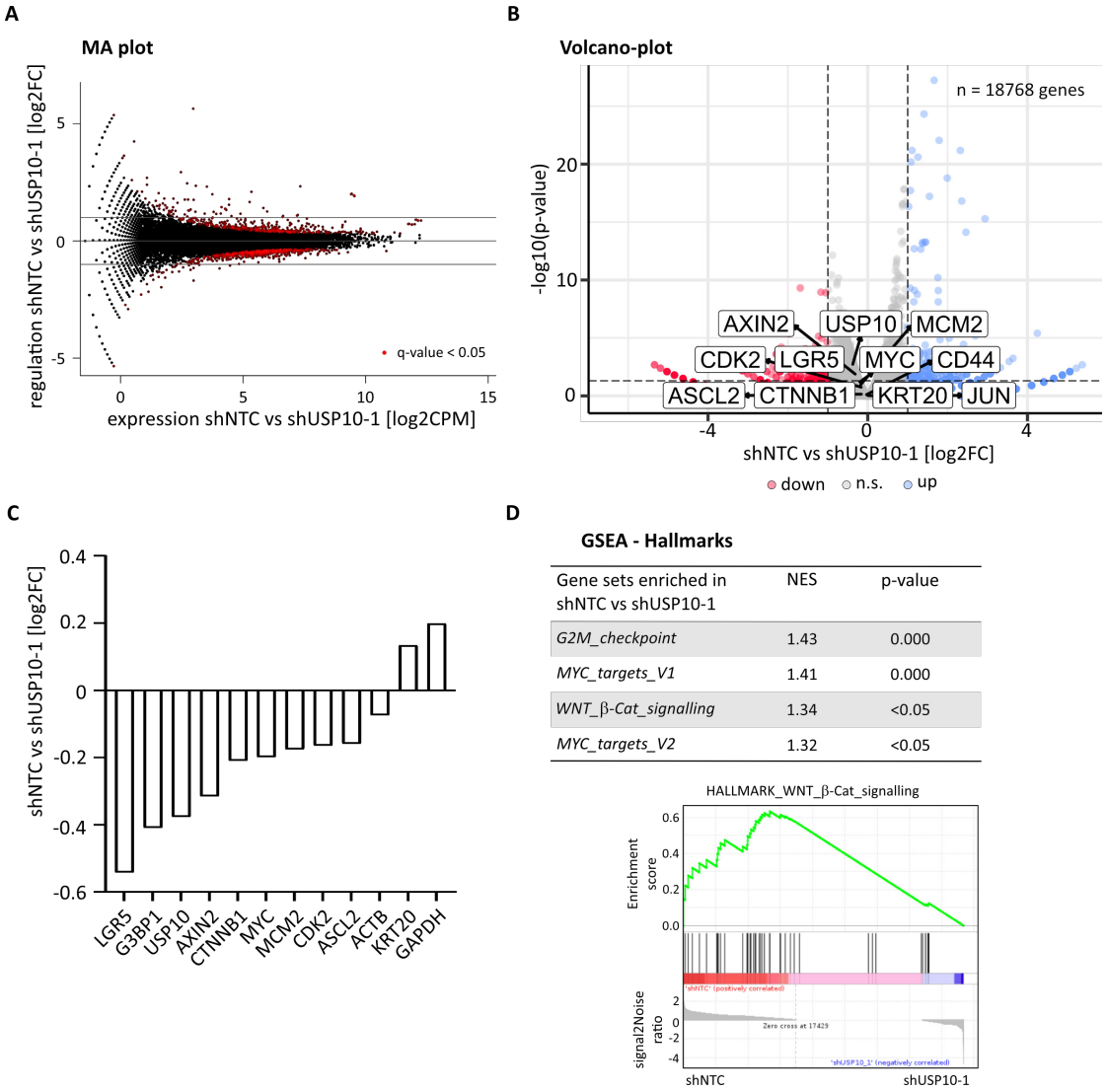

Figure 3.10: **Transcriptional analysis of USP10 KD in APC mutant HT29 cells**
A MA plot of shNTC vs shUSP10-1. Reduction of USP10 leads to only minor changes in gene expression. Significantly altered genes are labelled in red. **B** Volcano-plot of differential expressed genes upon KD of USP10. Up- and down-regulated genes are highlighted in red and blue, respectively. Genes-of-interest are labelled using enhanced volcano package in R. **C** Bargraph of log2 fold-changes of genes-of-interest from (B). **D** GSEA of shUSP10-1 vs shNTC.

Given that *LGR5* was the strongest differential expressed gene among the WNT signalling-related target genes, and that WNT signalling was significantly altered upon loss of USP10, it became interesting to analyse additional intestinal stem cell niche genes. To address this question, normalised counts from the suitable replicates from each condition (replicate 1,2 and replicate 2,3 from shNTC and shUSP10, respectively) were utilized to generate heatmaps for an intestinal stem cell gene list (please see [89] for further details). In figure 3.11 A and B, heatmaps for WNT signalling gene set and the intestinal stem cell gene set are shown. Closer analysis of the WNT signalling target gene set in shUSP10 cells (see figure 3.11 A), revealed a switch in expression of distinct genes,

including cyclins *CCNA2* and *CCND1*, EGF-receptor and the WNT signalling regulator *SOX9* (upper part of heatmap), which were downregulated in USP10 depleted cells.
Secondly, and while WNT controls proliferation and differentiation, next, the impact on stem cell niche was investigated. Figure 3.11 B represents the heatmap for intestinal stem cell genes in control and shUSP10 HT-29 cells. ShRNA mediated depletion of USP10 resulted in a significant downregulation of stem cell related genes. As an example, *LGR5*, *CD44* as well as *ASCL2* were downregulated upon USP10 depletion by shRNA. Furthermore, it was observed that the transcription factor *MEX3A*, which was described to regulate the pool of LGR5+ stem cells ([90]), is strongly downregulated in shUSP10 cells.
Despite the significant repression of the majority of stem cell genes, upon targeting of USP10, a subset of stem cell-related genes was upregulated in shUSP10 HT-29 cells. For example *IGFBP4*, a gene which was described to inhibit cancer cell growth among various cancer types, or *MARVELD1*, which was recently shown to downregulate β-Catenin expression and inhibit its translocation to the nucleus ([91]), were found to be upregulated in shUSP10 cells, when compared to control cells. This demonstrates the complex involvement of USP10 in WNT signalling and stem cell homeostasis.

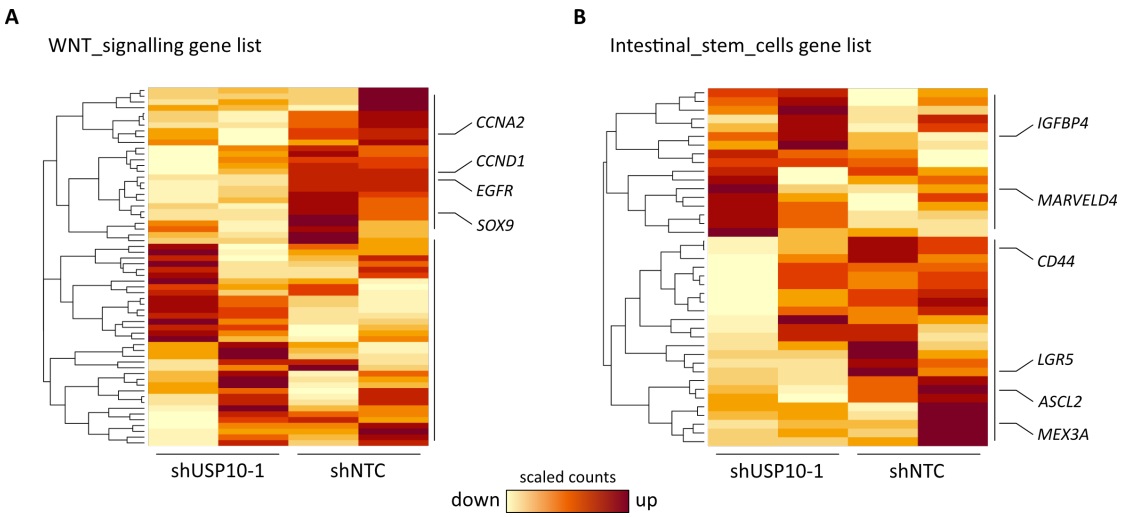

Figure 3.11: **Conditional knock-down of USP10 alters WNT signalling and stem cell identity**
A Heatmap of normalised counts of replicates #2, #3 from shUSP10-1 and replicates #1, #2 from shNTC regarding WNT signalling target genes. **B** Heatmap of normalised counts of replicates #1, #2 from shUSP10-1 and replicates #2, #3 from shNTC regarding intestinal stem cell genes.

Overall, by performing RNA sequencing, it was shown that acute depletion of USP10 in APC mutant HT-29 cells significantly affects the WNT signalling cascade and interfered with the expression of β-Catenin target genes. Additionally, loss of USP10 affected the expression of bona fide stem cell markers, such as *LGR5*. Furthermore, intestinal markers of stemness, such as *ASCL2*, *CD44* and *SOX9*, which are involved in the regulation of the pool of LGR5+ stem cells, were identified to be differentially expressed in shUSP10 cells.

3.1.5 Overexpession of USP10 in APC mutant HT29 cells activates transcription of stem cell markers and leads to increased proliferation

By analysing transcriptional changes upon USP10 knock-down in HT-29 cells, *LGR5* and additional stem cell markers, together with WNT signalling target genes were controlled in a USP10 dependent fashion. To investigate whether USP10 directly affects the protein abundance of these stem cell markers, DOX-inducible GFP-tagged USP10 WT overexpressing (OE) HT-29 lines were established and analysed.
As USP10 is a catalytically active deubiquitylase, a catalytical inactive mutant (C to A) was utilised as well, including a GFP-only control cell line. In figure 3.12 A a representative western blot of transduced HT-29 cells, overexpressing GFP-tagged USP10 variants, are shown. GFP has a molecular weight of about 27 kDa and therefore, the exogenous USP10 variants are detectable with a higher molecular weight, than the endogenous protein. Overexpression of USP10 WT increased β-Catenin, while the USP10 CA mutant as well as GFP expression on its own failed to increase β-Catenin. Surprisingly, it was also observed that the overexpression of USP10-WT resulted in elevated abundance of endogenous USP10, which is most likely caused by a possible auto-regulation of USP10. Interestingly, with the expression of USP10 WT, but not USP10 CA mutant, the mRNA expression of *USP10* and *CTNNB1* increased about 3.5-fold and 2.5-fold, respectively. Furthermore, a decrease in *KRT20* expression, which is a marker of differentiation, was observed (see figure 3.12 B). Consistent with the literature, cells overexpressing USP10 WT also showed an increase in proliferation, compared to GFP-control and USP10 CA mutant expressing cells, as can be seen in figure 3.12 C.
Next, to investigate whether USP10 overexpression also affects stem cell marker abundance, GFP-control, USP10 WT and USP10 CA mutant expressing cells were plated for immunofluorescent (IF) imaging analysis. Following exposure to 0.5 ţg/mL DOX for five days, cells were fixed and subjected to IF staining to detect the protein amount of USP10, β-Catenin, OLFM4, LGR5, ASCL2 and CD44. Analysis of staining intensity was performed using Operetta high-content microscopy. In figure 3.12 D, representative immunofluorescence images of all proteins-of-interest are shown and the intensity was quantified and plotted. For USP10, an increase in intensity was observed in cells transduced with either USP10 WT and CA mutant, compared to GFP-control cells. Next, the analysis of the intestinal stem cell marker expression in HT-29 cells revealed that all other proteins showed a significant increased abundance, when USP10 WT was overexpressed. Conversely, overexpression of the catalytic dead mutant or GFP alone, did not alter the overall abundance of stem cell markers, suggesting that USP10, as well as its catalytic activity, are involved in the control of stem cell marker expression.

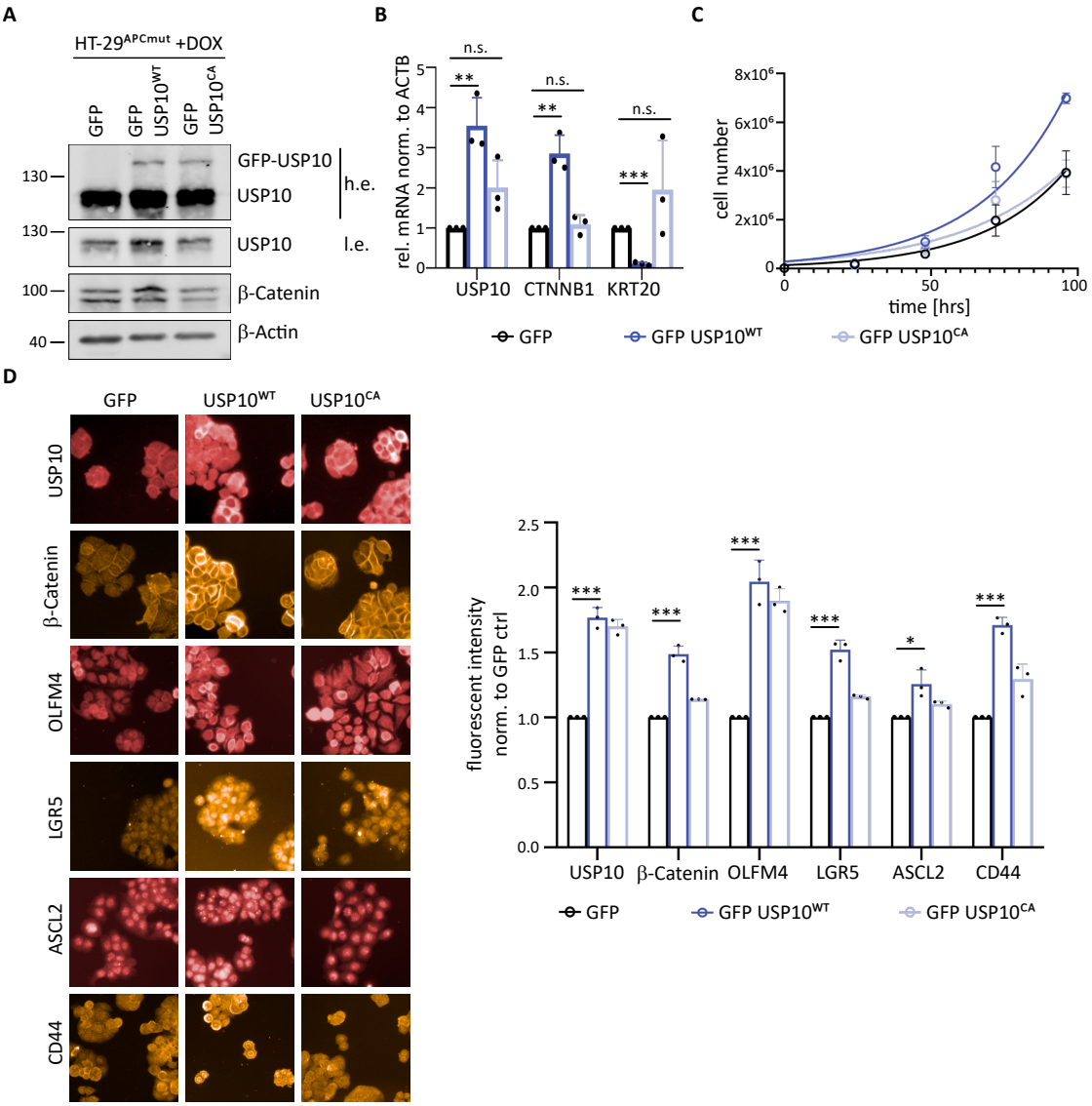

Figure 3.12: **Conditional overexpression of USP10 WT, but not catalytical inactive mutant, affects the expression of WNT target genes and impacts proliferation of cells**

A Representative western blot of DOX-inducible overexpression of GFP, GFP USP10^{WT} and GFP USP10^{CA} mutants in HT-29 cells. β-Actin served as loading control. For USP10, high exposure (h.e.) and low exposure (l.e.) blots are shown (n=3). **B** qRT-PCR analysis of GFP USP10^{WT} and GFP USP10^{CA} mutants compared to GFP control mRNA. Error bars reflect S.D. of three independent experiments. Significance was calculated using unpaired t-test *p-value<0.05 **p-value<0.005 ***p-value<0.001. **C** Growth-curve of USP10^{WT} and USP10^{CA} expressing cells compared to GFP control cells. Absolute cell number was counted over 4 days, error bars reflect S.D. (n=3). **D** Representative immunofluorescence images of conditional USP10 overexpression in HT-29 cells and quantification. Mean intensity over well was measured and normalised to GFP control cells intensity. Error bars reflect S.D. of three independent experiments. Significance was calculated using unpaired t-test. *p-value<0.05 **p-value<0.005 ***p-value<0.001

By performing RNA sequencing analysis of HT-29 cells depleted for USP10, in com-

bination with high-content microscopy of HT-29 cells overexpressing either WT or CA USP10, a direct regulation of the WNT signalling cascade, including target genes and intestinal stem cell markers, was discovered. The finding that only USP10 WT overexpression led to an increase of β-Catenin, LGR5, ASCL2 and CD44 protein, but not the expression of the catalytical inactive mutant, stresses the requirement of the deubiquitylating activity to fulfil its function in WNT signalling and CRC.

3.2 Usp10 is involved in intestinal homeostasis and transformation of murine intestinal organoids

USP10 is a novel regulator of β-Catenin stability in distinct human CRC-derived cell lines. Furthermore, USP10 KD experiments in hyper-proliferative midguts of *Drosophila melanogaster*, upon truncation of *Apc*, revealed a strong downregulation in the abundance of stem cells (data not shown in this work and reported in the Masterthesis by Saskia Tauch). Since β-Catenin is an important transcriptional co-activator of stem cell genes, and given that USP10 seems to be involved in the regulation of stemness, murine intestinal organoids were employed next. This system allows the cultivation of genetically non-altered, wild-type multicellular mini-intestines and their genetic modulation by CRISPR/Cas9. Furthermore, utilising this system enables not only control of disease onset and progression, but also the genetic alteration inflicted to initiate disease causing steps. It allows to study stem cell properties and tumour growth in respect to USP10 abundance in a novel *ex vivo* system.

3.2.1 Establishment of murine intestinal organoids to model the APC-dependence in an *ex vivo* system

During this thesis, the isolation and cultivation of murine intestinal organoids was established. In figure 3.13 A the schematic morphology of murine intestinal WT and transformed organoids, together with representative brightfield images is shown. WT organoids represent a multi-cellular system, reflecting the typical crypt-villus structure of the intestine, which can be seen by the morphology of outgrowing villi and crypts in-between (left site of fig 3.13 A). Upon transformation, nearly all cells are equally proliferative and the organoids grow in their typical cystic form (right site of Fig 3.13 A). To study the role of USP10 in tumourigenic organoids, WT organoids from a stable Cas9 expressing mouse were isolated and genetically modified by using CRISPR/Cas9. In figure 3.13 B, the schematic model for transformation is shown. In brief, three sgRNAs, targeting *Apc* exon 9, *Trp53* and *KRas*, together with the corresponding repair template, were packed in an adeno-associated virus (AAV) and used for infection of WT organoids. Targeting of exon 9 within the *Apc* gene creates a mutant variant, which is devoid of all AAR domains. These organoids were then selected via withdrawal of medium, as described by Matano *et al.* [75]. Deletion of *Apc*, irrespective of localisation, would lead to an R-spondin independent growth of organoids. Furthermore, hyperactive KRas signalling will negate the requirement for EGF supplementation. As shown in brightfield images in figure 3.13 C, after one week of selection, R-spondin and EGF independent

organoids could be established, which show the characteristic cystic morphology. The established organoids were further characterised using immunoblotting against β-Catenin and p-Erk1/2, as surrogate markers of *Apc* truncation and hyperactive KRas signalling, respectively (see figure 3.13 D). Organoids derived from a constitutive Cas9 mouse or *Apc*:*KRas*^{G12D} organoids served as either wild-type or CRC model specific control, respectively. Of note, the p53 status of these organoids is not critical for the following experiments and at the time of this thesis, genetic proof of CRISPR/Cas9 mediated deletion of *Trp53* is missing. However, based on the laboratory experience with *in vivo* CRISPR, it was assumed that deletion occurred in most organoids arising upon infection and medium-mediated selection [92].

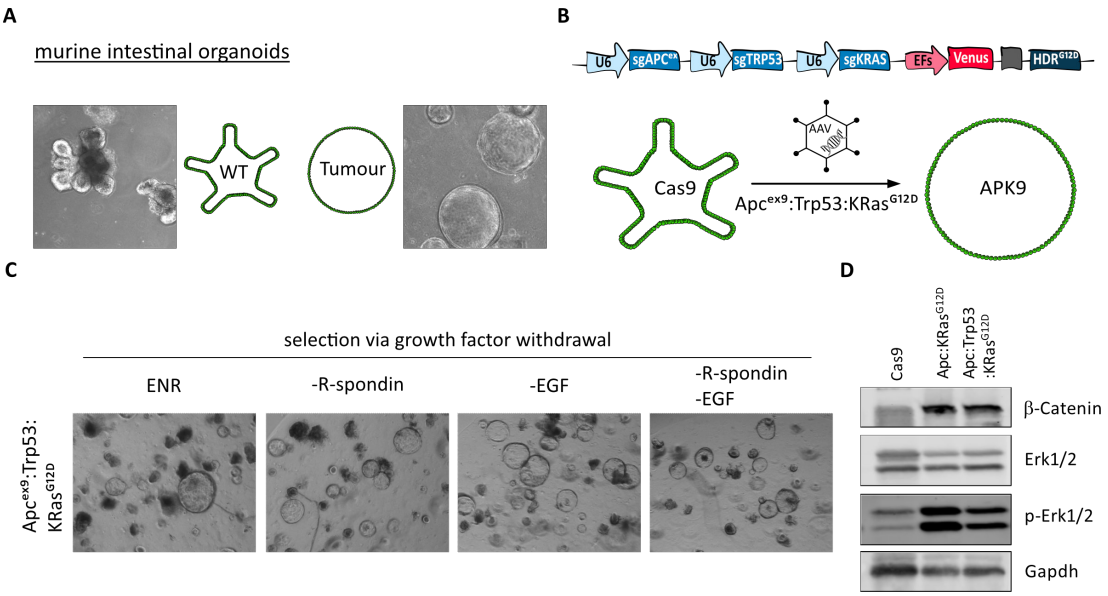

Figure 3.13: **Generation and characterisation of murine intestinal tumourigenic organoids**
A Brightfield images and corresponding scheme of WT and tumourigenic murine intestinal organoid morphology. **B** Schematic model of plasmids used for infection of Cas9 organoids. sgRNAs targeting *Apc* in exon 9, *Trp53* and *KRas* with corresponding HDR-template under the control of the U6-Promoter. Infection strategy via AAV and expected morphological change upon organoid transformation. **C** Representative brightfield images of infected organoids 1 week post infection (p.i.). Selection of successfully infected organoids was achieved via withdrawal of distinct medium-components. ENR - EGF, Noggin, R-spondin. **D** Western blot analysis of infected AK and APK9 organoids compared to control. β-Catenin and p-ERK1/2 served as downstream target for Apc truncation and KRas acivation, respectively. Gapdh served as loading control.

These novel genetically defined *Apc*:*Trp53*:*KRas*^{G12D} organoids (from now on referred to as mAPK9) were now employed to decipher the role of USP10 in an *ex vivo* multicellular intestinal cancer model system.

3.2.2 Altered levels of USP10 effect the expression of WNT signalling and differentiation genes in murine intestinal organoids

Firstly, to alter the abundance of USP10 in tumour organoids, two different shRNAs against Usp10, along with a non-targeting control shRNA were utilised to study effects of Usp10 depletion. Secondly, by overexpression of a human USP10 WT construct (see section 3.1.5), the role of Usp10 on the stem cell and differentiation program was investigated. As shown in figure 3.14 A, initial morphological analysis of mAPK9 organoids, transduced with shRNA Usp10-1 and -2, when compared to shNTC organoids, revealed that both organoid lines were slightly smaller and presented a less homogeneous cystic morphology. In contrast, overexpression of human USP10 WT did not affect the cystic growth of mAPK9 organoids. To validate the effect of the shRNAs as well as the overexpression, Usp10 protein level was validated via western blot (see figure 3.14 B). Both shRNAs led to a reduction in endogenous Usp10 down to 40 % remaining, whereas the hUSP10 WT overexpression led to an increase up to 130 %, when compared to shNTC organoids. Furthermore, the knock-down of Usp10 led to a reduction of β-Catenin protein to 50 % and 80 %, respective to shRNA. Surprisingly, no significant increase in β-Catenin could be observed upon hUSP10 overexpression. If an overall oncogenic saturation of β-Catenin abundance in mAPK9 organoids was already established, which could not be further enhanced, is currently unclear but will be addressed in the future. To investigate the afore observed effects of USP10 on β-Catenin and WNT signalling targets, and if these regulations are conserved in organoids, qRT-PCR was performed (see figure 3.14 C). Both shRNAs targeting Usp10 led to a strong decrease of *Usp10* mRNA, but did not affect *Ctnnb1* mRNA. However, the expression of Ctnnb1 target genes *Myc* and *Ccnd1* was decreased upon shUsp10-1 and -2. The stem cell marker *Lgr5*, however, showed varying results depending on the used shRNA against Usp10. For shUsp10-1, which showed the strongest effect on β-Catenin protein level, a 3.5-fold increase in *Lgr5* mRNA was observed. In contrast, upon shUsp10-2, which showed a milder effect on *Ctnnb1*, the *Lgr5* mRNA did not change significantly.
This was an interesting observation which cannot be fully explained at this point but could highlight a compensatory mechanism in tumour organoids to counter the antiproliferative effect of Usp10 loss. Further work is required to elucidate this mechanism. While the overexpression of human USP10 in organoids had no effect on β-Catenin protein abundance, also almost no significant alteration on mRNA for neither *Ctnnb1* nor the described Wnt signalling target genes, could be detected.

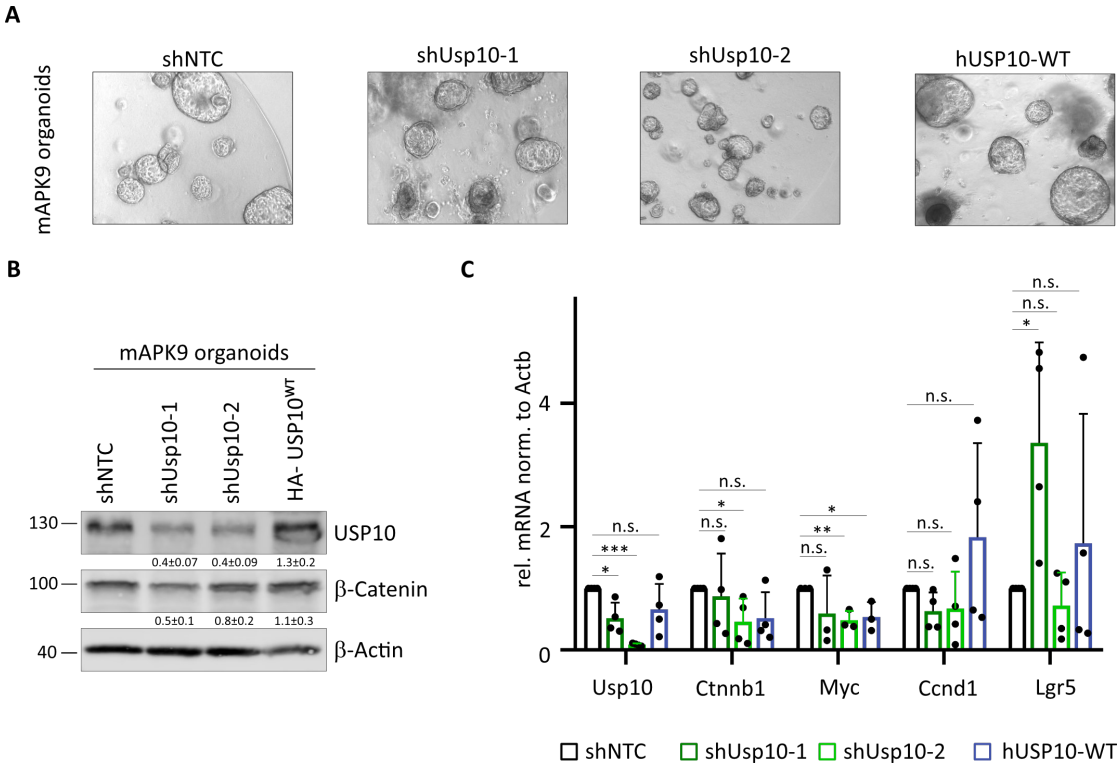

Figure 3.14: **Constitutive knock-down and overexpression of Usp10 in intestinal APK9 organoids alters β-Catenin protein and expression Wnt signalling target genes**
A Brightfield images of stable transformed murine intestinal organoids. Two different shRNAs against Usp10, human USP10 WT overexpression and shNTC expressing organoids are shown. **B**. Representative western blot of Usp10 and β-Catenin protein upon Usp10 KD and OE. β-Actin served as loading control. Quantification was calculated from three independent experiments. **C** qRT-PCR analysis of Usp10 KD and OE compared to mAPK9 control organoids. Error bars reflect S.D. of four independent experiments. *Actb* served as housekeeping gene. *p-value<0.05 **p-value<0.005 ***p-value<0.001

To get a more detailed overview of the physiological effects upon alteration of Usp10 levels in 3D, the generated and validated organoids were now subjected to RNA sequencing. In the previous experiment, where USP10 KD CRC-derived cell lines were applied to RNA sequencing, only minor changes in deregulation upon KD were observed (see figure 3.10 A). This minor impact on regulation of gene expression could be a) due to the role of USP10 as deubiquitylase and therefore mainly affecting protein level rather than mRNA or b) because of a lack of suitability of the model system, as human CRC lines only express low levels of stem cell genes and often present altered expression profiles when compared to the primary lesion. To answer this question, MA plots, comparing the regulation (log2CPM) vs expression (log2FC), were generated. Indeed, significant more changes in the transcriptional program upon KD of Usp10 in organoids could be observed, as shown in figure 3.15 A. Of note, the MA plots for the remaining conditions, shNTC vs shUsp10-2 and shNTC vs hUSP10-WT, resulted in a similar level of deregulated genes and are presented in the appendix.

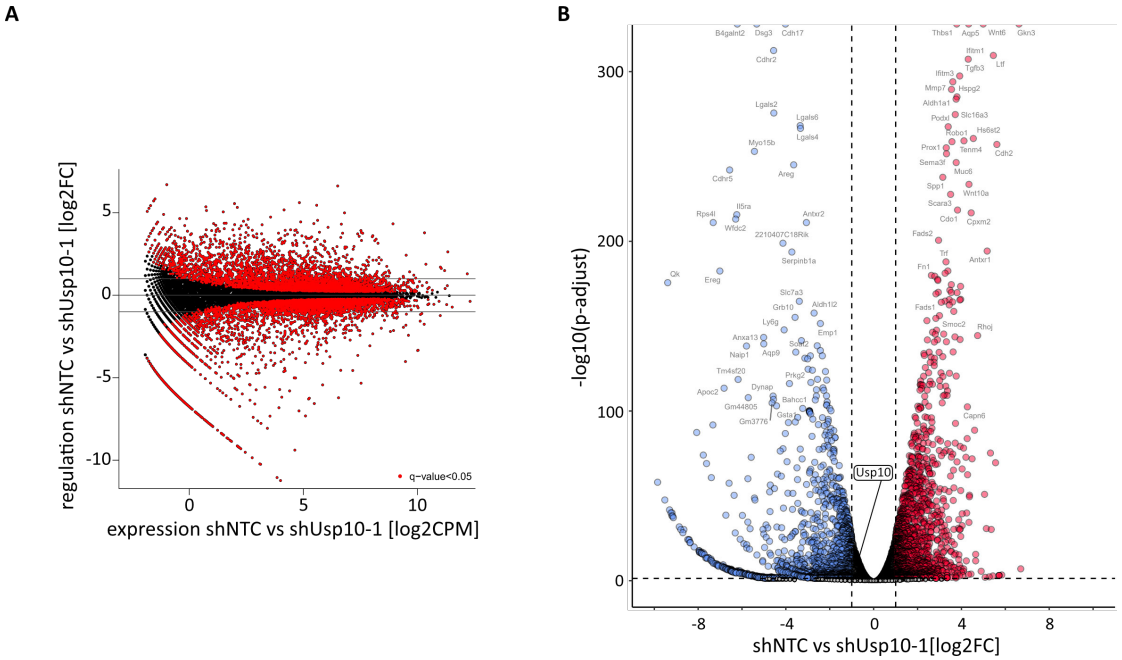

Figure 3.15: **RNAseq analysis of Usp10 knock-down murine APK9 organoids**
A Representative MA plot for shNTC vs shUsp10-1 in mAPK9 organoids. KD of Usp10 leads to huge changes in transcriptional program. **B** Representative volcano plot of differential expressed genes for shNTC vs shUsp10-1. Significantly expressed genes were defined with a log2FC greater than 1, -1 and a p-adjust greater than 0.05. Significantly up- and downregulated genes are coloured in red and blue, respectively. Genes with a p-adjust greater than $1e^{-100}$ and Usp10 are labelled.

To investigate and visualise the most significant deregulated genes upon knock-down and/or overexpression of Usp10 in mAPK9 tumour organoids, volcano plots of differentially expressed genes were generated and the volcano plot for shNTC vs shUsp10-1 is shown in figure 3.15 B. Since the extend of significant up-and downregulated genes was similar for all three condition, the remaining two volcanos can be found in the appendix. However, for all three conditions, namely shNTC vs shUsp10-1, shNTC vs shUsp10-2 and shNTC vs hUsp10-WT, the log2FC of expression was plotted against the -log10 of the p-adjust value. Genes with a log2FC greater than 1 and lower than -1 and a p-adjust lower than 0.05 were defined as significantly up- and downregulated, respectively. Although Usp10 itself was found to be downregulated upon shRNA-1 and -2 only 0.5-fold and 1.2-fold, respectively, the overall amount and distribution of significantly up- and downregulated genes was comparable for the two conditions. In case of the human USP10-WT overexpression, endogenous Usp10 was upregulated only mild (0.5 fold), which would be consistent with the effect observed already on western blot (see figure 3.14 B).
When comparing the most downregulated common genes between shUsp10-1 and -2 with the most upregulated genes upon hUSP10 overexpression (defined with a p-adjust value below $1e^{-100}$, labelled genes in the volcano plots), no overlap could be found. However, in previous experiments the level of regulation from Wnt signalling and stem cell genes was always rather moderate. Therefore it was decided to investigate not only the most differential expressed genes but to enlarge the range of analysed genes with a p-adjust value

below 0.05. In figure 3.16 A, a venn diagramm of all significantly downregulated genes upon shUsp10 and upregulated genes upon USP10 WT overexpression can be found and 169 genes match these conditions. To investigate the physiological consequences of KD and OE of *USP10* in mAPK9 organoids, a pathway analysis of these common deregulated genes was performed. Interestingly, among the 5 different pathways, altered in the described conditions, Wnt and cadherin signalling pathways were deregulated in a Usp10 dependent fashion, consistent with the data from the 2D cell culture experiments (see figure 3.16 B).

To get a more detailed overview of transcriptional changes upon alteration of Usp10 levels, a list of Wnt signalling target genes was generated and Reads Per Kilobase Million (RPKM) values for each condition and each replicate were analysed regarding this gene list. As shown in figure 3.16 C, three main clusters can be found. The first cluster, which comprises genes which are downregulated upon shUsp10-1 and -2 compared to shNTC organoids, included e.g. the transcription factors *Myc* and *Sox9*. The second cluster of the heatmap comprised for example the epithelial marker *Cdh1* and the WNT antagonist *Sox17*, among others. These genes are upregulated upon shUsp10-1 compared to control organoids and their expression is reduced in the hUSP10-WT overexpression [89]. In the third cluster, found in the upper part of the heatmap, genes which are exclusively upregulated upon USP10 WT overexpression are located. *Fgf20*, *Cd44* and *Twist1* are examples in that cluster and emphasise USP10s role as oncogene in CRC.
A major observation from the RNA sequencing in 2D, using the human CRC line HT-29, was the alteration in WNT signalling, stem cell markers and the differentiation program upon knock-down of USP10. To confirm if these regulations are transferable to the 3D organoid system, the differentially expressed genes upon shRNA mediated knock-down of Usp10 in mAPK9 organoids were analysed.

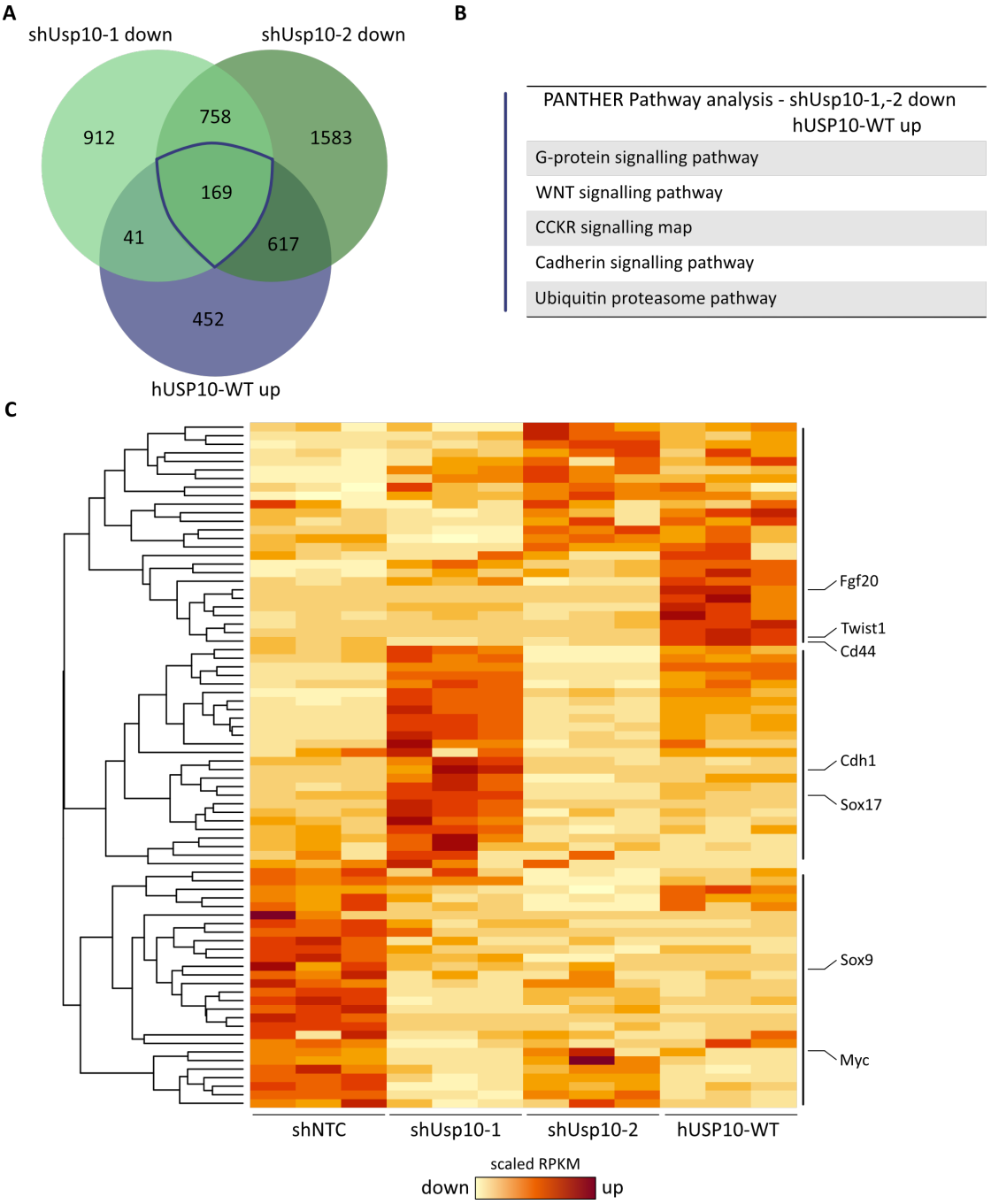

Figure 3.16: **Pathway analysis of differential expressed genes which are downregulated upon both shRNAs and upregulated upon hUSP10-WT overexpression**
A Venn diagram of DEG in all three conditions. 169 genes are downregulated in shUsp10-1 and -2 and upregulated upon hUSP10-WT overexpression. Venn diagram was generated using https://bioinformatics.psb.ugent.be/webtools/Venn/. **B** PANTHER pathway analysis of overlapping genes from (A). Analysis was performed using http://pantherdb.org/. **C** Heatmap of RPKM values from each condition for Wnt signalling target genes.

By performing RNA sequencing, similar changes in Wnt signalling pathway were observed in organoids when Usp10 was reduced (see figure 3.16). By analysing the ex-

pression of Wnt signalling genes among all four conditions it became obvious that the shUsp10-1 showed strongest effects, when compared to control organoids.
Based on this observation, it was decided to investigate the transcriptional changes in those two conditions in more detail. When analysing the changes in shUsp10-1 organoids regarding differentiation and late transit-amplifying gene (late TA gene) signatures (see figure 3.17 A), the expression of these genes was globally altered between the two conditions. For both gene signatures, the analysed genes cluster into two groups, pointing out major changes in the differentiation program as well as the late TA amplifying signature upon knock-down of Usp10.

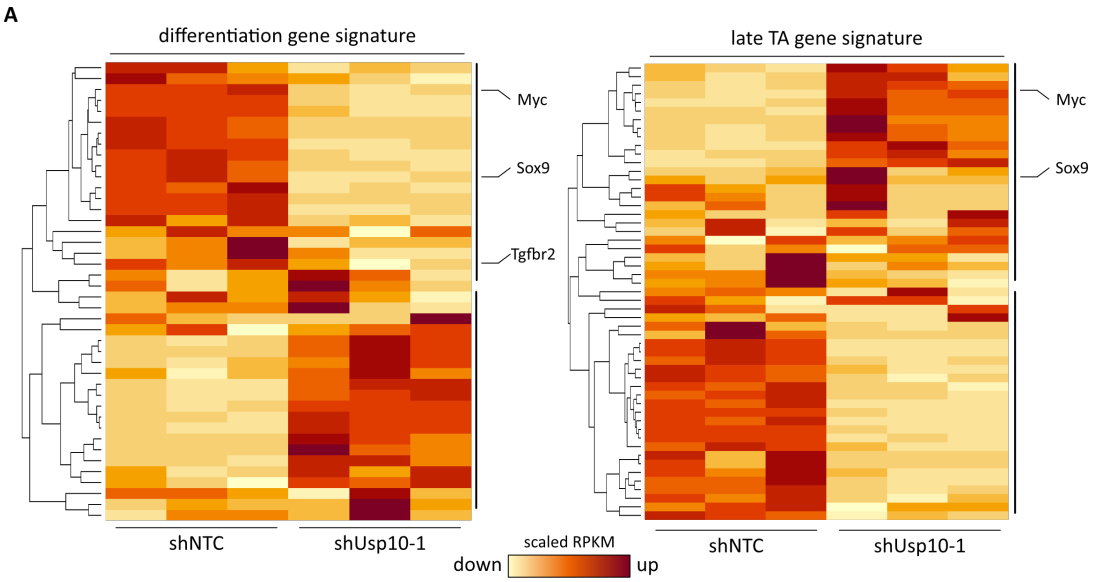

B

Gene sets enriched in shNTC	NES	p-value
KRAS_signalling_up	1.40	<0.05
incr_metastatic_potential	1.70	<0.005

Gene sets enriched in shUsp10-1	NES	p-value
GOBP_neg_reg_of_WNT_signalling_pathway	-1.97	0.000
KRAS_signalling_down	-1.39	<0.05

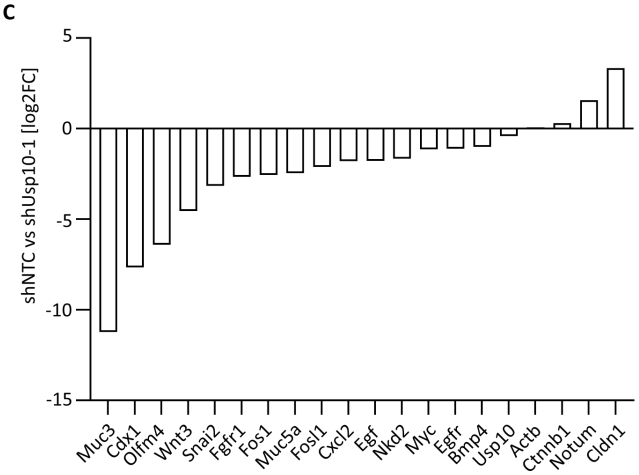

Figure 3.17: **Intestinal stem cell genes and Wnt signalling target genes are deregulated in shUsp10-1 organoids**
A Heatmap of RPKM values from shNTC vs shUsp10-1 regarding differentiation and late transit-amplifying gene signatures. **B** Gene set enrichment analysis for shNTC vs shUsp10-1. Gene sets enriched in shNTC and shUsp10-1 organoids are summarised. **C** Bar graph showing log2FC for genes-of-interest.

Consistently, when performing a gene set enrichment analysis, gene sets, corresponding to tumourigenic activities (metastasis and active KRas signalling), were enriched in control organoids. Furthermore, negative regulators of Wnt signalling and decreased KRas signalling gene sets were enriched upon knock-down of Usp10, as summarised in figure 3.17 B. As stated before, the changes in Wnt signalling and stem cell maintenance are rather mild and therefore the log2FC for distinct genes were analysed in figure 3.17 C. *Usp10* is only slightly reduced upon shUsp10-1, however the expression of other important members of the Wnt signalling pathway, for example *Muc3*, *Olfm4*, *Wnt3* and *Muc5a* is decreased significantly.
In summary, altered levels of USP10 in *in vitro* and *ex vivo* systems affected the abundance of the important transcriptional co-activator β-Catenin and thereby led to changes in the transcriptional program regarding Wnt signalling targets, stem cell properties and differentiation. The effects observed in 3D organoid models, were more pronounced compared to CRC-derived cell lines. This result is hardly surprising, since organoids exist of various different cell types and therefore resulting alterations in one cell can affect the neighbouring cells and even moderate transcriptional effects can potentiate to a stronger phenotype.

3.2.2.1 Usp10 contributes to epithelial-to-mesenchymal transition in tumour organoids

Among the top deregulated gene sets upon alteration of Usp10 abundance in mAPK9 organoids, another interesting pathway caught our attraction. In USP10 WT overexpressing as well as Usp10 KD organoids, epithelial-to-mesenchymal transition (EMT) related gene sets were significantly deregulated (see figure 3.18 A). This result was in line with the phenotypic observation that USP10-WT overexpressing HT-29 cells attached less to cell culture dishes and appeared more easy to detach. Firstly, to investigate whether EMT also played a role in 2D cell culture, USP10 WT and CA mutant HT-29 cells were analysed. A well known marker for epithelial cells is E-cadherin, being involved in cell-cell-contacts. Together with its counteracting mesenchymal marker protein N-Cadherin, those two proteins are ideal markers of EMT [93]. As shown in figure 3.18 B, HT-29 control and USP10 CA mutant cells express high levels of E-cadherin, compared to USP10 WT expressing cells. However, the expression of the mesenchymal marker protein N-cadherin was significantly increased upon USP10 WT overexpression, when compared to control cells. Additionally to the data from 2D HT-29 cells, EMT-related genes in mAPK9 organoids, dependent on Usp10 abundance, were investigated in more detail. Aiming this, a list of genes, involved in EMT, was generated and RPKM values from shNTC, shUsp10-2 and hUSP10 WT were analysed regarding this list. In figure 3.18 C and D, the corresponding heatmaps are shown. When comparing shNTC organoids to hUSP10 WT organoids, the majority of genes, e.g. *Zeb1*, *Notch1* and *Col1a1* are upregulated upon overexpression of USP10 WT. In line with this, cell-cell contact related genes, for example *Jup*, are downregulated in USP10 WT overexpressing organoids, when compared to shNTC (see figure 3.18 C). Conversely, genes which are known to be involved in EMT, e.g. *Vim*, *Cdh2* (encoding for N-Cadherin) and *Ctnnb1* itself, are downregulated upon knock-down of Usp10, when compared to shNTC organoids

(figure 3.18 D).
Noteworthy, the effects on EMT-related genes are even more striking upon Usp10 downregulation. According to literature, the mutational combination of *Apc*:*Trp53*:*KRas*^{G12D} already leads to an invasive phenotype of CRC and recapitulates an advanced stage, therefore, EMT-related genes are most likely already upregulated and downregulation of Usp10 affects these transcriptional changes even more.

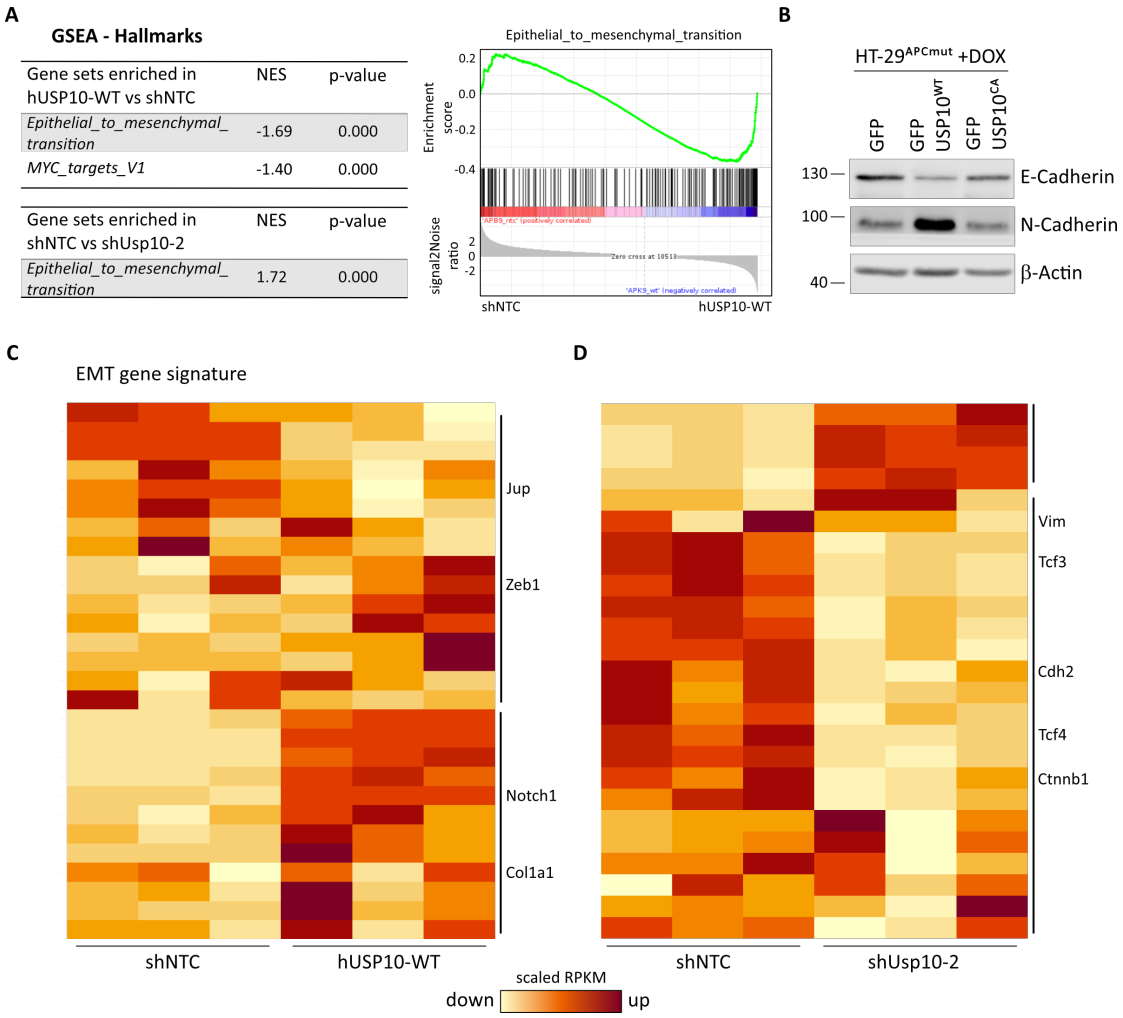

Figure 3.18: **Usp10 contributes to epithelial-mesenchymal-transition in tumour organoids and 2D HT-29 cells**
A Gene set enrichment analysis for shNTC vs shUsp10-1 and hUSP10-WT organoids. Representative GSEA plot is shown for epithelial_to_mesenchymal_transition enriched in hUSP10-WT. **B** Representative western bot for E-cadherin and N-Cadherin expression in USP10-WT and USP10 CA mutant overexpressing HT-29 cells, compared to GFP control cells. β-Actin served as loading control. (n=2) **C** Bar graph showing log2FC for genes-of-interest. **C** and **D** Heatmap of RPKM values from shNTC vs hUSP10-WT and shUsp10-1 regarding EMT gene signatures, respectively.

Conclusively, Usp10 overexpression contributes to EMT in 2D HT-29 cells and down-regulation of Usp10, in line with the previous observation, represses the transcription of mesenchymal marker proteins in murine tumour organoids.

The results of this thesis via genetic alteration of USP10 level inevitable lead to the question for targeted inhibition of USP10 and if it holds a therapeutic benefit. Small molecule inhibitors against USP10 would be ideally suited as novel therapeutic strategy, since previous data presented in this thesis highlighted the necessity of the catalytic activity for the *in vivo* function of USP10 in cell proliferation and stemness maintenance. This question will be explored in the following chapter.

3.3 Inhibition of USP10 in CRC-derived cell lines

Besides USP10s role as a novel regulator of β-Catenin stability in colorectal cancer, first described in this thesis, it was already established as an important oncogene in other cancers. As an example, in acute myeloid leukemia (AML), USP10 was described as a critical DUB for oncogenic FLT3. The authors could show that targeting USP10 provided a potential therapeutic window in treating oncogenic-FLT3-driven leukemia [94]. Furthermore, USP10 was also described in inhibiting the p53 signalling pathway via de-ubiquitylation and stabilisation of G3BP2 in prostate cancer [54].
However, there is no data available of targeting USP10 in colorectal cancer and therefore a potential therapeutic effect of targeting USP10 in CRC-derived cell lines should be investigated next.

3.3.1 Efficiency of commercial inhibitors on the Deubiquitylases USP7 and USP10 in CRC

The inhibition of deubiquitylases, as an anti-tumourigenic strategy is relatively new in the field and, so far, there are not many inhibitors for DUBs available. However, in 2011, a small molecule inhibitor of USP10 and USP13 was identified in a screen for inhibitors of autophagy. Liu *et al.* identified MBCQ, an inhibitor of phosphodiesterase type 5, and modified it to the specific and potent autophagy inhibitor-1 (Spautin-1) [95]. Spautin-1 was described for targeting USP10 and USP13 *in vitro* with IC_{50} from 0.6 to 0.7 ţM (Fig 3.19 A).
Besides Spautin-1, P22077 and HBX19818, both initially described as specific inhibitors for USP7, were reported to also target USP10 in FLT-3 driven AML with IC_{50} values *in vitro* of 8 ţM and 28.1 ţM, respectively (Fig 3.19 A) [94]. Since both enzymes, USP7 and USP10, share substrates as p53 and β-Catenin ([96], [46],[45], this thesis), both inhibitors were also tested for targeting USP10 in colorectal cancer.

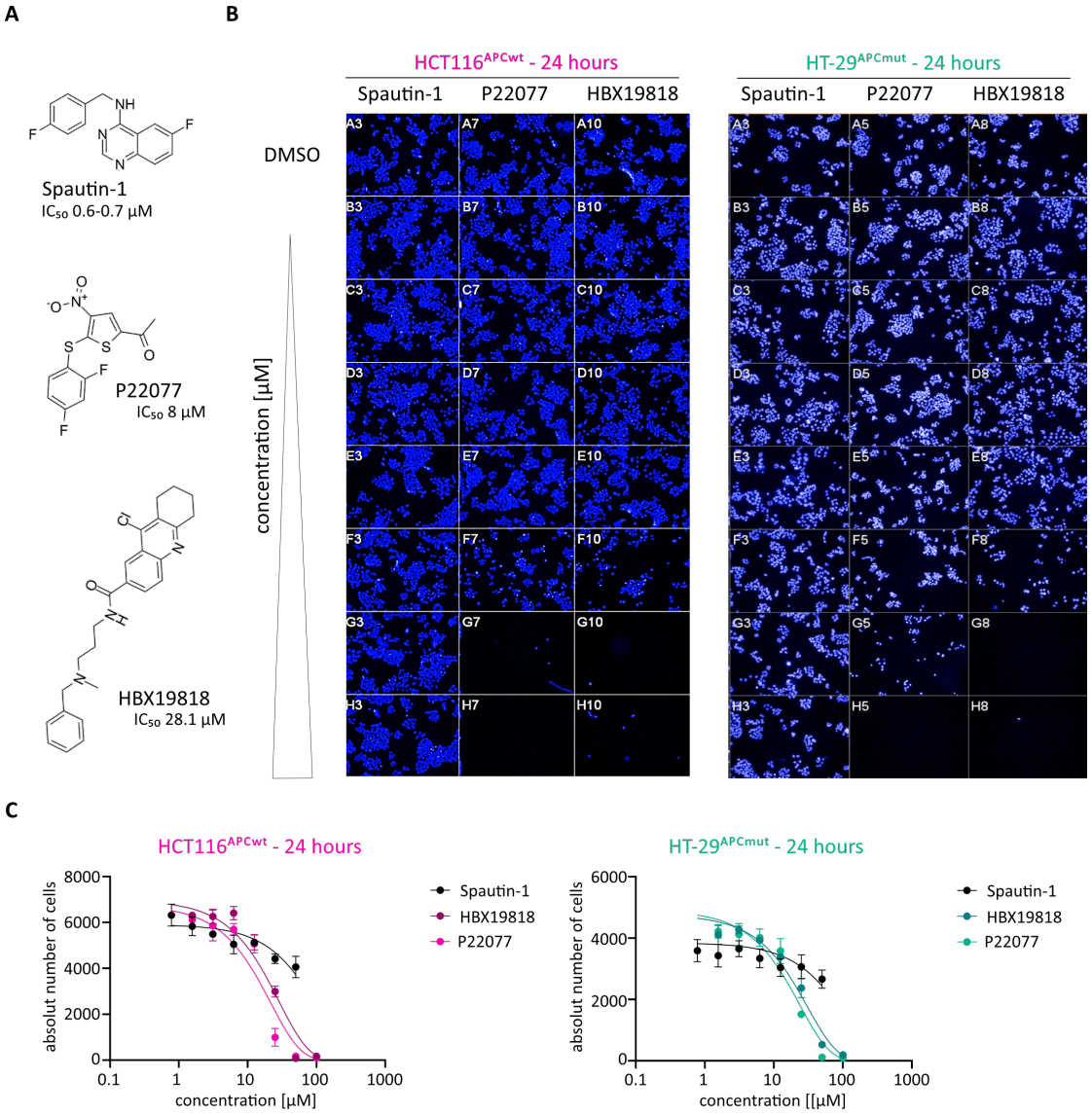

Figure 3.19: **Effects of USP7 and USP10 Inhibitors on cell viability in CRC cells**
A Structures and corresponding IC_{50} values of commercial available inhibitors, derived from medchemexpress.com. Inhibitors are selective for USP13, USP10 and USP7. IC_{50} values are for *in vitro* use only. **B** Representative images of EC_{50} determination. HCT116 and HT-29 cells were treated with increasing concentrations of indicated inhibitor for 24 hours. Cell number was determined via DAPI staining using the Operetta high content microscope (n=3). **C** Resulting dose-response curve generated from (B). For concentration a logarithmic scale was used. Error bars represent S.D.

To get a first insight into an effective working concentration (from hereinafter referred to as EC_{50}) of these small molecule inhibitors, a dose-response curve was generated. Therefore, HCT116 and HT-29 cells were plated on a 96-well plate, suitbale for microscopy, and treated with increasing concentrations of inhibitors. After 24 h of treatment, cells were fixated, counter-stained with DAPI and imaged using the Operetta high content screening microscope. Representative images are shown in figure 3.19 B. The relative

number of cells were quantified, using DAPI intensity, and dose-response curves were generated, as seen in figure 3.19 C. For the USP7 inhibitors P22077 and HBX19818 EC_{50} values of 25 ţM for HCT116 cells and 25 ţM for HT-29 cells could be estimated. For Spautin-1, the highest concentration of inhibitor, used in this assay, was not sufficient to ablate the tumour cells and therefore no EC_{50} could be calculated. Interestingly, non of the inhibitors had a different effect on APC wild-type or mutant cells, indicating an independent or alternative mechanism of action relative to the afore described APC dependent mechanism of USP10.

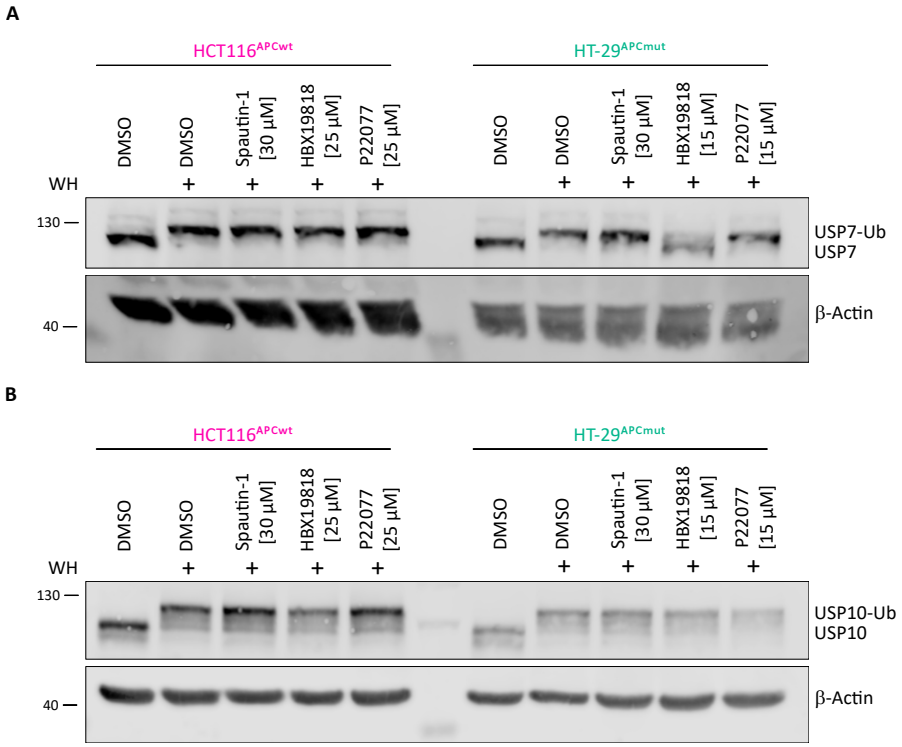

Figure 3.20: **Inhibitory effect of Spautin-1, HBX19818 and P2207 on USP10 and USP7 in CRC-derived cells**
A Western blot of warhead-assay to determine the inhibitory effect of the compounds on USP7. Cells were treated for 24 hours with indicated concentrations of the inhibitor. β-Actin served as loading control. **B** western blot of warhead-assay to determine the inhibitory effect of the compounds on USP10. Cells were treated for 24 hours with indicated concentrations of the inhibitor. β-Actin served as loading control.

To validate an inhibitory effect of the utilised inhibitors towards USP10, the so called ubiquitin-suicide probe/ warhead-assay was performed. In brief, ubiquitin-suicide probes can bind to active DUBs and therefore lead to a molecular weight shift of 8 kDA, when analysing the samples via SDS-PAGE. To determine the ratio of inactive/active USP10, control samples, without and with warhead, were loaded in the first two lanes of each WB. These controls are used to define base-line DUB activity, to be able to observe an inhibitory effect of the compounds. First, the effect of all inhibitors on USP7 was analysed. As shown in figure 3.20 A, none of the chosen concentrations resulted in an

inhibition of USP7 in HCT116 cells. However, in HT-29 cells, 15 ţM of HBX19818 inhibited the majority of USP7 protein. Since these two cell lines not only differ in their *APC* mutation, but also in their p53 and KRAS status, theses differences in mutational burden could putatively lead to an increased sensitivity of HT-29 cells to USP7 inhibition. Although this appeared as an interesting finding, the main aim of these experiments was to identify new inhibitors for USP10. Therefore, the inhibitory effect on USP10 was investigated next and the same cell lines were treated with similar concentrations of the substances. As seen in figure 3.20 B none of the inhibitors, at least with the applied concentrations, was efficient in targeting and inhibiting USP10. Surprisingly, also the published USP10 inhibitor Spautin-1 was not able to inhibit USP10, within the here used experimental set up.

3.3.2 Validation of inhibitory effects of novel USP10 compounds

As described before, the concept of targeting DUBs is still relatively new and thus, not many DUB inhibitors are commercially available. Based on the previous results with the commercial inhibitors, it was decided to develop and test novel small molecule compounds potentially targeting USP10. In cooperation with the University of Frankfurt and the Universiteit Leiden, four new compounds, identified in a drug screen should be tested for their ability to inhibit USP10. The four small molecule inhibitors, with the internal sample-IDs TMV-05, -06, -07 and TMV-12 were tested in the two human CRC-derived cell lines HCT116 and HT-29. First, dose-response curves with increasing concentration over 24 h were generated, using the Operetta high content screening microscope (figure 3.21 A). By comparing the inhibitors for each cell line, TMV-06 and TMV-07 were able to kill both cell lines and therefore, it was decided to use these inhibitors for further testing (figure 3.21 B).
To determine EC_{50} values, both inhibitors were compared in the different cell lines. Interestingly, HCT116 cells were more sensitive to the substances, compared to HT-29 cells. TMV-06 resulted in an EC_{50} value of less than 10 ţM and 32 ţM in HCT116 and HT-29 cells, respectively. The second compound, TMV-07, showed an EC_{50} value of 1 ţM and 2 ţM in HCT116 and HT-29 cells, respectively (figure 3.22 A).
Next, both cell lines were treated with two different concentrations of inhibitors, in the range of the calculated EC_{50} value, for 24 h and analysed using the warhead assay.

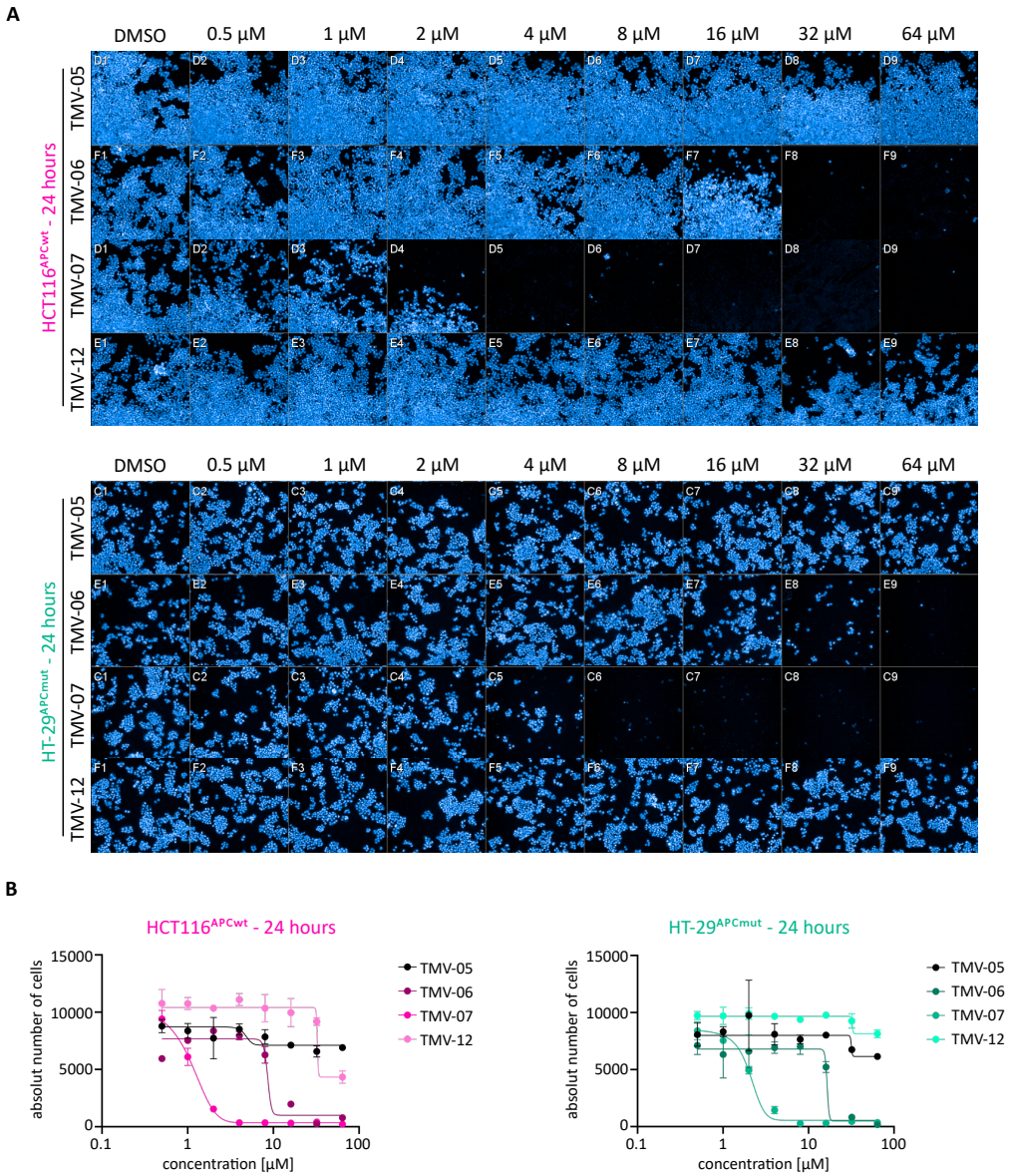

Figure 3.21: **Effects of novel USP10 inhibitors on cell viability in CRC-derived cell lines**
A Representative images of EC_{50} determination. HCT116 and HT-29 cells were treated with increasing concentrations of indicated inhibitor for 24 hours. Cell number was determined via DAPI staining using the Operetta high content microscope (n=3). **B** Resulting dose-response curve generated from (A). For concentration a logarithmic scale was used. Error bars represent S.D.

As a control for the warhead-assay, DMSO treated cell lysates were additionally mixed with 4 ţM of NEM, which is an inhibitor of cystein-proteases. As seen in the respective first two lanes of each WB, NEM led to a complete inactivation of USP10. In the third lane of each blot, DMSO samples with warhead were loaded, to define the base-line activity of USP10. In compound exposed cells, treated for 24 h with the indicated inhibitors, neither HCT116 nor HT-29 cells, demonstrated a reduction in USP10 activity for the concentrations used (figure 3.22 B).

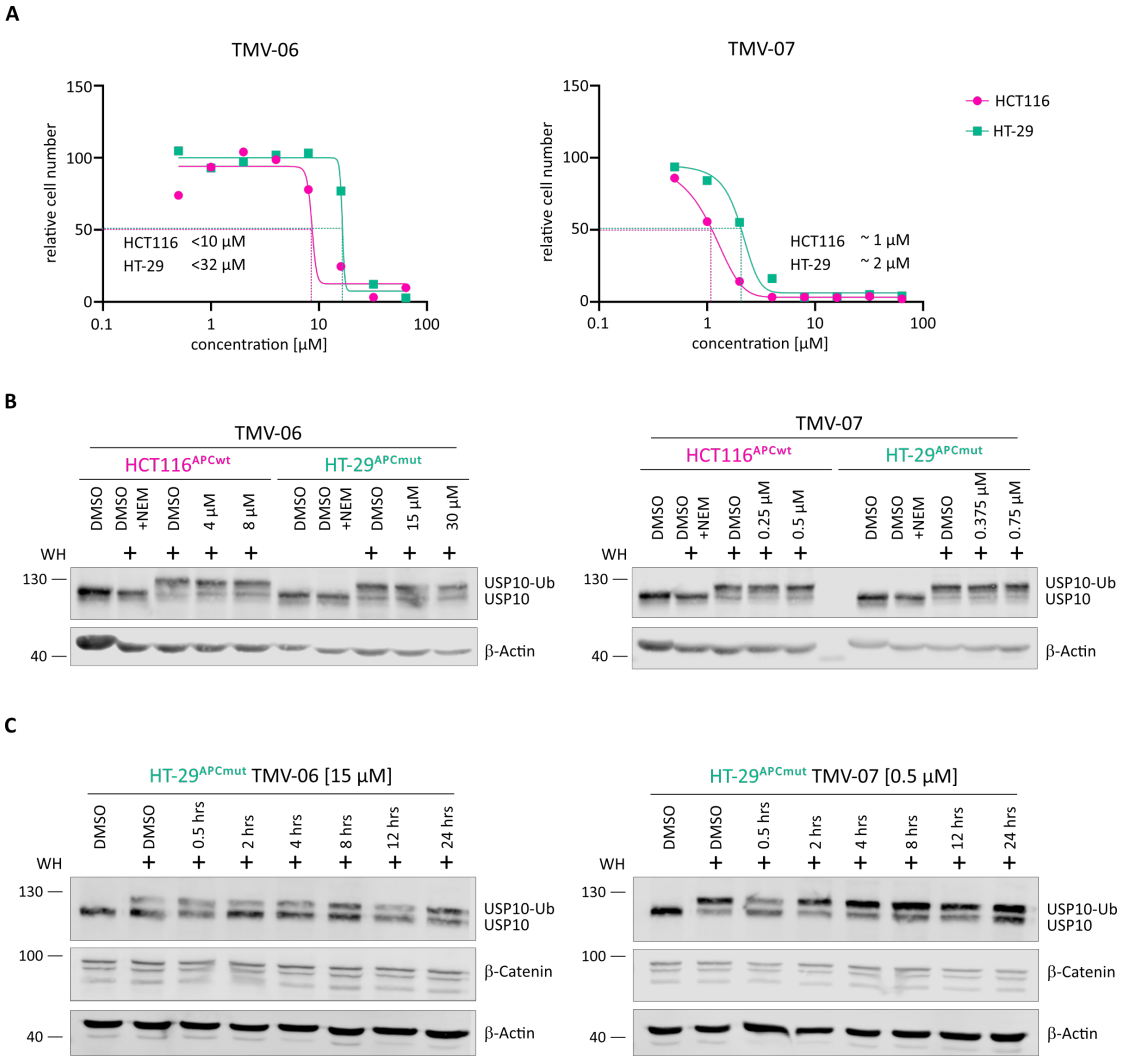

Figure 3.22: **Inhibitory effect of TMV-06 and TMV-07 on USP10 in CRC-derived cell lines**

A Dose-response curves for EC_{50} calculation of indicated inhibitor. HCT116 and HT-29 cells were compared, based on data from Fig 3.21. **B** Western blot from warhead-assay in HCT116 and HT-29 cells. Cells were treated for 24 hours with indicated concentration of the corresponding inhibitor. β-Actin served as loading control. **C** Western blot from warhead-assay in HT-29 cells. Cells were treated with indicated concentration of corresponding inhibitor and and effect on USP10 inhibition was analysed at indicated time-points. β-Actin served as loading control.

To rule out the possibility that new transcribed and translated protein is masking the inhibitory effect on USP10, a time-course experiment, with shorter time-points, was performed next. Therefore, HT-29 cells were treated with 15 ţM and 0.5 ţM of TMV-06 and -07, respectively, followed by harvesting of cells and subsequent warhead-assay at following time points: 0.5, 2, 4, 8, 12 and 24 h. Interestingly, there was a slight switch from active USP10 to inactive USP10 at about 2 h of treatment with TMV-06. Since the amount of active USP10 in the control sample is slightly less than in previous experiments, it would be important to repeat that experiment. For TMV-07 a putative

inhibitory effect could be observed already after 0.5 h of treatment. Surprisingly, already two hours later, almost all USP10 proteins seem to be active again (figure 3.22 C).

Taken together, these experiments support the need for novel USP10 inhibitors, which show a clear inhibition of USP10 protein *in vivo*. So far, none of the commercial available inhibitors neither the first trial of new synthesised compounds showed a clear inhibition of USP10 in the here chosen experimental set up. As shown in figure 3.22 C, a slight reduction of active USP10 was achieved by using short treatments with TMV-06 and -07. Although the effects seen here are not strong, this finding would be worth for further investigation.

3.4 Development of a novel mouse model for colorectal cancer

With the identification of a novel tumour-specific mechanism *in vitro* and *ex vivo*, the need for a fast and easy to generate mouse model also arises. The majority of the existing mouse models for colorectal cancer are either time-consuming (in case of classical breeding) or technically challenging (injection of organoids into the submucosa). To overcome these challenges, it was decided to develop a novel technique for the easy and fast generation of mouse models, reflecting a variety of different genotypes.

As already described in lung by Hartmann *et al.* in 2021, the injection of viral particles, encoding for CRISPR/Cas9 gRNAs or the Cre-recombinase into the organ-of-interest can revolutionise and accelerate the development of tissue-specific cancer models [92]. While the instillation of virus into the lung is already well established, CRISPR/Cas9-based gene editing of the colon was previously unattended. Therefore, the adaptation of this method for the gastrointestinal tract will be investigated in this part of the thesis. As summarised in figure 3.23 A and B, two different strategies, for the generation of oncogenic hits in the GI tract, were tested. For the transformation of WT mice, different combination of gRNAs were cloned into the lentiCRISPRv2 plasmid which also encodes for the Cas9 enzyme. In figure 3.23 A the schematic model of the plasmid, the different gRNA combinations and the timeline for the experiment is shown.

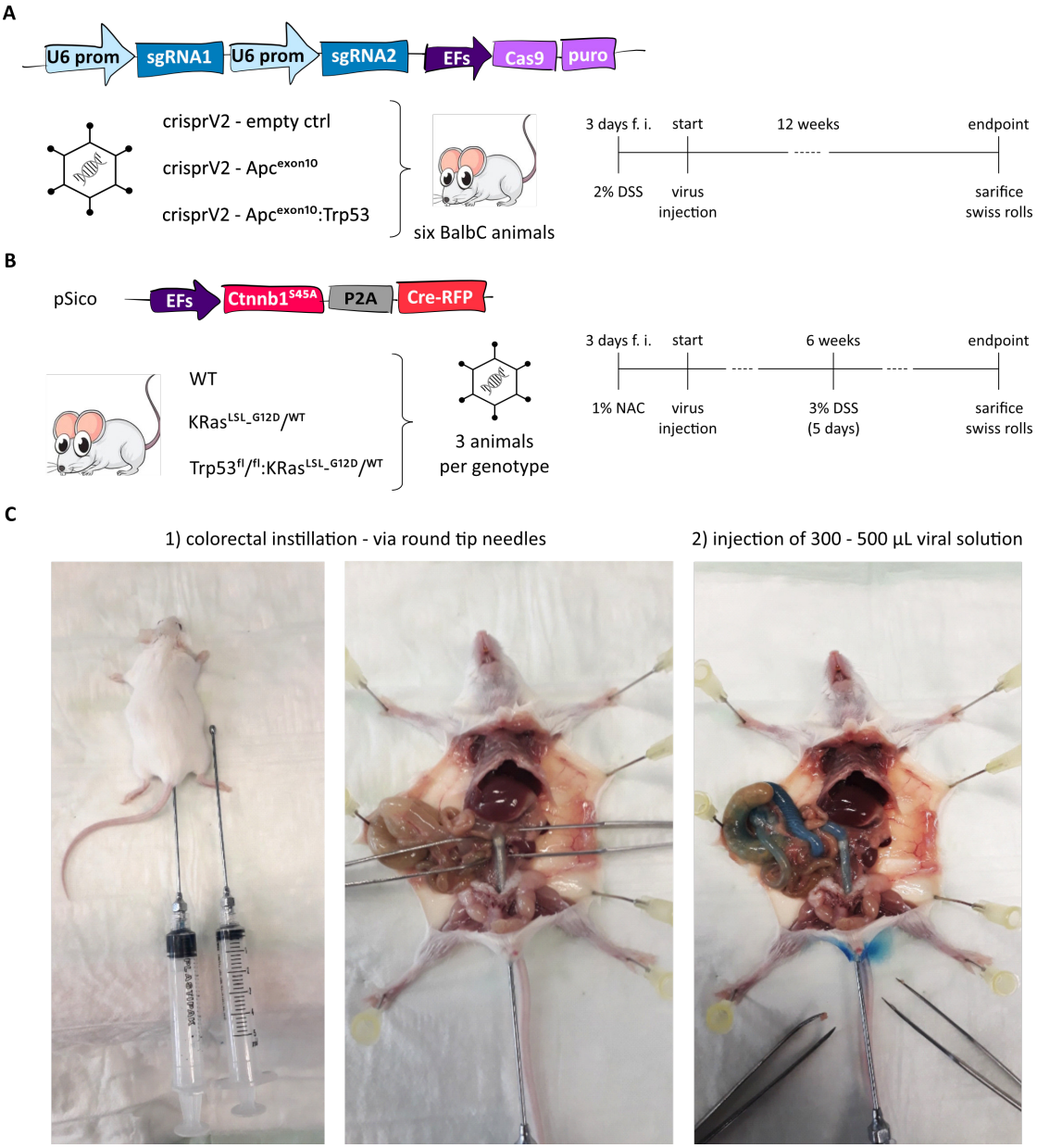

Figure 3.23: **Overview of the experimental set up to develop novel CRC mouse models** **A** Plasmid map of the used crispV2 backbone including gRNAs targeting *Apc* and *Trp53*. Right-side: Time-line for the experiment. **B** Plasmid map and genotypes of the animals used. Right-side: Time-line for the experiment. **C** Representative images of the colorectal instillation of viral particles. 500 µL of blue liquid were injected into the colon by using a round-tip needle.

In brief, a control plasmid only encoding for Cas9, an sgRNA targeting *Apc* exon 10 and a combination of gRNAs targeting *Apc* and *Trp53* were packed into lentivirus. To induce mild intestinal inflammation and to damage to the epithelial monolayer in the colon, allowing the dissemination of intestinal contents, wild-type BalbC mice were treated with 2 % DSS for 3 days before infection ([59]), followed by injection of 500 µL of concentrated

lentivirus, dissolved in PBS. The mice were then sacrificed and analysed after twelve weeks.
For the second approach, C56BL6/J control animals, C56BL6/J *KRas*$^{LSL\text{-}G12D/WT}$ and C56BL6/J *Trp53*$^{fl/fl}$: *KRas*$^{LSL\text{-}G12D/WT}$ animals were infected with lentivirus encoding for a Cre-recombinase and an oncogenic *Ctnnb1* mutant (see figure 3.23 B). These animals were treated for 3 days pre infection with 1 % N-acetylcystein, which was demonstrated to reduce the amount of secreted mucous in mice [97], infected with the virus and after 6 weeks they obtained a second injury, caused by 5 days of 3 % DSS. Animals were sacrificed and analysed 6 weeks later.
Both methods have the colorectal instillation of viral particles, with the help of a round-tip needle, in common. To define the amount of virus needed, the method was recapitulated by injecting blue liquid into the colon of a dead animal. As shown in figure 3.23 C, the needle was introduced up to approximately 2 cm into the colon and 500 µL of liquid were injected. As can be seen in the right part of figure 3.23 C, 500 µL of liquid are sufficient to flush the whole colon, the caecum and the first part of the ileum. With these experimental set up, the success of the method will be investigated in the following parts on a histological level.

3.4.1 Introduction of organ-specific tumourigenic mutations via CRISPR/ Cas9

One requirement for the novel mouse model, is an easy implementation of various genetic alterations into mice of every genotype. To address this, in a first attempt, gRNAs targeting *Apc*^{ex10} and *Trp53:Apc*^{ex10}, together with a control plasmid, were utilised.
In figure 3.24 A, representative low magnifications of hematoxylin and eosin (H&E) staining from small intestine as well as colon are shown. In the first row, untransformed wild-type gut rolls from control animals are depicted. The colon consists of a thin layer of ordered crypts and in the lower part of the presented section, small inflammatory regions can be seen (figure 3.24 A, arrow). These regions consist of infiltrating immune cells, which is most likely caused by the immune-response to the virus infection carried out prior. In the small intestine, the typical crypt-villus structure can be seen. In contrast to the untransformed animal, CRISPR/Cas9 mediated targeting of *Apc* and *Apc:Trp53* led to an increase in length of the small intestine and colon (fig 3.24). Furthermore, in the colon of both animals, regions with a thicker mucosa and longer crypts were identified. Surprisingly, the small intestine of both animals, showed significant differences, when compared to the control animal. In the presented low magnification image, an increase in villus-length is visible and each animal has at least one largely transformed region (marked with a dashed square).

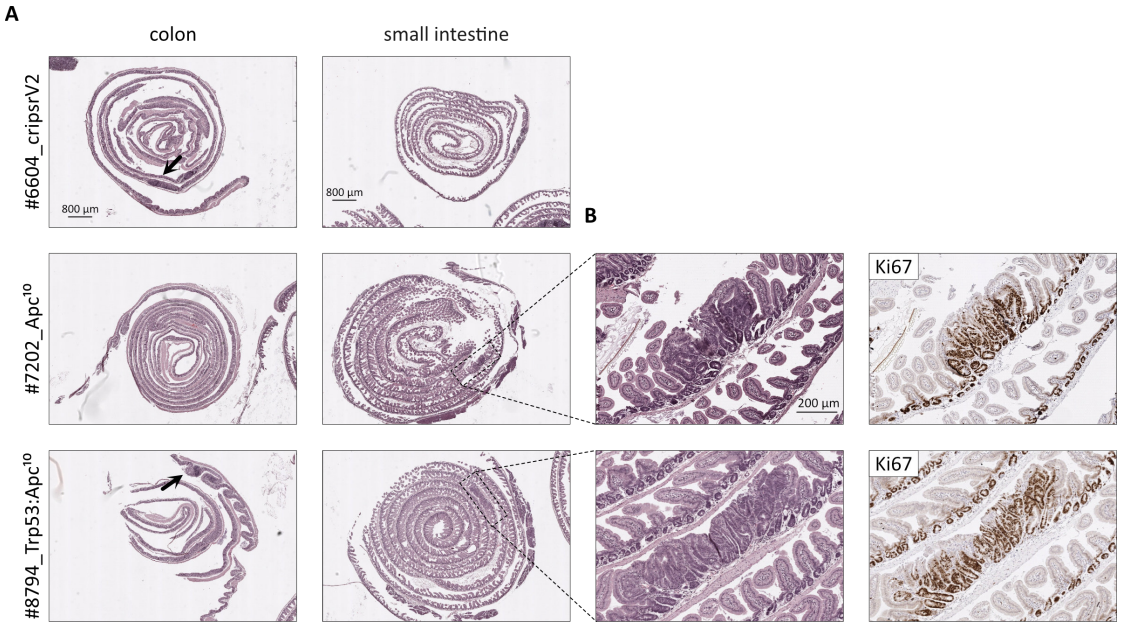

Figure 3.24: **Genetic modification of *Apc* and *Apc:Trp53* via CRSIPR/Cas9 introduces hyper-proliferative lesions in the small intestine**
A Low magnification images of colon and small intestine gut roles. H&E stainings from three representative animals are shown. Dashed squares highlight lesions in the small intestine. Arrows indicate immune infiltration. **B** Higher magnification from (A). Disordered and hyper-proliferative regions from the small intestine are shown. Ki67 IHC staining was performed to label proliferative cells.

A high magnification image, to investigate these areas in more detail, is shown in figure 3.24 B. In the H&E staining of both animals the typical crypt-villus structure is nearly completely lost and appears disordered, highly cellular crypts are overgrowing the regular structure. To investigate if these lesions are indeed hyper-proliferative transformations, a Ki67 IHC staining was performed. Ki67 is a marker of proliferating cells and its expression is restrained to the crypts, in particular to the stem- and transit-amplifying cell compartment, in a normal gut. In contrast to wild-type tissue, the observed lesions, were highly positive for Ki67 throughout the whole transformed area. Of course, additional proof-of-principle Apc and Trp53 IHC stainings need to be done, but the degree of disorganisation and the amount of Ki67 positive cells in these regions provide already a solid basis for the further optimisation of this method.

3.4.2 Introduction of the Cre-recombinase via lentiviral transduction

In a second approach, a combination of the classic mouse models with the new viral-based method should be investigated. Genetically engineered mice with a conditional allele for oncogenic KRas ($KRas^{LSL\text{-}G12D/WT}$) and in combination with a conditional homozygous loss of *Trp53* ($Trp53^{fl/fl}$:$KRas^{LSL\text{-}G12D/WT}$) were infected with a lentivirus encoding for a hyperactive $Ctnnb1^{S45A}$ variant and a Cre-recombinase. Morphologically,

the used animals show no abnormal intestinal structures prior to Cre-recombinase mediated recombination of the conditional alleles. Therefore, transformation onset only appears, when the viral-mediated transduction of the intestinal mucosa was successful.

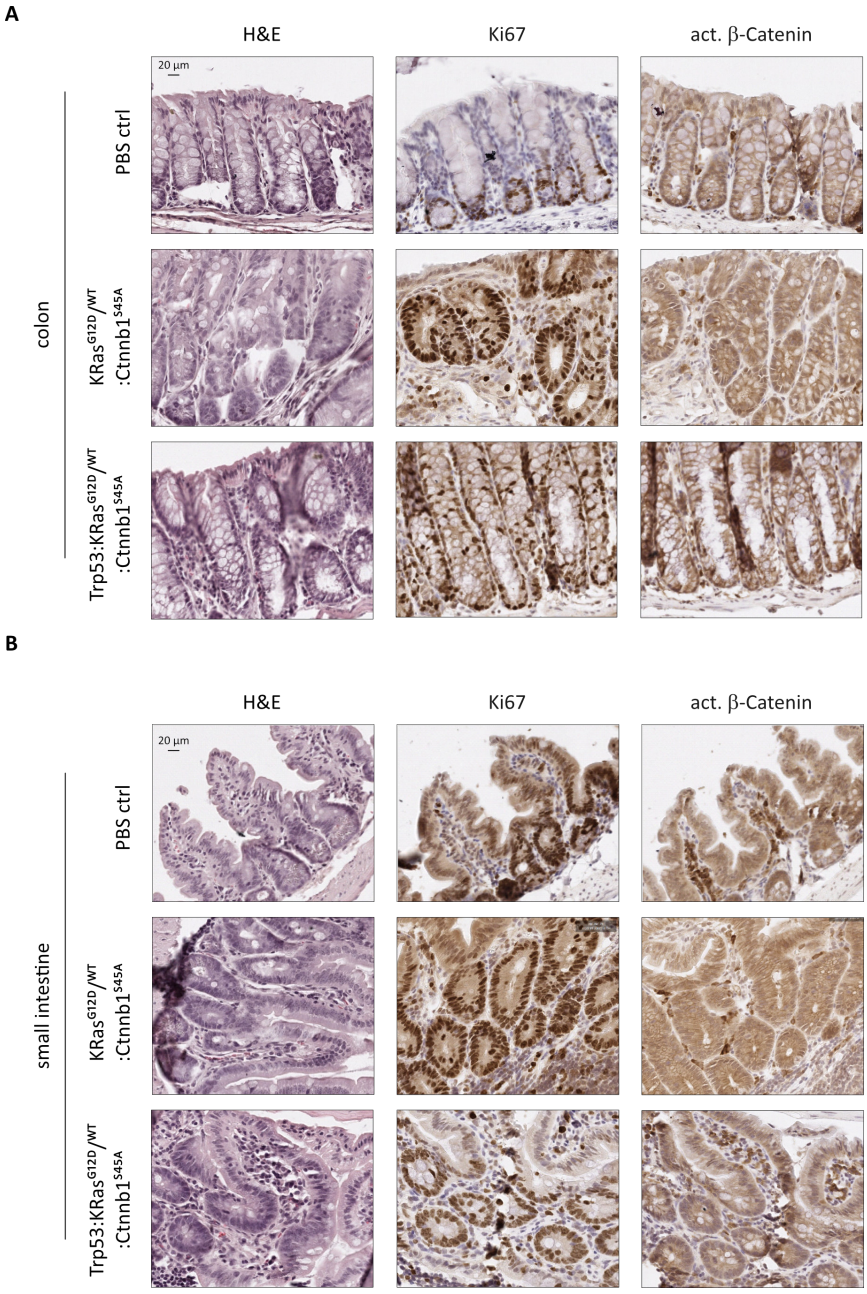

Figure 3.25: **Hyper-active KRas and Wnt signalling lead to hyper-proliferating lesions** **A** High magnification of transformed regions in the colon. Representative H&E staining show disordered intestinal structures. Ki67 and active β-Catenin IHC stainings label proliferating cells and cells with active Wnt signalling. **B** High magnification of transformed regions in the small intestine. Representative H&E staining show disordered intestinal structures. Ki67 and active β-Catenin IHC staining label proliferating cells and cells with active Wnt signalling.

Mice were treated and infected as described in figure 3.23 B (right site) and sacrificed 12 weeks post injection. The colon as well as the small intestine of each animal were analysed using the Swiss Gut role technique and high magnifications of representative H&E staining are shown in figure 3.25 A and B, respectively. A section from a transformed region is shown for each genotype compared to control animals (upper panel of figure 3.25 A and B). For both genotypes, the loss of the typical colon and small instestinal organisation along with an increase in cells throughout the crypts is remarkably. To analyse these lesions in more detail, IHC staining of Ki67 along with active β-Catenin was performed additionally. Again, a strong increase in Ki67 positive cells was observed. Another important marker for transformation, especially in the GI tract, is active β-Catenin. In a healthy GI tract, active β-Catenin is exclusively found in the nuclei of crypt cells, with active Wnt signalling. Therefore, an increase in active β-Catenin staining provides an evidence of increased Wnt signalling. Although it is not as clear as a marker protein as Ki67 in the intestine, an increase in staining intensity is observable in the $KRas^{G12D}$ and $Trp53{:}KRas^{G12D/WT}$ animals. Of note, since together with the Cre-recombinase a hyperactive β-Catenin mutant was introduced, one would expect a stronger staining for active β-Catenin. However, further IHC staining and quantitative analysis need to be done which is in line with the results from the CRISPR/Cas9-based approach.

Although for both animal experiments further staining and quantitative analysis from these staining are missing, transformed areas, especially in the small intestine, were detectable. The degree of transformation, specifically for the first CRISPR/Cas9 based approach, provides important preliminary evidence for the success of such a method.

4 Discussion

4.1 USP10 is a novel regulator of β-Catenin stability in APC-truncated CRC

Colorectal cancer is mostly driven by deregulated WNT signalling, resulting in hyper-stabilisation of the proto-oncoprotein β-Catenin and constant transcription of its target genes [98], [99]. It is widely accepted that alterations in the WNT signalling pathway prevent ubiquitylation and therefore degradation of β-Catenin by the 26S proteasome. Initial work of this group could show, however, that β-Catenin is still ubiquitylated in CRC-derived cell lines and therefore, attempts to identify novel DUBs, stabilising β-Catenin, were made. In an initial siRNA-based DUB library screen USP10 was identified to regulate β-Catenin stability in HT-29 cells. During this thesis it was demonstrated that USP10 indeed interacts with β-Catenin in an APC-truncation dependent manner and regulates its stability as well as affects the transcription of its target genes.

According to literature, *CTNNB1* mRNA as well as the corresponding protein is upregulated in CRC and with the analysis of publicly available data, the same was shown for USP10. Interestingly, the expression of *USP10* does not change significantly throughout different CRC stages, suggesting that USP10 is not only involved in tumour-initiation, but also for tumour-maintenance (figure 3.1 and 3.2). In line with this assumption, a strong reduction of *USP10*, mediated via shRNA or complete knock-out via CRISPR/Cas9, is lethal in longitudinal cultured human CRC-derived cell lines. This was further corroborated by analysis of publicly available dependency data from the Dependency Map project of the Broad institute (depmap.org). Conducting and curating several genome wide CRISPR screens in a plethora of human tumour cell lines identified *USP10* as a common essential gene (figure 3.7). Consistent with the elevated expression of *USP10* in CRC, a high expression also correlates with a poor overall survival probability of patients. Interestingly, only a small sample size of patients with CRC could be defined for low *USP10* expression, confirming the common abundance of USP10. When analysing the protein abundance and distribution of USP10 in *in vivo* tissue, a cell type independent low expression could be observed. It is worth noting that, while all cells expressed low levels of *USP10*, the overall abundance was not homogenous. Elevated levels of USP10 were observed in proliferating crypts and intestinal stem cells (figure 3.3), presumably due to its various described functions not only in pathology but also in physiology (reviewed in [100]).

At the beginning of this thesis, interaction studies in different CRC-derived cell lines were performed. Interestingly, an endogenous interaction of the two proteins could only be demonstrated in two different CRC cell lines, with a very short *APC* truncation. Colo320 and HT-29 cells, have a short remaining APC protein in common, which harbours none of the AAR domains anymore. In line with an APC-truncation dependent interaction is the observation that a direct effect of USP10 abundance on β-Catenin ubiquitylation, was only observed in HT-29 cells, but not in APC full-length HCT116 cells (see figures 3.5, 3.6, 3.8 and 3.9).

These results are consistent with previously published data regarding a comparable mode

of action for USP7 and β-Catenin, made by the team of Vivian Li [45]. In this study, the authors described a reverse binding of USP7 and the E3-ligase β-TrCP for β-Catenin, depending on the loss of the mutational cluster region in APC. The observation presented in this thesis extends the interaction landscape of β-Catenin in APC truncated CRC even more, as USP10 requires an even shorter APC truncation to enable binding and regulation of β-catenin.
These general observation on β-Catenin protein abundance regulation in CRC raises the intriguing and important question how complex the overall regulation of β-Catenin in an APC dependent, and probably even independent fashion, truly is. The initial siRNA screen, conducted as the priming nexus of this thesis, identified not only known deubiquitylating enzymes and did not only highlight USP10, but other factors as well. Further work is required to decipher the complexity of the β-Catenin regulatory network and one can only speculate at this point that not only APC truncations but other mutations, PTMs or tissue specific signalling cascades are indeed involved in the control and fine-tuning of WNT signalling in CRC.
Furthermore do the findings reported in this thesis, that the loss of all AAR domains is required to facilitate the interaction of USP10 with β-Catenin, raise the question how common these truncating mutations are in CRC patients. In figure 4.1 A and B, a mutational analysis using the cBioportal webtool is shown. According to the TCGA PanCancer data set, approximately 80 % of CRC are driven by truncating mutations in *APC*, however, as evident by the genetic patient data available, a plethora of various truncations are present. Closer stratification of the *APC* mutant cohort revealed that, strikingly, 30 % out of CRC patients harbour mutations in *APC*, which result in a loss of all AAR motifs and, therefore, presumably enable the interaction of USP10 with β-Catenin.

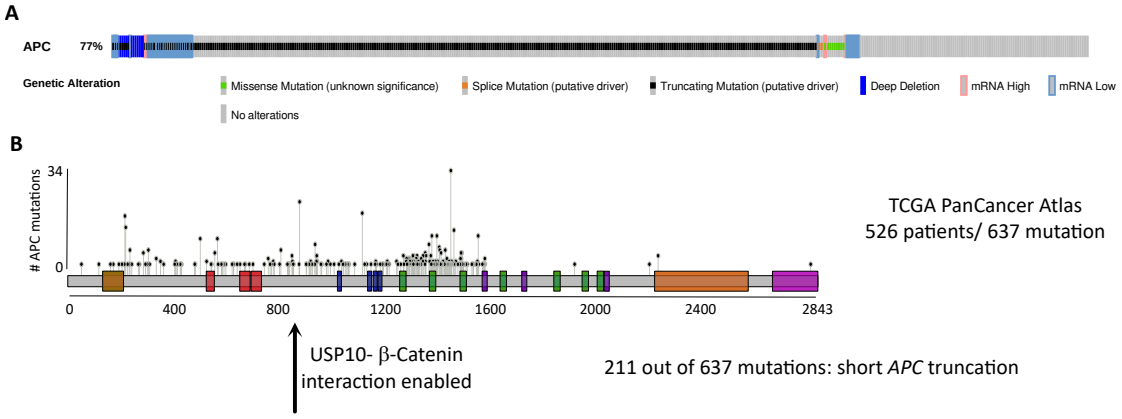

Figure 4.1: **APC truncating mutation in CRC**
A Overview and percental occurrence of APC mutations in CRC patients. Plot was generated using TCGA PanCancer data set using cBioportal. **B** Lollipop plot showing number and position of APC truncating mutations in CRC. Lollipop plot was generated using cBioportal. Arrow indicates short APC truncation variant.

The observation that different DUBs can regulate the same substrate, depending on the mutational background or in a tissue-specific context, is a relatively new observation and could serve as an entry point not only for highly selective cancer engagement and, hence, new therapeutic strategies. However, when keeping in mind the numbers of so

far identified E3-ligases and DUBs, it would not be surprising that several DUBs share substrates, depending on a certain stimulus. In this study, the extend of APC truncation would allow different DUBs to bind and regulate β-Catenin. Whether this also holds true for other substrates of USP7 and USP10, remains unclear.

The proposed model of USP10 and β-Catenin interaction relies on the involvement/loss of function mutations of APC. Although a truncating mutation in *APC* at amino acid 800 or less would lead to a very short protein, other laboratories have shown that the destruction complex still forms, however, fails to fully regulate β-Catenin abundance, leading to enhanced levels of WNT signalling [45]. Based on this observation, the next question would be whether alteration in USP10 would influence the activity of WNT signalling pathway. To address this question, two different strategies were pursued: Transcriptional consequences were analysed upon reduction of USP10 (see figures 3.10 and 3.11) and changes in protein amount were investigated in USP10 WT and catalytic inactive (CA) mutant overexpressing cells (figure 3.12). Interestingly, on mRNA and protein level, changes in the abundance of WNT signalling targets, such as LGR5, OLFM4, ASCL2 and CD44 ([101], [102], [103], [104]) could be observed in both experiments, with repressed expression upon loss of *USP10*, while enhanced when USP10, not the CA mutant, was overexpressed. This data clearly demonstrated the intricate interconnection and involvement of USP10 in the WNT signalling pathway, at least in CRC.
Although the changes on mRNA were rather mild, significant changes on protein level were observed upon USP10 overexpression. With the experimental set up performed in this thesis, it still remains unclear whether USP10 directly regulates also WNT signalling targets, such as LGR5, ASCL2, OLFM4 and CD44 for example, or whether these changes result from altered β-Catenin abundance. To further address this question, chromatin-immunoprecipitation (ChIP) or CUT&RUN experiments could be performed ([105]), allowing to study either the recruitment of β-Catenin to its cognate binding sites and how this is affected in a USP10-dependent fashion, or if USP10 is recruited to these promoters. Furthermore, Assay for Transposase-Accessible Chromatin using sequencing (ATACseq) experiments in Usp10 KD organoids could be done, to investigate putative changes in open chromatin, which would indicate an indirect but rather global role of USP10 in transcription of these genes [106]. Nevertheless, data from this thesis report USP10 as novel WNT signalling activator and provide preliminary evidence that USP10 contributes to stem cell homeostasis.

4.2 Organoids as model system to study USP10s effect on WNT signalling and stem cell homeostasis

4.2.1 Alterations in Usp10 level affect β-Catenin dependent Wnt signalling target genes

While utilising 2D cell culture model systems in cancer research is widely accepted, the lack of tissue architecture, heterogeneity and complexity makes them unsuitable to study

complex physiological consequences. To overcome these limitations, intestinal organoids as 3D model system have been developed and well established in the past [70]. Organoids allow the longitudinal culture of unperturbed stem cells and posses the key feature to truthfully recapitulate the stem cell nice and -lineage. Hence, this 3D system is uniquely suitable to model the differentiated cell-type heterogeneity similar to the *in vivo* tissue of origin (reviewed in [107], [108]).
The results of this thesis so far point towards a *de novo* role of the deubiquitylase USP10 in the regulation of stem cell and cancer stem cell homeostasis. Although this has not been described for USP10 so far, other DUBs, such as USP18 or USP21, have been described as regulators of stemness already [109], [110]. This makes it even more interesting to further investigate the role of USP10 in stemness.
To study these effects in a more relevant context, murine intestinal organoids were established, genetically modified and utilised to investigate the physiological consequences of the *de novo* USP10- β-Catenin interaction (see figures 3.13 and 3.14). By performing RNA sequencing of Apc^{ex9}:*Trp53*:$KRas^{G12D}$intestinal organoids, with altered *Usp10* levels, the importance of a suitable 3D system becomes obvious. The amount and extend of differentially expressed genes upon Usp10 alteration is significantly increased when compared to a similar experiment conducted in established human CRC-derived cell lines. To get a more comprehensive insight of transcriptional changes upon Usp10 alteration, genes which are downregulated upon shUsp10 and upregulated upon USP10 WT overexpression were analysed (figures 3.15 - 3.17). In line with the previous observations from 2D models, genes involved in Wnt and Cadherin signalling pathways were mainly deregulated in these conditions. Among these, *Lef1*, *Fzd2* and *Dkk2*, representing known Wnt signalling targets, were identified to be expressed in a *Usp10* dependent fashion [111], [112]. Additionally, the transcription factors *Tfap2a* and *Tead1* were identified to be deregulated upon alteration of USP10 abundance in organoids. Tfap2a is a transcription factor with increased expression in stem-like cancers and was described to act together with the Zeb1/2 network in promoting EMT [113]. *Tead1* expression is also found to be upregulated in tumours and, interestingly, was described to increase the expression of *Myc*, *Sox9* and *Tead4* together with β-Catenin and Yap [114]. Another gene which was strongly regulated by USP10 depletion and overexpression is *Fgf9*. Fgf9 is not only a regulator of Wnt signalling pathway in CRC, but was also described to mediate cisplatin resistance in colorectal cancer [115].
Besides the Wnt and Cadherin signalling pathways, the analysed genes were involved in three other signalling pathways. Firstly, alterations in the ubiquitin signalling pathway were identified. This is not surprising at all, as Usp10 is a deubiquitylating enzyme and in the literature interactions with other members of the UPS can be found. For example, interactions with the E3-ligase-components CUL3 and CUL4A/B were described by Liu *et al.* 2019 already [116]. Furthermore, interactions with other DUBs and, as already mentioned, shared substrates are also known [117], [95].
Secondly, the G-protein signalling pathway was among the top deregulated pathways. Interestingly, G-protein coupled receptors (GPCR) are indeed involved in the regulation of the intestinal homeostasis. Feng *et al.* reviewed recently that alterations in GPCR signalling can effect inflammatory bowel diseases through deregulated intestinal homeostasis [118].
Thirdly, the cholecystokinin (CKK) receptor signalling pathway is tightly regulated by Usp10 expression. In the literature no connection between Usp10 and the CCKR pathway can be found so far. However, with a closer look into that pathway, an important

connection to the results of this thesis can be drawn. Cholecystokinin, the name giver of that pathway, is structural very similar to gastrin and those two proteins belong to over 30 gut hormone genes, and play important roles in digestive processes and gut motility [119]. Together with their corresponding receptors CCK2R and CCK1R, they regulate important processes in the intestinal epithelium, like cell proliferation and apoptosis and therefore, under certain circumstances, can lead to cancer [120]. Indeed, CCK2R and CCK1R are often found to be upregulated in CRC, indicating aberrant production of gastrin/CCK. Although gastrin/CCK are essential for normal gastric mucosa, when produced in access it evolves its growth-promoting functions. Moreover, Watson *et al.* demonstrated that an inhibition of that pathway, by immune neutralisation for example, reduces growth, invasion and metastasis of CRC [121].
In summary, the pathways which were upregulated upon overexpression and downregulated upon knock-down of Usp10 in murine tumourigenic intestinal organoids are involved in proliferation and stem cell maintenance. Their regulation plays an important role in CRC establishment, progression and metastasis. These findings provide solid evidence for Usp10 being an important oncoprotein in colorectal cancer.

4.2.2 USP10 contributes to EMT in colorectal cancer

It is known that canonical WNT-signalling via β-Catenin can activate the transcription of EMT genes and therefore contribute to invasion and metastasis (reviewed in [122]).
When comparing genes downregulated upon Usp10 knock-down and upregulated upon USP10 overexpression (see figure 3.18), also Fgf9 and Fgfr1 were significantly altered. Those proteins were described in the activation of FAK, AKT and ERK/MAPK signalling and, even more interesting, were reported to induce the expression of key mediators of EMT (N-Cadherin, Vimentin and Snai1 for example) [123].
Moreover, in the gene expression analysis of shUsp10-2 vs shNTC regarding an EMT gene signature list, several known EMT genes were downregulated. Among others, including *Ctnnb1* itself, *Tcf3* and *4*, which drive the expression of EMT target genes, were found to be altered in a USP10 dependent fashion. Besides that, also *Vim* and *Cdh2*, which are upregulated in later stages of cancer, were found to be strongly decreased. Vimentin was described to be low expressed in early stages, but its expression increases with invasive potential of various cancer types [124]. *Cdh2*, the gene encoding for N-cadherin, is known for its EMT-dependent expression. The expression of the cell-cell contact protein E-Cadherin (*Cdh1*) is found to be alternated to N-Cadherin. In more detail, only one of the two proteins can be expressed in a cell, determining an epithelial or mesenchymal state [125]. In line with this, *Cdh1* was upregulated upon *Usp10* knock-down and *Cdh2* is found to be downregulated in shUsp10 but upregulated in USP10 overexpressing cells. Additionally to *Cdh2*, also *Zeb1*, *Notch1* and *Col1a1* were upregulated upon overexpression of USP10 WT. All these genes encode for proteins which drive the invasive program of cancer cells and inhibit the epithelial state of a cancer cell [126], [113] and [127].
Taken together, depletion/ reduction of USP10 decreases the expression and abundance of factors involved in the control of the invasive potential of tumourigenic organoids. Conversely, the loss of the DUB increased expression of epithelial marker proteins. As stated before, the WNT signalling pathway is well known for its capacity to induce EMT

and therefore, it remains unclear whether USP10 is a direct activator of EMT or whether its a downstream effect upon altered WNT signalling. Current literature suggests that USP10 is a direct mediator of EMT. In 2018, Ouchida *et al.* demonstrated that USP10 regulates the stability of SLUG in cancer cells [128]. However, this study was cancer-type unspecific and further research would be necessary to clarify USP10s exact role in EMT. For example, with the analysis of patient-derived liver metastasis material, one could analyse the abundance of USP10 compared to the primary tumour. Furthermore, by utilising 2D cell culture as 3D spheroids, the invasive capacity of USP10 KD and OE spheroids could be measured *in vitro*. In summary, USP10 indeed contributes to EMT, but further research needs to be done to clarify the explicit role of USP10 in this process.

4.2.3 USP10 as a *de novo* repressor of clonal competition capacity?

With the analysis of our sequencing data from APK9 organoids it became clear that alterations in Usp10 lead to changes in the stemness and differentiation program. Interestingly, there were two publications quite recently, which described that tumourigenic $Apc^{-/-}$ cells actively repress the growth and activate the differentiation program of their neighbouring WT cells, due to the secretion of Notum (figure 4.2 A left side) [129], [130]. To identify the genetic program which is altered upon Notum exposure, Flanagan *et al.* cultured WT organoids in WT- and $Apc^{-/-}$- derived medium and applied them to RNA sequencing. A heatmap of the top differential expressed genes is shown in figure 4.2 A, right side. Interestingly, WT organoids, treated with $Apc^{-/-}$ conditioned medium, showed a decrease in stemness and an increase in differentiation. Noticeable, genes identified as important mediators were also deregulated upon loss of Usp10 in mAPK9 organoids. In figure 4.2 B, a comparison of up- and downregulated genes from recent studies to the data from this thesis is shown.
The transcriptional program of shUsp10 organoids is similar to WT organoids in WT-conditioned medium, meaning surrounded by WT cells. In contrast, the shNTC organoids differentially express genes which WT organoids express when surrounded by hyper-proliferative $Apc^{-/-}$ organoids.
Given the fact, that in the here used organoid culture, not all cells are transformed but a heterogeneous mixture of cells is present, one could speculate that downregulation of Usp10 decreases the super-competing properties of tumourigenic cells and therefore decrease the influence of these cells, on their neighbour cells.

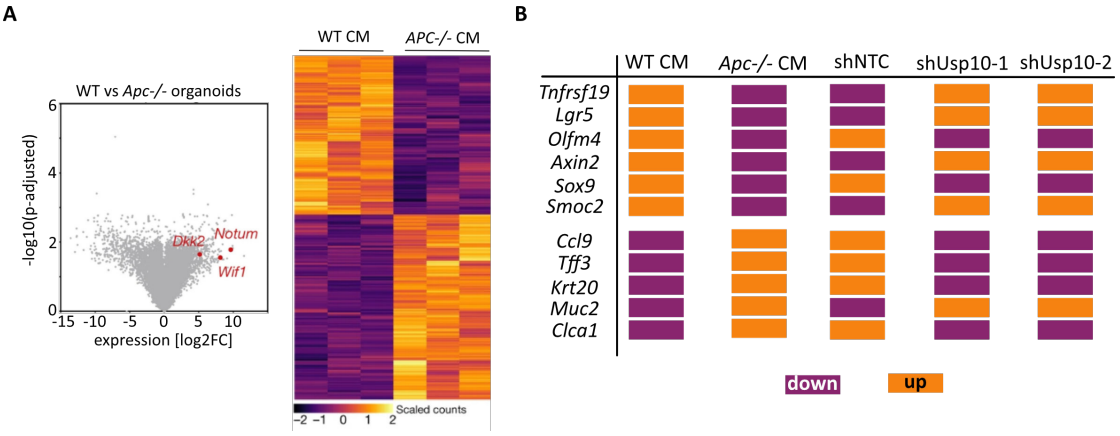

Figure 4.2: **Usp10 KD organoids loose their super-competitor capacity**
A Gene expression pattern of WT organoids treated with WT and $APC^{-/-}$ medium. Adapted from Flanagan *et al.* [130]. **B** Gene expression pattern of shNTC, shUsp10-1 and shUsp10-2 organoids compared to organoids from (A) for stemness and differentiation genes.

The here provided hypothesis is, of course, preliminary and only based on a comparison of the transcription of a minute set of genes. As already mentioned above, due to the infection strategy of shNTC and shUsp10 mAPK9 organoids, one needs to keep in mind that not all cells are transformed and organoids are still very heterogeneous. To study the effect of USP10 on clonal capacity, organoids would be required to be infected and grown from single cells. With these clonal organoids the effect of shUsp10 cultured medium on WT organoids could be investigated and compared to the results from the publication. Additionally, by performing co-culturing experiments, the effect of Usp10 KD on its neighbouring cells could be analysed. Another very elegant strategy to investigate the level of heterogeneity and the clonal capacity of shUsp10 compared to shNTC organoids would be spatial transcriptomics. By performing a spatial transcriptomics experiment, one does not only get the transcriptomic information of cells, but additionally spatially resolved information [131]. With such a method, a resolution down to 3- 5 cells is possible and a direct effect of a transformed cell on a WT cell, dependent on Usp10 level, could be investigated. When combining this method with single cell RNA sequencing, an even more detailed view would be possible.
Nevertheless, the data provided so far lead to the assumption that USP10 indeed is a regulator of intestinal homeostasis by its ability to contribute to the regulation of stemness and differentiation and could thereby putatively also effect the clonal capacity of tumourigenic cells.

4.3 Inhibition of USP10 as putative therapeutic strategy for CRC

Extensive research on deubiquitylating enzymes, such as USP10, has been made in the past decades. During the time, more and more substrates and thus, novel cellular processes which are regulated by DUBs have been identified. It is no surprise in so far that a similar amount of effort went into the investigation of their putative therapeutic

targeting. With bortezomib, an inhibitor of the proteasome, a first inhibitor of the UPS is already in the clinics and shows promising results in the therapy of multiple myeloma and mantle cell lymphoma [132]. But of cause, in terms of targeted therapy, the development of specific DUB inhibitors is still ongoing.
For USP10, the first described inhibitor is Spautin-1 and was published in 2014. Although it was described by several studies in targeting USP10 direct or indirectly ([133], [134], [135]), in this thesis, no direct inhibition of USP10 could be observed. A possible explanation for that could be the experimental set up. Here, two different CRC cell lines were treated for 24 h with Spautin-1 and an inhibitory effect was investigated using the so called warhead assay (reviewed in [136]). In contrast to the other studies, the direct inhibition of USP10 was target of observation and not the physiological downstream effect. Therefore, a short-lived change in activity was possibly overseen. Noteworthy, in the original study, where Spautin-1 was developed, the proposed mechanism is based on an interaction and regulation of USP13 and USP10 [95]. No efforts were made so far, to investigate whether this interaction is also true in colorectal cancer.
Spautin-1 is the only commercially available selective USP10 inhibitor so far, but two other USP7 inhibitors, P22077 and HBX19818, have been also described in inhibiting USP10. In a study from Weisberg *et al.* in 2017, the inhibition of USP10 by P22077 and HBX19818 results in the degradation of oncogenic FLT3 in acute myeloid leukemia [94]. Based on these results, similar experiments were performed with those two inhibitors. However, no direct inhibition of USP10 could be observed again. In this case, the most reasonable explanation is the duration of treatment. In the publication, the inhibitor treatment was only for a few hours, however in the here used experimental set up, 24 h treatment was performed. Not much is known about USP10 turnover, but given its strong expression in cancer cells, it could be that novel transcribed and translated protein replaced the inhibited USP10.
In summary, with the commercial available inhibitors, no inhibitory effect on USP10 protein could be proven so far. This is in line with the test of *de novo* inhibitors, which were tested in cooperation with the Universities of Frankfurt and Leiden. The tested inhibitors were identified in an *in vitro* screen but could not proof inhibitory capacity for USP10 in a cellular system (figures 3.19 - 3.22). However, as a conclusion from the experiments with the commercial inhibitors, shorter timepoints and effects on downstream targets of USP10 should be included in the future experiments.
Albeit none of the inhibitors tested in this thesis showed promising effects on USP10 in cellular systems, the need of small molecule inhibition of USP10 still exists. For a long time, the main focus on inhibition of the UPS was on E3 ligase inhibitions, the development of Protacs or broad proteasome inhibitors and DUBs are relatively new [137], [138]. But there are several challenges, researchers developing DUB drugs are facing. Firstly, although most USPs have the USP domain in common, and a mode-of-action is proposed, crystal structures, which are inevitable for efficient drug design, are rare. The mode-of-action for most USPs relies on structures from USP5, 7 and 8. However, this is not enough structural knowledge to design potent inhibitors, blocking the active center of a DUB (reviewed in [100]). Secondly, DUBs seem to have a certain set of substrates *in vivo*, but often selectivity is not only based on the substrate, but on an interplay of ubiquitin-chain, substrate, activation of a DUB via PTMs and tissue-context [139], [140], [141]. Thirdly, which is in line with the first problem, several DUBs show similar features and domains. USP25 and USP28 for example, are structurally highly homologous but have distinct physiological functions [142], [143]. This similarity between various

DUBs makes the discovery of potent and selective small molecule inhibitors even more challenging.
The here described *de novo* interaction between USP10 and β-Catenin would also open the possibility to develop protein-protein-interaction inhibitors. This approach could be an option to target distinct cellular processes via DUB inhibition [144], [145].

4.4 The development of a fast and easy-to-use mouse model for CRC

With the identification of USP10 as putative novel stem cell marker and *de novo* regulator of β-Catenin in APC-truncated CRC, the question for a suitable *in vivo* model arose. As introduced before, various genetic models of CRC exist, recapitulating patient-relevant mutations. However, utilising these models to test novel hypotheses by classical breeding is time consuming and expensive (reviewed in [62]). Both factors are not always given in a PhD timespan. Additional to classical mouse genetics, novel options, as the implantation of genetically engineered organoids exist but are technically very challenging [77], [79]. To overcome this, a fast and easy-to-use mouse model, based on CRISPR/Cas9, should be developed during this thesis.
Based previous publication from this lab, such as Hartmann *et al.*, lentiviral particles should be used as transport vehicles to infect cells with CRISPR/Cas9 *in vivo* and generate tumours with our genetic needs [92].
Various attempts to establish and optimise this method, also for the colon, were done during the time of this thesis. The two most prominent trials were described here (figures 3.23 - 3.25). With the lentiviral introduction of guide RNAs targeting *APC* and *Trp53* into constitutively Cas9 expressing mice, transformed lesions in the small intestine could be caused. Furthermore, atypical changes and extended crypt length in the colon (data not shown) could be observed too. With the expression of the proliferating marker protein Ki67, it was proven that lesions in the small intestine hyper-proliferate. Additionally, the grade of disorganisation of the typical crypt-villus structure and the increase in number of cells, provide evidences of early adenomas (as reviewed in [146]). Another typical histo-pathological marker for adenomas, caused by deregulated WNT-signalling, is the abundance of nuclear β-Catenin [147]. Of note, since β-Catenin is also present in untransformed crypts, a convincing IHC staining is challenging. In addition to the IHC staining of marker proteins, also other characteristics of transformed areas could be investigated. Especially for hyper-proliferative lesions histological parameters could be measured: an increase in number of cells found in a crypt as well as the length of crypts and villi determine the grade of transformation for colon and intestine, respectively.
As stated before, only two out of several different trials were described in this thesis. With the described experiments here, small lesions, mainly in the small intestine were achieved. However, not every animal developed lesions and the main purpose was to achieve transformation in the colon, because this reflects patient-relevant disease. During optimisation, differences in duration and concentration of DSS pre-treatment were tried. Additionally, NAC and low-percentage EtOH treatment were also tested. To achieve more lesions in the colon, than in the intestine, reduced volume of virus was tested too. As shown in figure 3.23, 500 µL of virus was enough to not only flush the colon, but also the caecum and the first part of the ileum. Another problem we faced,

was remaining excrement in the colon, which presumably prevented the whole liquid to get inside. To overcome this, mice were also put on temporal starvation (in line with animal care guidelines), before injection.
Taken together, it is known from other organs that lentiviral infection *in vivo* can be used as an elegant tool to introduce tumours [92]. However, the lung for example is a very suitable organ to take liquid. In contrast, the GI tract is anatomically designed for the opposite. Therefore, the colorectal instillation of sufficient amount of virus for a suitable time-frame of infection remains challenging and needs to be further optimised.

4.5 Conclusion

At the beginning of this thesis, USP10 was identified in an siRNA based DUB library screen as novel regulator of β-Catenin. Therefore, interaction studies and KO and KD experiments should be performed to validate this finding. As presented here, the initial observation and the methods and tools, developed during this project, resulted in the identification of a novel mode of action of USP10 on β-Catenin. In various experiments it could be demonstrated that the regulation of β-Catenin by USP10 is dependent on the APC truncating mutation in CRC. Furthermore, the transcriptional consequences of USP10 depletion and overexpression lead to the observation that USP10 not only stabilises β-Catenin but also affects the stemness and differentiation program of cells.

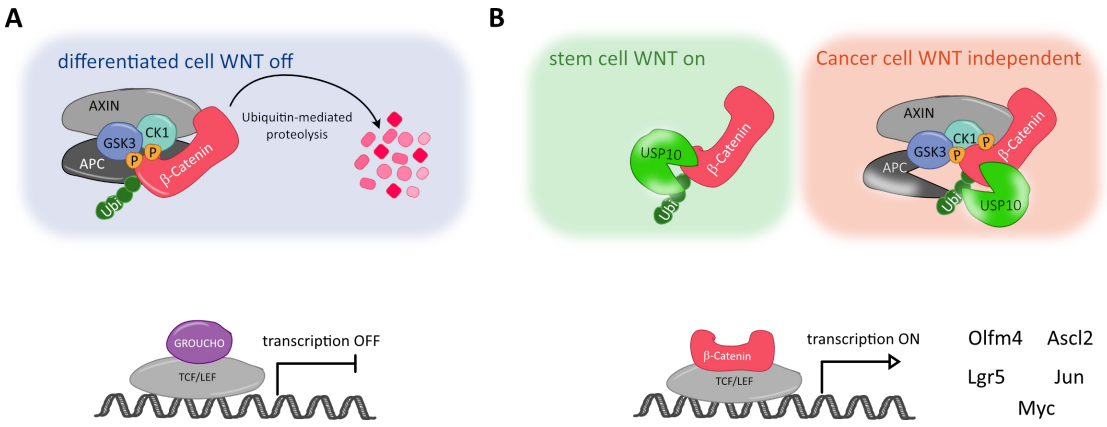

Figure 4.3: **Proposed model of USP10-β-Catenin interaction in CRC**
A USP10 is not able to interact with and stabilise β-Catenin when the destruction complex is intact and WNT signalling is off. Transcription of β-Catenin target genes is off. **B** In stem cells, with active WNT signalling, USP10 can further stabilise β-Catenin and activate the transcription of its target genes. In APC-truncated cancer cells, USP10-β-Catenin interaction is enabled and leads to increased expression of its target genes, promoting tumourigenesis.

In figure 4.3, a model, depending on APC-truncation or cell fate, is summarised.
In differentiated cells, where the WNT signalling cascade is not active, the destruction complex forms and leads to the proteasomal degradation of β-Catenin. The transcription of its target genes is switched off and cells do not actively proliferate (see figure 4.3 A). In this state of a cell, the majority of the β-Catenin pool is in the cytosol and gets

recruited to the cell membrane where it participates in cell-cell contacts and supports the epithelial cell type character. Consistently, the expression of USP10 is also low in these cells.
However, in stem cells at the bottom of the crypts, which are exposed to WNT ligands, USP10 elevated levels of USP10 are found. In the presence of WNT, the destruction complex does not form and β-Catenin is stabilised, translocates to the nucleus and activates the transcription of its target genes, such as *JUN*, *MYC*, and *ASCL2*. We hypothesis that USP10 already interacts with and stabilises β-Catenin in these actively proliferating stem cells (see figure 4.3 B, left part).
Furthermore, in tumour-cells, which are driven by the short APC variant, the destruction complex still forms but is less efficient and potentially enables USP10 to bind and deubiquitylate β-Catenin. This hypothesis is driven by the interaction studies we performed in CRC cell lines with various APC truncation length and are supported by the literature [45].
Taken together, in this thesis USP10 was identified as a novel regulator of β-Catenin stability in CRC in line with a putative role in stem cell homeostasis. The level of USP10 expression correlates with the proliferation capacity of an intestinal cell. Furthermore, USP10 overexpression contributes to EMT in 2D as well as 3D cell culture. With this thesis USP10s role as oncogene in CRC could be proven and contributes to the understanding of tissue specific roles for DUBs.

5 Bibliography

[1] *WHO | World Health Organization.*

[2] R. L. Siegel, K. D. Miller, H. E. Fuchs, and A. Jemal. "Cancer Statistics, 2021". In: *CA. Cancer J. Clin.* 71.1 (Jan. 2021), pp. 7–33. ISSN: 1542-4863.

[3] P. Correa, J. P. Strong, A. Reif, and W. D. Johnson. "The epidemiology of colorectal polyps: prevalence in New Orleans and international comparisons." eng. In: *Cancer* 39.5 (May 1977), pp. 2258–2264. ISSN: 0008-543X (Print).

[4] *Risks and causes of bowel cancer | Cancer Research UK.*

[5] J. P. Lockhart-Mummery and C. E. Dukes. "The pancancerous changes in the rectum and colon". In: *Surg. , Gynecol. Obstet.* 46 (1928), pp. 591–596.

[6] R. Jackman and C. W. Mayo. "The adenoma-carcinoma sequence in cancer of the colon". In: *Surg. , Gynecol. Obstet.* 93.3 (1951), pp. 327–330.

[7] T. Muto, H. J. Bussey, and B. C. Morson. "The evolution of cancer of the colon and rectum." eng. In: *Cancer* 36.6 (Dec. 1975), pp. 2251–2270. ISSN: 0008-543X (Print).

[8] A. Leslie, F. A. Carey, N. R. Pratt, and R. J. Steele. "The colorectal adenoma-carcinoma sequence". In: *Br. J. Surg.* 89.7 (2002), pp. 845–860. ISSN: 0007-1323.

[9] F. De Palma, V. D'Argenio, J. Pol, G. Kroemer, M. Maiuri, and F. Salvatore. "The Molecular Hallmarks of the Serrated Pathway in Colorectal Cancer". In: *Cancers (Basel).* 11.7 (July 2019), p. 1017. ISSN: 2072-6694.

[10] E. J. Kuipers, W. M. Grady, D. Lieberman, T. Seufferlein, J. J. Sung, P. G. Boelens, C. J. Van De Velde, and T. Watanabe. "Colorectal cancer". In: *Nat. Rev. Dis. Prim. 2015 11* 1.1 (Nov. 2015), pp. 1–25. ISSN: 2056-676X.

[11] J. L. Tsao and D. Shibata. "Further evidence that one of the earliest alterations in colorectal carcinogenesis involves APC." In: *Am. J. Pathol.* 145.3 (Sept. 1994), p. 531. ISSN: 00029440.

[12] S. E. Goelz, B. Vogelstein, S. R. Hamilton, and A. P. Feinberg. "Hypomethylation of DNA from Benign and Malignant Human Colon Neoplasms". In: *Science (80-.).* 228.4696 (1985), pp. 187–190. ISSN: 00368075.

[13] K. R. Cho, J. D. Oliner, J. W. Simons, L. Hedrick, E. R. Fearon, A. C. Preisinger, P. Hedge, G. A. Silverman, and B. Vogelstein. "The DCC Gene: Structural Analysis and Mutations in Colorectal Carcinomas". In: *Genomics* 19.3 (Feb. 1994), pp. 525–531. ISSN: 0888-7543.

[14] C.-H. Heldin, K. Miyazono, and
bibinitperiod Peter. "TGF-signalling from cell membrane to nucleus through SMAD proteins". In: *Nat. ľ Macmillan Publ. Ltd* 390 (1997).

[15] M. J. O'Brien and D. Gibbons. "The adenoma-carcinoma sequence in colorectal neoplasia". In: *Surg. Oncol. Clin. N. Am.* 5.3 (1996), pp. 513–530. ISSN: 10553207.

[16] J. Guinney et al. "The consensus molecular subtypes of colorectal cancer". In: *Nat. Med. 2015 2111* 21.11 (Oct. 2015), pp. 1350–1356. ISSN: 1546-170X.

[17] R. Dienstmann, L. Vermeulen, J. Guinney, S. Kopetz, S. Tejpar, and J. Tabernero. "Consensus molecular subtypes and the evolution of precision medicine in colorectal cancer". In: *Nat. Rev. Cancer 2017 172* 17.2 (Jan. 2017), pp. 79–92. ISSN: 1474-1768.

[18] N. Barker. "Adult intestinal stem cells: critical drivers of epithelial homeostasis and regeneration". In: *Nat. Rev. Mol. Cell Biol. 2013 151* 15.1 (Dec. 2013), pp. 19–33. ISSN: 1471-0080.

[19] M. J. Parsons, T. Tammela, and L. E. Dow. "WNT as a driver and dependency in cancer". In: *Cancer Discov.* 11.10 (Oct. 2021), pp. 2413–2429. ISSN: 21598290.

[20] T. Sato, J. H. Van Es, H. J. Snippert, D. E. Stange, R. G. Vries, M. Van Den Born, N. Barker, N. F. Shroyer, M. Van De Wetering, and H. Clevers. "Paneth cells constitute the niche for Lgr5 stem cells in intestinal crypts". In: *Nat. 2010 4697330* 469.7330 (Nov. 2010), pp. 415–418. ISSN: 1476-4687.

[21] S. Ikeda, S. Kishida, H. Yamamoto, H. Murai, S. Koyama, and A. Kikuchi. "Axin, a negative regulator of the Wnt signaling pathway, forms a complex with GSK-3beta and beta-catenin and promotes GSK-3beta-dependent phosphorylation of beta-catenin". In: *EMBO J.* 17.5 (Mar. 1998), pp. 1371–1384. ISSN: 0261-4189.

[22] S. Amit, A. Hatzubai, Y. Birman, J. S. Andersen, E. Ben-Shushan, M. Mann, Y. Ben-Neriah, and I. Alkalay. "Axin-mediated CKI phosphorylation of beta-catenin at Ser 45: a molecular switch for the Wnt pathway". In: *Genes Dev.* 16.9 (May 2002), pp. 1066–1076. ISSN: 0890-9369.

[23] H. Aberle, A. Bauer, J. Stappert, A. Kispert, and R. Kemler. "β-catenin is a target for the ubiquitinproteasome pathway". In: *EMBO J.* 16.13 (July 1997), pp. 3797–3804. ISSN: 1460-2075.

[24] C. Liu, Y. Li, M. Semenov, C. Han, G. H. Baeg, Y. Tan, Z. Zhang, X. Lin, and X. He. "Control of β-catenin phosphorylation/degradation by a dual-kinase mechanism". In: *Cell* 108.6 (Mar. 2002), pp. 837–847. ISSN: 00928674.

[25] A. J. Quyn, P. L. Appleton, F. A. Carey, R. J. Steele, N. Barker, H. Clevers, R. A. Ridgway, O. J. Sansom, and I. S. Näthke. "Spindle orientation bias in gut epithelial stem cell compartments is lost in precancerous tissue". In: *Cell Stem Cell* 6.2 (Feb. 2010), pp. 175–181. ISSN: 1875-9777.

[26] B. M. Boman and J. Z. Fields. "An APC:WNT Counter-Current-Like Mechanism Regulates Cell Division Along the Human Colonic Crypt Axis: A Mechanism That Explains How APC Mutations Induce Proliferative Abnormalities That Drive Colon Cancer Development". In: *Front. Oncol.* 3 (2013). ISSN: 2234-943X.

[27] C. Albuquerque, C. Breukel, R. Van Der Luijt, P. Fidalgo, P. Lage, F. J. Slors, C. Nobre Leitão, R. Fodde, and R. Smits. "The just-right' signaling model: APC somatic mutations are selected based on a specific level of activation of the β-catenin signaling cascade". In: *Hum. Mol. Genet.* 11.13 (June 2002), pp. 1549–1560. ISSN: 0964-6906.

[28] M. Buchert et al. "Genetic Dissection of Differential Signaling Threshold Requirements for the Wnt/β-Catenin Pathway In Vivo". In: *PLOS Genet.* 6.1 (Jan. 2010), e1000816. ISSN: 1553-7404.

[29] A. Ciechanover. "The unravelling of the ubiquitin system". In: *Nat. Rev. Mol. Cell Biol. 2015 165* 16.5 (Apr. 2015), pp. 322–324. ISSN: 1471-0080.

[30] R. B. Damgaard. "The ubiquitin system: from cell signalling to disease biology and new therapeutic opportunities". In: *Cell Death Differ. 2021 282* 28.2 (Jan. 2021), pp. 423–426. ISSN: 1476-5403.

[31] D. Komander and M. Rape. "The Ubiquitin Code". In: *Annu. Rev. Biochem.* 81.1 (2012), pp. 203–229.

[32] X. Tian, Z. Liu, B. Niu, J. Zhang, T. K. Tan, S. R. Lee, Y. Zhao, D. C. Harris, and G. Zheng. "E-cadherin/β-catenin complex and the epithelial barrier". In: *J. Biomed. Biotechnol.* 2011 (2011). ISSN: 1110-7251.

[33] J. Liu, J. Stevens, C. A. Rote, H. J. Yost, Y. Hu, K. L. Neufeld, R. L. White, and N. Matsunami. "Siah-1 mediates a novel beta-catenin degradation pathway linking p53 to the adenomatous polyposis coli protein". In: *Mol. Cell* 7.5 (May 2001), pp. 927–936. ISSN: 1097-2765.

[34] M. Abed et al. "RNF4-Dependent Oncogene Activation by Protein Stabilization". In: *Cell Rep.* 16.12 (Sept. 2016), p. 3388. ISSN: 22111247.

[35] V. C. Chitalia et al. "Jade-1 inhibits Wnt signaling by ubiquitinating β-catenin and mediates Wnt pathway inhibition by pVHL". In: *Nat. Cell Biol.* 10.10 (2008), p. 1208. ISSN: 14657392.

[36] H. X. Hao et al. "ZNRF3 promotes Wnt receptor turnover in an R-spondin-sensitive manner". In: *Nature* 485.7397 (May 2012), pp. 195–202. ISSN: 1476-4687.

[37] S. Angers, C. J. Thorpe, T. L. Biechele, S. J. Goldenberg, N. Zheng, M. J. MacCoss, and R. T. Moon. "The KLHL12-Cullin-3 ubiquitin ligase negatively regulates the Wnt-beta-catenin pathway by targeting Dishevelled for degradation". In: *Nat. Cell Biol.* 8.4 (Apr. 2006), pp. 348–357. ISSN: 1465-7392.

[38] R. E. De Groot et al. "Huwe1-mediated ubiquitylation of dishevelled defines a negative feedback loop in the Wnt signaling pathway". In: *Sci. Signal.* 7.317 (Mar. 2014). ISSN: 19379145.

[39] N. Baloghova, T. Lidak, and L. Cermak. "Ubiquitin Ligases Involved in the Regulation of Wnt, TGF-β, and Notch Signaling Pathways and Their Roles in Mouse Development and Homeostasis". In: *Genes 2019, Vol. 10, Page 815* 10.10 (Oct. 2019), p. 815. ISSN: 2073-4425.

[40] H. B. Park, J. W. Kim, and K. H. Baek. "Regulation of Wnt Signaling through Ubiquitination and Deubiquitination in Cancers". In: *Int. J. Mol. Sci. 2020, Vol. 21, Page 3904* 21.11 (May 2020), p. 3904. ISSN: 1422-0067.

[41] B. Madana et al. "USP6 oncogene promotes Wnt signaling by deubiquitylating Frizzleds". In: *Proc. Natl. Acad. Sci. U. S. A.* 113.21 (May 2016), E2945–E2954. ISSN: 1091-6490.

[42] D. V. Tauriello, A. Haegebarth, I. Kuper, M. J. Edelmann, M. Henraat, M. R. Canninga-van Dijk, B. M. Kessler, H. Clevers, and M. M. Maurice. "Loss of the tumor suppressor CYLD enhances Wnt/beta-catenin signaling through K63-linked ubiquitination of Dvl". In: *Mol. Cell* 37.5 (Mar. 2010), pp. 607–619. ISSN: 1097-4164.

[43] X. Huang, C. Langelotz, B. K. Hetfeld-Pcho, W. Schwenk, and W. Dubiel. "The COP9 Signalosome Mediates β-Catenin Degradation by Deneddylation and Blocks Adenomatous Polyposis coli Destruction via USP15". In: *J. Mol. Biol.* 391.4 (Aug. 2009), pp. 691–702. ISSN: 0022-2836.

[44] J. Shi, Y. Liu, X. Xu, W. Zhang, T. Yu, J. Jia, and C. Liu. "Deubiquitinase USP47/UBP64E Regulates β-Catenin Ubiquitination and Degradation and Plays a Positive Role in Wnt Signaling". In: *Mol. Cell. Biol.* 35.19 (Oct. 2015), p. 3301. ISSN: 0270-7306.

[45] L. Novellasdemunt, V. Foglizzo, L. Cuadrado, P. Antas, A. Kucharska, V. Encheva, A. P. Snijders, and V. S. Li. "USP7 Is a Tumor-Specific WNT Activator for APC-Mutated Colorectal Cancer by Mediating β-Catenin Deubiquitination". In: *Cell Rep.* 21.3 (Oct. 2017), pp. 612–627. ISSN: 2211-1247.

[46] J. Yuan, K. Luo, L. Zhang, J. C. Cheville, and Z. Lou. "USP10 Regulates p53 Localization and Stability by Deubiquitinating p53". In: *Cell* 140.3 (Feb. 2010), pp. 384–396. ISSN: 0092-8674.

[47] A. G. Jochemsen and Y. Shiloh. "USP10: Friend and Foe". In: *Cell* 140.3 (Feb. 2010), pp. 308–310. ISSN: 0092-8674.

[48] J. Sun, T. Li, Y. Zhao, L. Huang, H. Sun, H. Wu, and X. Jiang. "USP10 inhibits lung cancer cell growth and invasion by upregulating PTEN". In: *Mol. Cell. Biochem.* 441.1-2 (Apr. 2018), pp. 1–7. ISSN: 15734919.

[49] G. H. Han, D. B. Chay, J. M. Yi, H. Cho, J. Y. Chung, and J. H. Kim. "Loss of Both USP10 and p14ARF Protein Expression Is an Independent Prognostic Biomarker for Poor Prognosis in Patients With Epithelial Ovarian Cancer". In: *Cancer Genomics Proteomics* 16.6 (Nov. 2019), pp. 553–562. ISSN: 1109-6535.

[50] K. Kim, T. Huh, Y. Park, D. H. Koo, H. Kim, I. Hwang, C. H. Choi, J. M. Yi, and J. Y. Chung. "Prognostic significance of USP10 and p14ARF expression in patients with colorectal cancer". In: *Pathol. - Res. Pract.* 216.6 (June 2020), p. 152988. ISSN: 0344-0338.

[51] J. S. Song, J. M. Yi, H. Cho, C. H. Choi, Y. Park, E. J. Chung, J. Song, J. Y. Chung, and S. M. Hong. "Dual loss of USP10 and p14ARF protein expression is associated with poor prognosis in patients with small intestinal adenocarcinoma". In: *Tumor Biol.* 40.10 (Oct. 2018). ISSN: 14230380.

[52] N. Kumari, A. Saei, C. Lalith, V. Serra, S. Jha, and P. Eichhorn. "Identifying the oncogenic role of USP10 as the regulator of PTEN function in breast cancer". In: *Ann. Oncol.* 29 (Mar. 2018), pp. iii10–iii11. ISSN: 0923-7534.

[53] J. M. Grunda et al. "Increased expression of thymidylate synthetase (TS), ubiquitin specific protease 10 (USP10) and survivin is associated with poor survival in glioblastoma multiforme (GBM)". In: *J Neurooncol* 80 (2006), pp. 261–274.

[54] K. ichi Takayama, T. Suzuki, T. Fujimura, S. Takahashi, and S. Inoue. "Association of USP10 with G3BP2 inhibits p53 signaling and contributes to poor outcome in prostate cancer". In: *Mol. Cancer Res.* 16.5 (May 2018), pp. 846–856. ISSN: 15573125.

[55] J. Groden, A. Thliveris, W. Samowitz, M. Carlson, L. Gelbert, H. Albertsen, G. Joslyn, J. Stevens, L. Spirio, and M. Robertson. "Identification and characterization of the familial adenomatous polyposis coli gene." eng. In: *Cell* 66.3 (Aug. 1991), pp. 589–600. ISSN: 0092-8674 (Print).

[56] A. R. Moser, H. C. Pitot, and W. F. Dove. "A dominant mutation that predisposes to multiple intestinal neoplasia in the mouse". In: *Science* 247.4940 (1990), pp. 322–324. ISSN: 0036-8075.

[57] A. R. Moser, C. Luongo, K. A. Gould, M. K. McNeley, A. R. Shoemaker, and W. F. Dove. "ApcMin: A mouse model for intestinal and mammary tumorigenesis". In: *Eur. J. Cancer* 31.7-8 (July 1995), pp. 1061–1064. ISSN: 0959-8049.

[58] F. Bürtin, C. S. Mullins, and M. Linnebacher. "Mouse models of colorectal cancer: Past, present and future perspectives". In: *World J. Gastroenterol.* 26.13 (Apr. 2020), p. 1394. ISSN: 22192840.

[59] I. Okayasu, S. Hatakeyama, M. Yamada, T. Ohkusa, Y. Inagaki, and R. Nakaya. "A novel method in the induction of reliable experimental acute and chronic ulcerative colitis in mice". In: *Gastroenterology* 98.3 (1990), pp. 694–702. ISSN: 0016-5085.

[60] I. Okayasu, M. Yamada, T. Mikami, T. Yoshida, J. Kanno, and T. Ohkusa. "Dysplasia and carcinoma development in a repeated dextran sulfate sodium-induced colitis model". In: *J. Gastroenterol. Hepatol.* 17.10 (2002), pp. 1078–1083. ISSN: 0815-9319.

[61] H. S. Cooper, L. Everley, W. C. Chang, G. Pfeiffer, B. Lee, S. Murthy, and M. L. Clapper. "The role of mutant Apc in the development of dysplasia and cancer in the mouse model of dextran sulfate sodium-induced colitis". In: *Gastroenterology* 121.6 (2001), pp. 1407–1416. ISSN: 0016-5085.

[62] R. Jackstadt and O. J. Sansom. "Mouse models of intestinal cancer". In: *J. Pathol.* 238.2 (Jan. 2016), pp. 141–151. ISSN: 1096-9896.

[63] H. Shibata et al. "Rapid colorectal adenoma formation initiated by conditional targeting of the APC gene". In: *Science (80-.).* 278.5335 (Oct. 1997), pp. 120–133. ISSN: 00368075.

[64] O. J. Sansom et al. "Loss of Apc in vivo immediately perturbs Wnt signaling, differentiation, and migration". In: *Genes Dev.* 18.12 (June 2004), p. 1385. ISSN: 08909369.

[65] F. El Marjou, K. P. Janssen, B. H. J. Chang, M. Li, V. Hindie, L. Chan, D. Louvard, P. Chambon, D. Metzger, and S. Robine. "Tissue-specific and inducible Cre-mediated recombination in the gut epithelium". In: *Genesis* 39.3 (July 2004), pp. 186–193. ISSN: 1526-954X.

[66] R. Rad et al. "A genetic progression model of Braf(V600E)-induced intestinal tumorigenesis reveals targets for therapeutic intervention". In: *Cancer Cell* 24.1 (July 2013), pp. 15–29. ISSN: 1878-3686.

[67] K. Takaku, M. Oshima, H. Miyoshi, M. Matsui, M. F. Seldin, and M. M. Taketo. "Intestinal tumorigenesis in compound mutant mice of both Dpc4 (Smad4) and Apc genes". In: *Cell* 92.5 (Mar. 1998), pp. 645–656. ISSN: 0092-8674.

[68] E. Sakai et al. "Combined Mutation of Apc, Kras, and Tgfbr2 Effectively Drives Metastasis of Intestinal Cancer". In: *Cancer Res.* 78.5 (Mar. 2018), pp. 1334–1346. ISSN: 1538-7445.

[69] W. M. S. Russell and R. Burch. "The Principles of Humane Experimental Technique". In: *Med. J. Aust.* 1.13 (Mar. 1960), pp. 500–500. ISSN: 0025-729X.

[70] T. Sato et al. "Single Lgr5 stem cells build crypt-villus structures in vitro without a mesenchymal niche". In: *Nat. 2009 4597244* 459.7244 (Mar. 2009), pp. 262–265. ISSN: 1476-4687.

[71] T. Sato et al. "Long-term expansion of epithelial organoids from human colon, adenoma, adenocarcinoma, and Barrett's epithelium". In: *Gastroenterology* 141.5 (Nov. 2011), pp. 1762–1772. ISSN: 15280012.

[72] P. Mali, L. Yang, K. M. Esvelt, J. Aach, M. Guell, J. E. DiCarlo, J. E. Norville, and G. M. Church. "RNA-guided human genome engineering via Cas9". In: *Science (80-.).* 339.6121 (Feb. 2013), pp. 823–826. ISSN: 10959203.

[73] L. Cong et al. "Multiplex genome engineering using CRISPR/Cas systems". In: *Science (80-.).* 339.6121 (Feb. 2013), pp. 819–823. ISSN: 10959203.

[74] G. Schwank et al. "Functional Repair of CFTR by CRISPR/Cas9 in Intestinal Stem Cell Organoids of Cystic Fibrosis Patients". In: *Cell Stem Cell* 13.6 (Dec. 2013), pp. 653–658. ISSN: 1934-5909.

[75] M. Matano, S. Date, M. Shimokawa, A. Takano, M. Fujii, Y. Ohta, T. Watanabe, T. Kanai, and T. Sato. "Modeling colorectal cancer using CRISPR-Cas9mediated engineering of human intestinal organoids". In: *Nat. Med. 2015 213* 21.3 (Feb. 2015), pp. 256–262. ISSN: 1546-170X.

[76] M. Fujii et al. "A Colorectal Tumor Organoid Library Demonstrates Progressive Loss of Niche Factor Requirements during Tumorigenesis". In: *Cell Stem Cell* 18.6 (June 2016), pp. 827–838. ISSN: 1875-9777.

[77] A. Fumagalli et al. "Genetic dissection of colorectal cancer progression by orthotopic transplantation of engineered cancer organoids". In: *Proc. Natl. Acad. Sci. U. S. A.* 114.12 (Mar. 2017), E2357–E2364. ISSN: 10916490.

[78] K. P. O'Rourke et al. "Transplantation of engineered organoids enables rapid generation of metastatic mouse models of colorectal cancer". In: *Nat. Biotechnol.* 35.6 (June 2017), pp. 577–582. ISSN: 1546-1696.

[79] J. Roper et al. "In vivo genome editing and organoid transplantation models of colorectal cancer and metastasis". In: *Nat. Biotechnol.* 35.6 (June 2017), pp. 569–576. ISSN: 15461696.

[80] B. Langmead and S. L. Salzberg. "Fast gapped-read alignment with Bowtie 2". In: *Nat. Methods 2012 94* 9.4 (Mar. 2012), pp. 357–359. ISSN: 1548-7105.

[81] M. D. Robinson, D. J. McCarthy, and G. K. Smyth. "edgeR: a Bioconductor package for differential expression analysis of digital gene expression data". In: *Bioinformatics* 26.1 (Jan. 2010), pp. 139–140. ISSN: 1367-4803.

[82] Y. Liao, G. K. Smyth, and W. Shi. "featureCounts: an efficient general purpose program for assigning sequence reads to genomic features". In: *Bioinformatics* 30.7 (Apr. 2014), pp. 923–930. ISSN: 1367-4803. arXiv: 1305.3347.

[83] H. Li, B. Handsaker, A. Wysoker, T. Fennell, J. Ruan, N. Homer, G. Marth, G. Abecasis, and R. Durbin. "The Sequence Alignment/Map format and SAMtools". In: *Bioinformatics* 25.16 (Aug. 2009), pp. 2078–2079. ISSN: 1367-4803.

[84] G. J. M Rosa et al. "ggplot2: Elegant Graphics for Data Analysis by WICKHAM, H." In: *Biometrics* 67.2 (June 2011), pp. 678–679. ISSN: 1541-0420.

[85] C. Fellmann et al. "An optimized microRNA backbone for effective single-copy RNAi". In: *Cell Rep.* 5.6 (Dec. 2013), pp. 1704–1713. ISSN: 22111247.

[86] C. Moolenbeek and E. J. Ruitenberg. "The 'Swiss roll': a simple technique for histological studies of the rodent intestine". In: *Lab. Anim.* 15 (1981), pp. 57–59.

[87] C. Hu et al. "The USP10-HDAC6 axis confers cisplatin resistance in non-small cell lung cancer lacking wild-type p53". In: *Cell Death \& Dis. 2020 115* 11.5 (May 2020), pp. 1–18. ISSN: 2041-4889.

[88] S. wen Ouyang, T. ting Liu, X. sheng Liu, F. xiang Zhu, F. ming Zhu, X. ni Liu, and Z. hai Peng. "USP10 regulates Musashi-2 stability via deubiquitination and promotes tumour proliferation in colon cancer". In: *FEBS Lett.* 593.4 (Feb. 2019), pp. 406–413. ISSN: 1873-3468.

[89] D. Y. Fu, Z. M. Wang, Li-Chen, B. L. Wang, Z. Z. Shen, W. Huang, and Z. M. Shao. "Sox17, the canonical Wnt antagonist, is epigenetically inactivated by promoter methylation in human breast cancer". In: *Breast Cancer Res. Treat.* 119.3 (Feb. 2010), pp. 601–612. ISSN: 01676806.

[90] B. Pereira et al. "MEX3A regulates Lgr5+ stem cell maintenance in the developing intestinal epithelium". In: *EMBO Rep.* 21.4 (Apr. 2020), e48938. ISSN: 1469-3178.

[91] J. Zhang, Q. Li, Q. Sun, B. Wang, Y. Cui, C. Lou, Y. Yao, and Y. Zhang. "Epigenetic modifications inhibit the expression of MARVELD1 and in turn tumorigenesis by regulating the Wnt/β-catenin pathway in pan-cancer". In: *J. Cancer* 13.1 (2022), pp. 225–242. ISSN: 18379664.

[92] O. Hartmann et al. "Implementation of CRISPR/Cas9 Genome Editing to Generate Murine Lung Cancer Models That Depict the Mutational Landscape of Human Disease". In: *Front. Cell Dev. Biol.* 9 (Mar. 2021), p. 201. ISSN: 2296634X.

[93] D. M. Gonzalez and D. Medici. "Signaling mechanisms of the epithelial-mesenchymal transition". In: *Sci. Signal.* 7.344 (Sept. 2014), re8. ISSN: 19379145.

[94] E. L. Weisberg et al. "Inhibition of USP10 induces degradation of oncogenic FLT3". In: *Nat. Chem. Biol. 2017 1312* 13.12 (Oct. 2017), pp. 1207–1215. ISSN: 1552-4469.

[95] J. Liu et al. "Beclin1 Controls the Levels of p53 by Regulating the Deubiquitination Activity of USP10 and USP13". In: *Cell* 147.1 (Sept. 2011), p. 223. ISSN: 10974172.

[96] Y. Sheng, V. Saridakis, F. Sarkari, S. Duan, T. Wu, C. H. Arrowsmith, and L. Frappier. "Molecular recognition of p53 and MDM2 by USP7/HAUSP". In: *Nat. Struct. Mol. Biol. 2006 133* 13.3 (Feb. 2006), pp. 285–291. ISSN: 1545-9985.

[97] R. C. De Lisle, E. Roach, and K. Jansson. "Effects of laxative and N-acetylcysteine on mucus accumulation, bacterial load, transit, and inflammation in the cystic fibrosis mouse small intestine". In: *Am. J. Physiol. Gastrointest. Liver Physiol.* 293.3 (Sept. 2007). ISSN: 0193-1857.

[98] N. Harada, Y. Tamai, T. O. Ishikawa, B. Sauer, K. Takaku, M. Oshima, and M. M. Taketo. "Intestinal polyposis in mice with a dominant stable mutation of the beta-catenin gene". In: *EMBO J.* 18.21 (Nov. 1999), pp. 5931–5942. ISSN: 0261-4189.

[99] K. W. Kinzler and B. Vogelstein. "Lessons from hereditary colorectal cancer". In: *Cell* 87.2 (Oct. 1996), pp. 159–170. ISSN: 0092-8674.

[100] U. Bhattacharya, F. Neizer-Ashun, P. Mukherjee, and R. Bhattacharya. "When the chains do not break: the role of USP10 in physiology and pathology". In: *Cell Death Dis. 2020 1112* 11.12 (Dec. 2020), pp. 1–10. ISSN: 2041-4889.

[101] S. H. Tan, P. Phuah, L. T. Tan, S. Yada, J. Goh, L. B. Tomaz, M. Chua, E. Wong, B. Lee, and N. Barker. "A constant pool of Lgr5+ intestinal stem cells is required for intestinal homeostasis". In: *Cell Rep.* 34.4 (Jan. 2021), p. 108633. ISSN: 22111247.

[102] L. G. van der Flier, A. Haegebarth, D. E. Stange, M. van de Wetering, and H. Clevers. "OLFM4 Is a Robust Marker for Stem Cells in Human Intestine and Marks a Subset of Colorectal Cancer Cells". In: *Gastroenterology* 137.1 (July 2009), pp. 15–17. ISSN: 00165085.

[103] J. Schuijers, J. P. Junker, M. Mokry, P. Hatzis, B. K. Koo, V. Sasselli, L. G. Van Der Flier, E. Cuppen, A. Van Oudenaarden, and H. Clevers. "Ascl2 acts as an R-spondin/Wnt-responsive switch to control stemness in intestinal crypts". In: *Cell Stem Cell* 16.2 (Feb. 2015), pp. 158–170. ISSN: 1875-9777.

[104] V. J. Wielenga, R. Smits, V. Korinek, L. Smit, M. Kielman, R. Fodde, H. Clevers, and S. T. Pals. "Expression of CD44 in Apc and Tcf mutant mice implies regulation by the WNT pathway". In: *Am. J. Pathol.* 154.2 (1999), pp. 515–523. ISSN: 0002-9440.

[105] P. J. Skene and S. Henikoff. "An efficient targeted nuclease strategy for high-resolution mapping of DNA binding sites". In: *Elife* 6 (Jan. 2017). ISSN: 2050084X.

[106] J. D. Buenrostro, B. Wu, H. Y. Chang, and W. J. Greenleaf. "ATAC-seq: A Method for Assaying Chromatin Accessibility Genome-Wide". In: *Curr. Protoc. Mol. Biol.* 109 (2015), p. 21.29.1. ISSN: 19343647.

[107] K. E. Boonekamp, T. L. Dayton, and H. Clevers. "Intestinal organoids as tools for enriching and studying specific and rare cell types: advances and future directions". In: *J. Mol. Cell Biol.* 12.8 (Aug. 2020), pp. 562–568. ISSN: 17594685.

[108] C. Corrò, L. Novellasdemunt, and V. S. Li. "Making Cell Culture More Physiological: A brief history of organoids". In: *Am. J. Physiol. - Cell Physiol.* 319.1 (July 2020), p. C151. ISSN: 15221563.

[109] K.-i. Arimoto, Y. Zhang, M. Yan, S. Miyauchi, S. Weng, S. A. Stoner, T. Shima, Y. Komeno, K. Lam, and D.-E. Zhang. "Usp18 Is Required for Normal Stem Cell Maintenance". In: *Blood* 128.22 (Dec. 2016), pp. 3863–3863. ISSN: 0006-4971.

[110] D. Pei. "Deubiquitylating Nanog: novel role of USP21 in embryonic stem cell maintenance". In: *Signal Transduct. Target. Ther. 2017 21* 2.1 (Apr. 2017), pp. 1–3. ISSN: 2059-3635.

[111] D. J. Flanagan et al. "Frizzled7 Functions as a Wnt Receptor in Intestinal Epithelial Lgr5+ Stem Cells". In: *Stem Cell Reports* 4.5 (May 2015), p. 759. ISSN: 22136711.

[112] J. H. Shin et al. "Dickkopf-2 regulates the stem cell marker LGR5 in colorectal cancer via HNF4α1". In: *iScience* 24.5 (May 2021), p. 102411. ISSN: 2589-0042.

[113] Y. Dimitrova, A. J. Gruber, N. Mittal, S. Ghosh, B. Dimitriades, D. Mathow, W. A. Grandy, G. Christofori, and M. Zavolan. "TFAP2A is a component of the ZEB1/2 network that regulates TGFB1-induced epithelial to mesenchymal transition". In: *Biol. Direct* 12.1 (Apr. 2017), pp. 1–17. ISSN: 17456150.

[114] O. Guillermin et al. "Wnt and Src signals converge on YAP-TEAD to drive intestinal regeneration". In: *EMBO J.* 40.13 (July 2021), e105770. ISSN: 1460-2075.

[115] Z. Zhang, Y. Zhang, X. Qin, Y. Wang, and J. Fu. "FGF9 promotes cisplatin resistance in colorectal cancer via regulation of Wnt/β-catenin signaling pathway". In: *Exp. Ther. Med.* 19.3 (Dec. 2020). ISSN: 1792-0981.

[116] H. Liu, W. Lu, H. He, J. Wu, C. Zhang, H. Gong, and C. Yang. "Inflammation-dependent overexpression of c-Myc enhances CRL4DCAF4 E3 ligase activity and promotes ubiquitination of ST7 in colitis-associated cancer". In: *J. Pathol.* 248.4 (Aug. 2019), pp. 464–475. ISSN: 1096-9896.

[117] P. R. Elliott et al. "SPATA2 Links CYLD to LUBAC, Activates CYLD, and Controls LUBAC Signaling". In: *Mol. Cell* 63.6 (Sept. 2016), pp. 990–1005. ISSN: 1097-4164.

[118] Z. Feng, R. Sun, Y. Cong, and Z. Liu. "Critical roles of G protein-coupled receptors in regulating intestinal homeostasis and inflammatory bowel disease". In: *Mucosal Immunol. 2022 155* 15.5 (June 2022), pp. 819–828. ISSN: 1935-3456.

[119] L. R. Johnson. "Gastrointestinal hormones and their functions". In: *Annu. Rev. Physiol.* 39 (1977), pp. 135–158. ISSN: 0066-4278.

[120] Q. Zeng, L. Ou, W. Wang, and D. Y. Guo. "Gastrin, Cholecystokinin, Signaling, and Biological Activities in Cellular Processes". In: *Front. Endocrinol. (Lausanne).* 11 (Mar. 2020), p. 112. ISSN: 16642392.

[121] S. A. Watson, P. A. Clarke, T. M. Morris, and M. E. Caplin. "Antiserum raised against an epitope of the cholecystokinin B/gastrin receptor inhibits hepatic invasion of a human colon tumor." In: *Cancer Res.* 60.20 (Oct. 2000), pp. 5902–5907. ISSN: 0008-5472.

[122] A. Dongre and R. A. Weinberg. "New insights into the mechanisms of epithelialmesenchymal transition and implications for cancer". In: *Nat. Rev. Mol. Cell Biol. 2018 202* 20.2 (Nov. 2018), pp. 69–84. ISSN: 1471-0080.

[123] M. M. Chang, S. Z. Wu, S. H. Yang, C. C. Wu, C. Y. Wang, and B. M. Huang. "FGF9/FGFR1 promotes cell proliferation, epithelial-mesenchymal transition, M2 macrophage infiltration and liver metastasis of lung cancer". In: *Transl. Oncol.* 14.11 (Nov. 2021). ISSN: 1936-5233.

[124] S. Usman, N. H. Waseem, T. K. N. Nguyen, S. Mohsin, A. Jamal, M. T. Teh, and A. Waseem. "Vimentin Is at the Heart of Epithelial Mesenchymal Transition (EMT) Mediated Metastasis". In: *Cancers (Basel).* 13.19 (Oct. 2021), p. 4985. ISSN: 20726694.

[125] K. Gravdal, O. J. Halvorsen, S. A. Haukaas, and L. A. Akslen. "A switch from E-cadherin to N-cadherin expression indicates epithelial to mesenchymal transition and is of strong and independent importance for the progress of prostate cancer". In: *Clin. Cancer Res.* 13.23 (Dec. 2007), pp. 7003–7011. ISSN: 1078-0432.

[126] M. Natsuizaka et al. "Interplay between Notch1 and Notch3 promotes EMT and tumor initiation in squamous cell carcinoma". In: *Nat. Commun.* 8.1 (Dec. 2017). ISSN: 2041-1723.

[127] Z. Zhang, Y. Wang, J. Zhang, J. Zhong, and R. Yang. "COL1A1 promotes metastasis in colorectal cancer by regulating the WNT/PCP pathway". In: *Mol. Med. Rep.* 17.4 (Apr. 2018), pp. 5037–5042. ISSN: 1791-3004.

[128] A. T. Ouchida, M. Kacal, A. Zheng, G. Ambroise, B. Zhang, E. Norberg, and H. Vakifahmetoglu-Norberg. "USP10 regulates the stability of the EMT-transcription factor Slug/SNAI2". In: *Biochem. Biophys. Res. Commun.* 502.4 (Aug. 2018), pp. 429–434. ISSN: 1090-2104.

[129] S. M. van Neerven et al. "Apc-mutant cells act as supercompetitors in intestinal tumour initiation". In: *Nat. 2021 5947863* 594.7863 (June 2021), pp. 436–441. ISSN: 1476-4687.

[130] D. J. Flanagan et al. "NOTUM from Apc-mutant cells biases clonal competition to initiate cancer". In: *Nat. 2021 5947863* 594.7863 (June 2021), pp. 430–435. ISSN: 1476-4687.

[131] P. L. Ståhl et al. "Visualization and analysis of gene expression in tissue sections by spatial transcriptomics". In: *Science (80-.).* 353.6294 (July 2016), pp. 78–82. ISSN: 10959203.

[132] P. G. Richardson et al. "A phase 2 study of bortezomib in relapsed, refractory myeloma". In: *N. Engl. J. Med.* 348.26 (June 2003), pp. 2609–2617. ISSN: 1533-4406.

[133] C. R. Schott, L. Ludwig, A. J. Mutsaers, R. A. Foster, and G. A. Wood. "The autophagy inhibitor spautin-1, either alone or combined with doxorubicin, decreases cell survival and colony formation in canine appendicular osteosarcoma cells". In: *PLoS One* 13.10 (Oct. 2018). ISSN: 19326203.

[134] R. J. Correa, Y. R. Valdes, T. M. Peart, E. N. Fazio, M. Bertrand, J. McGee, M. Préfontaine, A. Sugimoto, G. E. DiMattia, and T. G. Shepherd. "Combination of AKT inhibition with autophagy blockade effectively reduces ascites-derived ovarian cancer cell viability". In: *Carcinogenesis* 35.9 (2014), p. 1951. ISSN: 14602180.

[135] Y. Liao, Z. Guo, X. Xia, Y. Liu, C. Huang, L. Jiang, X. Wang, J. Liu, and H. Huang. "Inhibition of EGFR signaling with Spautin-1 represents a novel therapeutics for prostate cancer". In: *J. Exp. Clin. Cancer Res.* 38.1 (Apr. 2019). ISSN: 17569966.

[136] A. Shanmugham and H. Ovaa. "DUBs and disease: activity assays for inhibitor development." In: *Curr. Opin. Drug Discov. Devel.* 11.5 (Sept. 2008), pp. 688–696. ISSN: 1367-6733.

[137] M. Békés, D. R. Langley, and C. M. Crews. "PROTAC targeted protein degraders: the past is prologue". In: *Nat. Rev. Drug Discov. 2022 213* 21.3 (Jan. 2022), pp. 181–200. ISSN: 1474-1784.

[138] A. Paramore and S. Frantz. "Bortezomib. Market analysis". In: *Nat. Rev. Drug Discov.* 2.8 (2003), pp. 611–612. ISSN: 14741776.

[139] D. D. Sahtoe and T. K. Sixma. "Layers of DUB regulation". In: *Trends Biochem. Sci.* 40.8 (Aug. 2015), pp. 456–467. ISSN: 0968-0004.

[140] T. E. Mevissen and D. Komander. "Mechanisms of Deubiquitinase Specificity and Regulation". In: *Annu. Rev. Biochem.* 86 (June 2017), pp. 159–192. ISSN: 1545-4509.

[141] J. A. Harrigan, X. Jacq, N. M. Martin, and S. P. Jackson. "Deubiquitylating enzymes and drug discovery: emerging opportunities". In: *Nat. Rev. Drug Discov. 2017 171* 17.1 (Sept. 2017), pp. 57–78. ISSN: 1474-1784.

[142] M. Gersch, J. L. Wagstaff, A. V. Toms, B. Graves, S. M. Freund, and D. Komander. "Distinct USP25 and USP28 Oligomerization States Regulate Deubiquitinating Activity". In: *Mol. Cell* 74.3 (May 2019), 436–451.e7. ISSN: 1097-4164.

[143] F. Sauer, T. Klemm, R. B. Kollampally, I. Tessmer, R. K. Nair, N. Popov, and C. Kisker. "Differential Oligomerization of the Deubiquitinases USP25 and USP28 Regulates Their Activities". In: *Mol. Cell* 74.3 (May 2019), 421–435.e10. ISSN: 10974164.

[144] T. Maculins et al. "Discovery of Protein-Protein Interaction Inhibitors by Integrating Protein Engineering and Chemical Screening Platforms". In: *Cell Chem. Biol.* 27.11 (Nov. 2020), 1441–1451.e7. ISSN: 2451-9448.

[145] J. Choi, J. S. Yun, H. Song, N. H. Kim, H. S. Kim, and J. I. Yook. "Exploring the chemical space of proteinprotein interaction inhibitors through machine learning". In: *Sci. Reports 2021 111* 11.1 (June 2021), pp. 1–10. ISSN: 2045-2322.

[146] K. Washington, A. Elizabeth, and D. Zemper. "Apc-related models of intestinal neoplasia: a brief review for pathologists". In: *Surg. Exp. Pathol. 2019 21* 2.1 (Apr. 2019), pp. 1–9. ISSN: 2520-8454.

[147] P. Pollard et al. "The Apc1322T Mouse Develops Severe Polyposis Associated With Submaximal Nuclear β-Catenin Expression". In: *Gastroenterology* 136.7 (June 2009), 2204–2213.e13. ISSN: 00165085.

6 Appendix

MA plots from shNTC vs shUsp10-2 and shNTC vs hUSP10-WT

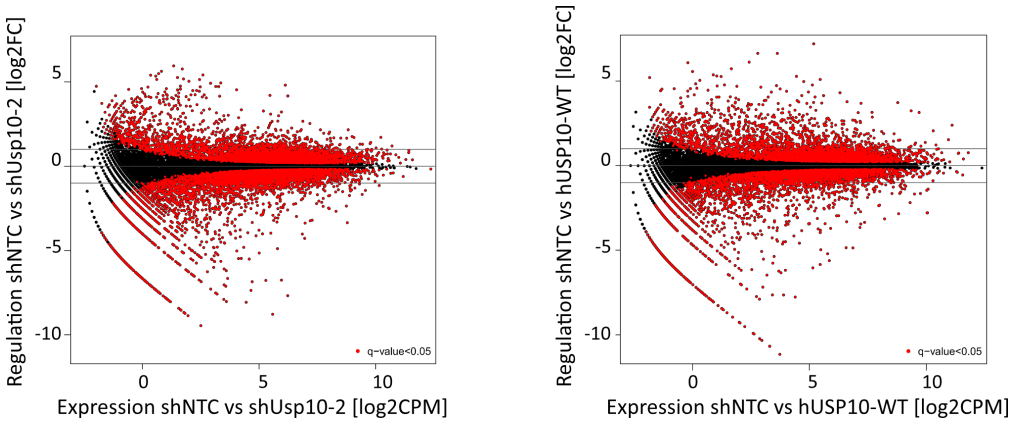

Figure 6.1: **MA plots shNTC vs shUsp10-2 and shNTC vs hUSP10 WT**
MA plot of log2CPM vs log2FC for each condition. Significant deregulated genes were defined with a p-value lower than 0.05.

Volcano plots from shNTC vs shUsp10-2 and shNTC vs hUSP10-WT

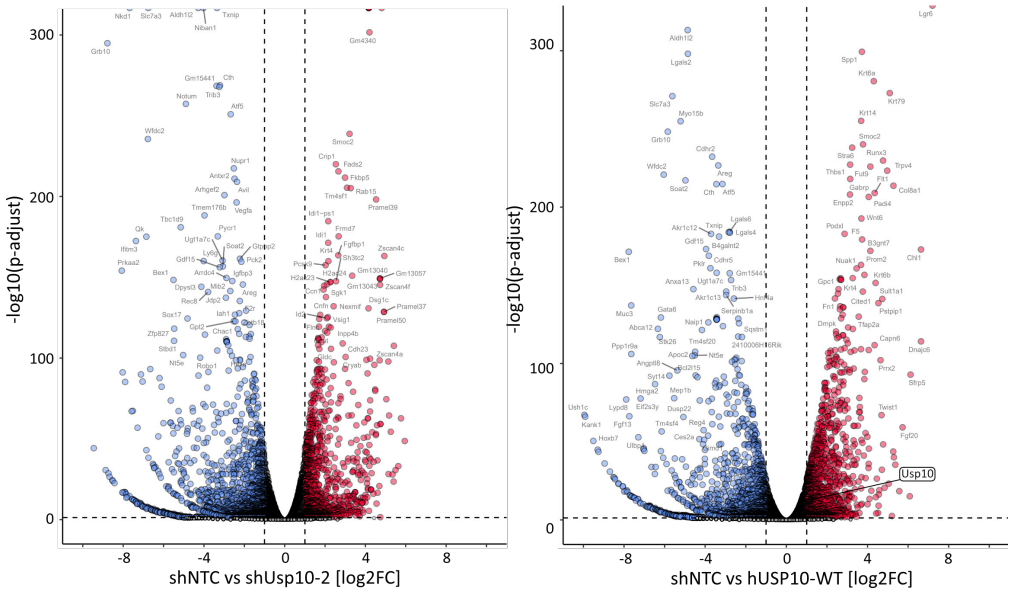

Figure 6.2: **Volcano plots shNTC vs shUsp10-2 and shNTC vs hUSP10 WT**
Significantly expressed genes were defined with a log2FC greater than 1, -1 and a p-adjust greater than 0.05. Significantly up- and downregulated genes are coloured in red and blue, respectively. Genes with a p-adjust greater than $1e^{-100}$ and Usp10 are labelled.

List of abbreviations

AAR	amino acid repeats
AAV	Adeno-accociated virus
AMPKα	adenosine monophosphate-activated protein kinase
AOM	Aoxymethan
APC	Adenomatous Polyposis Coli
ATAC	Assay for Transposase-Accessible Chromatin
ATM	Ataxia telangiectasia mutated
ATR	Ataxia telangiectasia and Rad3-related
BMP	Bone morphogenic proteins
β-TrCP	b-transducin repeat containing protein
CBC	crypt base collumnar
CCK	Cholecystokinin
CFTR	Cystic fibrosis transmembrane conductance regulator
ChIP	Chromatin Immunoprecipitation
CID	catenin inhibitory domain
CIMP	CpG island methylator phenotype
CIN	Chromosomal instability
CK1a	Casein kinase 1
CMS	consensus molecular subtype
CRC	Colorectal Cancer
CRISPR	clustered regularly interspaced short palindromic repeats
CSN	Cop9-signalosome
CYLD	Cylindromatosis tumour suppressor gene
DGE	differential gene expression
DMSO	Dimethylsolfoxid
DNA	Deoxyribonucleic acid
DOX	Doxycyclin
DSS	Dextran sulfate sodium
DUB	Deubiquitylase
DVL	Dishevelled
EC50	effective concentration
EGF	epidermal growthfactor
EGFR	EGF receptor
EMT	epithelial to mesenchymal transition
FACS	Fluorescent activated cell sorting
FAP	familial adenomatous polyposis
fl	flox
FZD	Frizzled
G3BP1/2	GTPase- activating protein-binding protein1/2
GEMM	genetically engineered mouse model
GFP	Green-fluorescent protein
GI	gatro instestinal
GPCR	G-protein coupled receptor
gRNA	guide RNA
GSEA	Gene set enrichment analysis
GSK3b	Glycogen synthase kinase 3 beta,

H&E	Hematxoylin and Eosin
HCC	Hepatocellular carcinoma
HECT	homologues to the 6-AP Carboxyl Terminuns
IC50	inhibitory concentration
IF	Immunofluorescence
IHC	Immunohistochemistry
IP	Immunoprecipitation
KD	knock-down
KM	Kaplan-Meier
KO	knock-out
LGR5	Leucine-rich repeat-containing G-protein coupled receptor 5
logCPM	log Counts per million
logFC	log FoldChange
LOH	loss-of-hetereozygocity
MIN	multiple intestinal neoplasia
MSI	Microstalellite instable
NAC	N-acetylcystein
NEM	N-Ethylmaleimide
NSG	NOD scid gamma
NTC	Non-targeting control
OE	Overexpression
PI3K	Phosphoinositide 3-kinases
PTEN	Phosphatase and tensin homolog
PTM	post-translational modification
RBR	Ring-between-Ring
RCC	Rebal cell carcinoma
RING	Really interetsing new gene
RNA	Ribonuclei acid
RPKM	Reads per kilobase million
SAMP	Axin-binding sites
SCF	Skp1-Cullin-F-box
SCNA	somatic copy number alterations
shRNA	short hairpin RNA
siRNA	short interfering RNA
Spautin-1	specific and potent autophagy inhibitor
TA	transit-aplifying
TCGA	The cancer genome atlas
TGFβ	transforming growthfactor b
TGFBR2	TGFβ-receptor2
TMA	Tissue micro array
TRE	Tetracycline responsive element
TUBE	Tandem Ubiquitin Binding Entities
Ub	Ubiquitin
UPS	Ubiquitin Proteasome Pathway
USP	Ubiquitin Specific Protease
VHL	Von Hippel-Lindau
WB	Western blot
WT	wild-type

List of Figures

Acknowledgments

My first and biggest thanks goes to the boss, Dr. Markus Diefenbacher. You've been the best Doktorvater a PhD student could ask for. Thank you for your patience, your ideas, the endless discussions, for challenging me almost every day and to let me do, what I really want to do, at least most of the time;). Thank you for giving me the chance to work on this fantastic project, to learn all methods I wanted to learn and for all the support during this thesis. I could learn a lot from you not only scientifically but also for my future career.

A big acknowledgment goes also to Prof. Martin Eilers, for the fruitful discussions in our small groups, the scientific input and the friendly reminder to focus on my project. Additionally, I would like to thank Prof. Amir Orian and Prof. Ivan iki for being members of my thesis committee and for their scientific help to my project, their ideas and for all the helpful comments and the discussions during the thesis committee meetings. I would like to thank the GRK2243, and especially Prof Alexander Buchberger, for being an amazing Ubiquitin-family in Würzburg, for supporting my project with great ideas and critical questions and for enabling me, to attend so many conferences and workshops. This scientific exchange, as well in the GRK as on these Ubiquitin meetings have broaden my scientific horizon.

A huge shout out goes the past and present members of the Diefenbacher Lab. Oli, Carmina, Cristian, Saskia, Thomas, Niki and Angela, thank you for the great time in the lab, so much fun in the office and all the delicious breakfasts during our Seminars. I would especially like to thank Saskia, my first Master student. She was not only scientifically participating in my project, I also learned how to teach and to supervise. Thank you for being the best first student.
And special thanks of course also to Oli and Carmina. Not only did you spend your time with me in the lab, but also beyond. Thank you for being not only the best colleagues, but also becoming really good friends.

I also would like to thank the whole Department of Biochemistry and Molecular Biology for the great working environment. In such a department one always finds help, answers to every question and friends. Special thanks goes to Isa, Carina and Sarah, you made the starting time in Würzburg very easy, not only in the lab but also in our spare time. PhD life is often happening in the lab, with retreats, coffee breaks, Mensa time and Feierabend-bier but also outside of the lab. Thanks to Daniel, Lorenz, Sinah, Mareike, Leonie, der andere Daniel, Basti, Katrin and Stefanie you've made my time here Würzburg very special and became friends instead of colleagues!

Finally, I want to thank my family, my mum, Jürgen and my brother and the extended family Elli, Kerstin and Nate. Thank you for all your support throughout this journey, for always believing in me, for putting up with all my whims as I finished this last part. Without your support, none of this would have been possible.

Publications

Reissland M, Tauch S, Prieto-Garcia C, Hartmann O, Sugino T, Schulte C, Schülein-Völk C, Ade C, Cossa G, Rosenfeldt M, Wiegering A, Potente M, Eilers M, Maric H, Li V, Maurice M, Diki I, Orian M, Gallant M & Diefenbacher ME: β-Catenin regulation by USP10 is essential for intestinal stem cell homeostasis and tumour progression. (*in preparation*)

Novak R, Ahmad YA, Timaner M, Bitman-Lotan E, Oknin-Vaisman A, Horwitz R, Hartmann O, **Reissland M**, Buck V, Rosenfeldt M, Nikomarov D, Diefenbacher ME, Shaked Y, Orian A. (2022): RNF4˜RGMb˜BMP6 axis required for osteogenic differentiation and cancer cell survival. *Cell Death Dis.*, 13(9):820. doi: 10.1038/s41419-022-05262-1.

Fischer T, Hartmann O, **Reissland M**, Prieto-Garcia C, Klann K, Pahor N, Schülein-Völk C, Baluapuri A, Polat B, Abazari A, Gerhard-Hartmann E, Kopp HG, Essmann F, Rosenfeldt M, Münch C, Flentje M, Diefenbacher ME. (2022): PTEN mutant non-small cell lung cancer require ATM to suppress pro-apoptotic signalling and evade radiotherapy. *Cell Biosci.*, 12(1):50. doi: 10.1186/s13578-022-00778-7.

Prieto-Garcia C, Hartmann O, **Reissland M**, Braun F, Bozkurt S, Pahor N, Fuss C, Schirbel A, Schülein-Völk C, Buchberger A, Calzado Canale MA, Rosenfeldt M, Dikic I, Münch C, Diefenbacher ME. (2022): USP28 enables oncogenic transformation of respiratory cells, and its inhibition potentiates molecular therapy targeting mutant EGFR, BRAF and PI3K. *Mol Oncol.*, 16(17):3082-3106. doi: 10.1002/1878-0261.13217

Prieto-Garcia C, Hartmann O, **Reissland M**, Fischer T, Maier CR, Rosenfeldt M, Schülein-Völk C, Klann K, Kalb R, Dikic I, Münch C, Diefenbacher ME. (2022): Inhibition of USP28 overcomes Cisplatin-resistance of squamous tumors by suppression of the Fanconi anemia pathway. *Cell Death Differ.*, 29(3):568-584. doi: 10.1038/s41418-021-00875-z

Hartmann O, **Reissland M**, Maier CR, Fischer T, Prieto-Garcia C, Baluapuri A, Schwarz J, Schmitz W, Garrido-Rodriguez M, Pahor N, Davies CC, Bassermann F, Orian A, Wolf E, Schulze A, Calzado MA, Rosenfeldt MT, Diefenbacher ME. (2021): Implementation of CRISPR/Cas9 Genome Editing to Generate Murine Lung Cancer Models That Depict the Mutational Landscape of Human Disease. *Front Cell Dev Biol.*, 9:641618. doi: 10.3389/fcell.2021.641618

Prieto-Garcia C, Hartmann O, **Reissland M**, Braun F, Fischer T, Walz S, Schülein-Völk C, Eilers U, Ade CP, Calzado MA, Orian A, Maric HM, Münch C, Rosenfeldt M, Eilers M, Diefenbacher ME. (2020): Maintaining protein stability of ΔNp63 via USP28 is required by squamous cancer cells. *EMBO Mol Med*, 12(4):e11101. doi: 10.15252/emmm.201911101

Affidavit

I hereby confirm that my thesis entitled “USP10 is a *de novo* tumour-specific regulator of β-Catenin and contributes to cancer stem cell maintenance and tumour progression” is the result of my own work. I did not receive any help or support from commercial consultants. All sources and/or materials are listed and specified in the thesis.

Furthermore, I confirm that this thesis has not been submitted as part of another examination process neither in identical nor in similar form.

Place, Date Michaela Reissland

Eidesstattliche Erklärung

Hiermit erkläre ich an Eides statt, die Dissertation "USP10 ist ein *de novo* tumorspezifischer Regulator von β-Catenin und trägt zur Erhaltung von Krebsstammzellen und zur Tumorprogression bei" eigenständig, d.h. selbstständig und ohne Hilfe eines kommerziellen Promotionsberaters, angefertigt und keine anderen als die von mir angegeben Quellen und Hilfsmittel verwendet zu haben.

Ich erkläre auSSerdem, dass die Dissertation weder in gleicher noch in ähnlicher Form bereits in einem anderen Prüfungsverfahren vorgelegt wurde.

Ort, Datum Michaela Reissland